

Neuronal pathology in targeted cortical experimental autoimmune encephalomyelitis and multiple sclerosis

Doctoral Thesis

In partial fulfillment of the requirements for the degree
“Doctor rerum naturalium (Dr. rer. nat.)”
in the Molecular Medicine Study Program
at the Georg-August University Göttingen

submitted by
Tanja Jürgens

born in
Nordenham, Germany

Göttingen, April 2013

Meinen Eltern

Members of the Thesis Committee:

Supervisor

Prof. Dr. W. Brück
Department of Neuropathology
University of Göttingen

Second member of the thesis committee

Prof. Dr. Dr. H. Ehrenreich
Department of Clinical Neurosciences
Max Planck Institute of Experimental Medicine, Göttingen

Third member of the thesis committee

Prof. Dr. M. Simons
Department of Neurology
Max Planck Institute of Experimental Medicine, Göttingen

Assistant supervisor

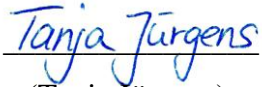
Prof. Dr. D. Merkler
Department of Pathology and Immunology
University of Geneva

Date of Disputation: 29.05.2013

AFFIDAVIT

AFFIDAVIT

Here I declare that my doctoral thesis entitled “Neuronal pathology in targeted cortical experimental autoimmune encephalomyelitis and multiple sclerosis” has been written independently with no other sources and aids than quoted.


(Tanja Jürgens)

Göttingen, April 2013

LIST OF PUBLICATIONS

Late motor decline after accomplished remyelination: impact for progressive multiple sclerosis.

Natalia Manrique-Hoyos, Tanja Jürgens, Mads Grønberg, Mario Kreutzfeldt, Mariann Schedensack, Tanja Kuhlmann, Christina Schrick, Wolfgang Brück, Henning Urlaub, Mikael Simons and Doron Merkler. *Annals of Neurology*, 2012.

Toll-like receptor activation reveals developmental reorganization and unmasks responder subsets of microglia.

Jörg Scheffel, Tommy Regen, Denise van Rossum, Stefanie Seifert, Sandra Ribes, Roland Nau Roham Parsa, Robert A. Harris, Hendrikus W. G. M. Boddeke, Han-Ning Chuang, Tobias Pukrop, Johannes T. Wessels, Tanja Jürgens, Doron Merkler, Wolfgang Brück, Mareike Schnaars, Mikael Simons, Helmut Kettenmann and Uwe-Karsten Hanisch. *Glia*, 2012.

Propagation of spreading depression inversely correlates with cortical myelin content.

Doron Merkler*, Florian Klinker*, Tanja Jürgens, Raoul Glaser, Walter Paulus, Bastian G. Brinkmann, Michael W. Sereda, Christine Stadelmann-Nessler, Rubem C.A. Guedes, Wolfgang Brück, David Liebetanz. *Annals of Neurology*, 2009.

(*equal contribution)

TABLE OF CONTENTS

AFFIDAVIT	I
LIST OF PUBLICATIONS	II
TABLE OF CONTENTS	III
ACKNOWLEDGEMENTS	VI
ABSTRACT	VII
ZUSAMMENFASSUNG.....	IX
LIST OF FIGURES.....	XI
LIST OF TABLES.....	XII
ABBREVIATIONS.....	XIII
1 INTRODUCTION	1
1.1 Multiple sclerosis.....	2
1.1.1 Etiology of MS	2
1.1.2 Diagnosis and clinical presentation	3
1.1.2.1 Diagnosis	3
1.1.2.2 Clinical disease courses in MS	4
1.1.2.3 Clinical correlates of cortical lesions.....	4
1.2 Myelin and myelin proteins	5
1.2.1 Proteolipid protein (PLP)	6
1.2.2 Myelin basic protein (MBP).....	6
1.2.3 Myelin oligodendrocyte glycoprotein (MOG)	6
1.3 Immunology of MS	6
1.3.1 Concept of autoimmune T cell responses.....	7
1.3.2 Role of CD4 ⁺ T cell effector subsets	8
1.3.3 Role of CD8 ⁺ T cells	9
1.3.4 Role of antibodies and B cells	9
1.4 Pathology of MS.....	11
1.4.1 Immunopathology.....	11
1.4.2 Demyelination	12
1.4.3 Remyelination.....	13
1.4.4 Neurodegeneration and atrophy.....	14
1.5 Animal models of MS	15
1.5.1 Experimental autoimmune encephalomyelitis (EAE).....	15

TABLE OF CONTENTS

1.5.2	Targeted EAE models.....	16
2	AIM OF THE STUDY	18
3	MATERIAL AND METHODS	19
3.1	Material.....	19
3.1.1	Reagents	19
3.1.2	Antibodies.....	22
3.1.3	Buffers and solutions	23
3.1.4	Laboratory animals	30
3.1.5	Human brain samples	30
3.1.6	Equipment.....	30
3.1.7	Consumables.....	33
3.1.8	Software.....	34
3.2	Methods	35
3.2.1	Genotyping of EGFP-M positive animals	35
3.2.2	Expression and purification of recombinant rat MOG ₁₋₁₂₅	36
3.2.3	SDS-PAGE	37
3.2.4	Animal experiments.....	37
3.2.5	Blood sampling.....	37
3.2.6	Induction of EAE.....	38
3.2.7	Intracerebral stereotactic injection.....	38
3.2.8	Enzyme-linked immunosorbent assay (ELISA)	40
3.2.9	Histology of mouse brain tissue	40
3.2.9.1	Tissue processing.....	40
3.2.9.1.1	Perfusion and sectioning.....	40
3.2.9.1.2	Deparaffinization and rehydration	41
3.2.9.2	Histochemistry	41
3.2.9.2.1	Bielschowsky's silver staining.....	41
3.2.9.3	Immunohistochemistry	42
3.2.9.3.1	Antigen retrieval for CD3, Mac-3, NeuN in paraffin-embedded sections	42
3.2.9.3.2	Immunohistochemistry for MBP and NeuN in paraffin-embedded sections.....	42
3.2.9.3.3	Immunohistochemistry for Mac-3 and CD3 in paraffin embedded sections	43
3.2.9.3.4	Immunohistochemistry for MBP in EGFP positive cryosections	43
3.2.10	Histology of human brain tissue.....	44
3.2.10.1	Human tissue collection.....	44
3.2.10.2	Golgi-Cox impregnation.....	44

TABLE OF CONTENTS

3.2.11	Image acquisition, processing and analyses of histological tissue sections	44
3.2.12	Statistical analyses	46
4	RESULTS	47
4.1	Development of a targeted EAE model of cortical demyelination	47
4.2	Immunization with MOG ₁₋₁₂₅ leads to high antibody titers in serum.....	47
4.3	Cortical demyelination is primarily located at subpial areas, reveals partial remyelination and mimics cortical MS lesions.....	48
4.4	Axonal preservation but incomplete remyelination in targeted cortical demyelinated lesions	51
4.5	Cortical inflammation is transient after lesion induction	53
4.5.1	Infiltration of T cells during demyelination	53
4.5.2	Different morphological phenotypes of macrophages/microglia are present in demyelinated cortex.....	54
4.6	Cortical EAE reveals no neuronal loss	57
4.6.1	Cortical thickness is slightly reduced after remyelination	57
4.6.2	Neuronal density is not reduced in targeted EAE.....	58
4.7	Visualization and shape analysis of dendrites and spines in the cerebral cortex of mice	59
4.8	Loss of dendritic spines and branches in the cortex of progressive MS cases	62
5	DISCUSSION.....	65
5.1	Targeted cortical EAE in mice allows reproducible lesion induction within a defined anatomical area	65
5.2	Active cortical demyelination and inflammation are transient and do not induce neuronal or axonal loss	66
5.3	Widespread but incomplete remyelination	70
5.4	Global dendritic spine loss in cortices of progressive MS patients.....	71
6	SUMMARY AND CONCLUSIONS.....	73
7	REFERENCES	74
8	CURRICULUM VITAE	92

ACKNOWLEDGEMENTS

I would like to thank my assistant supervisor Prof. Dr. Doron Merkler for the interesting project, the great support and guidance. At any time I could discuss with him open questions. In addition, I would like to thank him for teaching me many histological and animal experimental techniques, especially the stereotactic injections into the brain.

I also like to thank my supervisors Prof. Dr. Wolfgang Brück, Prof. Dr. Dr. Hannelore Ehrenreich, and Prof. Dr. Mikael Simons for being members of my Thesis Committee and their helpful discussions in these meetings.

Furthermore I would like to thank our collaboration partner Dr. Enikö Kövari, Division of Neuropsychiatry, Department of Psychiatry, University School of Medicine, Geneva for introducing me into the Golgi-Cox impregnation technique for our human samples and giving me the opportunity to cut the tissue blocks in their institute.

Moreover, I would like to thank my former colleagues in the Department of Neuropathology in Göttingen and my new colleagues in the Department of Pathology and Immunology in Geneva for the great working atmosphere. Special thanks go to Dr. Karin Steinbach, who supported me in any question in the lab and for proofreading my manuscript. Many thanks also to Mariann Vorm and Ingrid Wagner for their assistance in histological techniques, animal experimentation and any other laboratory business.

I also like to thank my grandparents and my brother Christian and Wiebke for their great support especially in the end of my thesis.

My very special thanks go to my parents, who supported and motivated me during my studies in all respects.

ABSTRACT

In the recent years it has become increasingly obvious that multiple sclerosis (MS) is not only a white matter (WM) disease of the central nervous system (CNS) but also involves frequently and extensively the grey matter (GM) in all MS disease subtypes. Particular cortical pathology including demyelinated lesions was reinvestigated in detail by improved immunohistochemical staining techniques and new magnetic resonance imaging (MRI) acquisition methods. Clinically, MS patients often suffer from physical disability and neuropsychological deficits affecting their quality of life. These symptoms were associated with GM lesions. Therefore, the pathomechanism(s) leading to GM pathology needs to be elucidated for the development of preventative or acute treatments.

Studying GM pathology requires appropriate animal models reflecting human cortical pathology. The most used rodent model in MS research, experimental autoimmune encephalomyelitis (EAE), rarely affects the cerebral cortex in 'conventional' immunization protocols. An EAE model targeting the cortex and reflecting human MS lesions has been described in the rat. GM lesions were induced by the injection of proinflammatory cytokines in a predetermined cortical area. Due to the lack of useful transgenic rat strains in order to study the mechanisms underlying GM pathology, the targeted EAE model needs to be established in mice.

This project focused on the establishment of a targeted cortical EAE mouse model and the histopathological characterization. Furthermore, cortical brain tissue of late disease-stage MS patients was studied focusing on dendritic pathology.

Targeted cortical EAE was induced in myelin oligodendrocyte glycoprotein (MOG)-immunized BiozziABH (antibody high) and F1 offsprings generated from BiozziABH and mice on a C57BL6/J background by intracortical injection of TNF- α and IFN- γ . Histological analyses revealed widespread subpial demyelination and inflammation in the cortex three days after cytokine injection in the affected hemisphere. Within three weeks inflammation resolved profoundly and demyelinated lesions showed partial remyelination. Axons remained well preserved in lesioned areas and neuronal loss could not be detected in the cortex. Furthermore, a method was established that allows detailed analysis of dendritic pathologies in mice.

Cerebral cortex autopsy specimen of progressive MS patients with a long-lasting disease revealed a reduction of dendritic spines in neurons located in the lower cortical layers in

ABSTRACT

chronically demyelinated lesions as well as in the surrounding normal appearing grey matter (NAGM).

In the present project a targeted cortical EAE mouse model was established reproducing key hallmarks of GM pathology observed in early-stage MS patients. The model is a useful tool to study early events in demyelinated cortex and to investigate therapeutic treatments such as increasing remyelination. Furthermore, the global loss of dendritic spines in the cerebral cortex of chronic MS patients might be attributed to neuropsychological deficits that are often observed.

ZUSAMMENFASSUNG

In den letzten Jahren ist zunehmend deutlich geworden, dass die Multiple Sklerose (MS) nicht nur eine Erkrankung der weißen Substanz des zentralen Nervensystems ist, sondern auch häufig und beträchtlich die graue Substanz in allen klinischen Verlaufsformen betrifft. Besonders die kortikale Pathologie mit entmarkten Läsionen wurde durch verbesserte immunhistochemische Färbetechniken und neuen magnetresonanztomographischen Verfahren ausführlicher untersucht. MS-Patienten leiden klinisch oft an körperlichen Beeinträchtigungen und neuropsychologischen Defiziten, welche die Lebensqualität beeinflussen. Diese Symptome wurden mit Läsionen in der grauen Substanz assoziiert. Mechanismen, die zu dieser Pathologie führen, müssen daher aufgeklärt werden um vorbeugende oder akute Behandlungen entwickeln zu können.

Zur pathologischen Untersuchung der grauen Substanz werden angemessene Tiermodelle benötigt, welche die humane kortikale Pathologie widerspiegeln. Das am häufigsten verwendete Tiermodell in MS-Studien ist die Experimentelle Autoimmune Enzephalomyelitis (EAE), die in ihrem 'konventionellen' Immunisierungsprotokoll nur selten den zerebralen Kortex betrifft. Ein EAE-Modell mit Einbezug des Kortex, das MS-Läsionen nachahmt, wurde in Ratten beschrieben. Hierzu wurden proinflammatorische Zytokine in eine vorbestimmte kortikale Region injiziert. Da spezifisch genveränderte Rattenstämme fehlen um die Mechanismen der Pathologie in der grauen Substanz zu untersuchen ist es notwendig das Tiermodell in Mäusen zu entwickeln.

Das Ziel dieses Projekts war die Entwicklung eines kortikalen EAE-Mausmodells sowie dessen histopathologische Charakterisierung. Desweiteren wurde kortikales Gehirnmaterial von MS-Patienten im späten Krankheitsstadium auf dendritische Pathologie untersucht.

Die kortikale EAE wurde in Myelin Oligodendrozyten Glykoprotein (MOG)-immunisierten BiozziABH (hohe Antikörper) und F1 Nachkommen, die aus BiozziABH und Mäusen mit einem C57BL6/J-Hintergrund generiert worden sind, durch die intrakortikale Injektion von TNF- α und IFN- γ induziert. Histologische Untersuchungen zeigten eine ausgedehnte subpiale Entmarkung und Entzündung im Kortex drei Tage nach der Zytokininjektion in der betroffenen Hirnhälfte. Die Entzündung ging innerhalb von drei Wochen fast vollständig zurück und entmarkte Regionen wiesen teilweise eine Remyelinisierung auf. Axone blieben in läSIONalen Regionen erhalten und neuronaler Verlust wurde im Kortex nicht beobachtet. Desweiteren wurde eine Methode etabliert, die es erlaubt detailliert dendritische Pathologien in der Maus zu untersuchen.

ABSTRACT (GERMAN)

Kortex-enhaltenes Autopsiematerial von progressiven MS-Patienten mit langandauerndem Krankheitsverlauf zeigte einen Verlust von dendritischen Dornfortsätzen (Spines) in Neurone, die in den unteren korikalen Layern sowohl in chronisch entmarkten Läsionen als auch im umliegenden normal erscheinendem Gewebe der grauen Substanz lokalisiert waren.

Im vorliegenden Projekt wurde ein kortikales EAE-Mausmodell entwickelt, das die humane MS-Pathologie der grauen Substanz in frühen Krankheitsstadien widerspiegelt. Dieses Modell ist für Untersuchungen früher Mechanismen im entmarkten Kortex und für die Erprobung therapeutischer Behandlungen wie die Erhöhung der Remyelinisierung nützlich. Darüberhinaus wurde ein ausgedehnter Verlust dendritischer Dornfortsätze im zerebralen Kortex in chronischen MS-Patienten gezeigt, der auf oft beobachtete neuropsychologische Defizite zurückgeführt werden könnte.

LIST OF FIGURES

Figure 1 Strategy of targeted cortical EAE39

Figure 2 Coronal sectioning of the injection site.....41

Figure 3 MOG₁₋₁₂₅-immunization induces high autoantibody titers47

Figure 4 Active demyelination can be observed three days after cytokine injection48

Figure 5 Targeted cortical demyelination is followed by partial remyelination50

Figure 6 Axonal preservation in incomplete remyelinated lesions52

Figure 7 Transient CD3⁺ T cell infiltration during demyelination54

Figure 8 Different morphological phenotypes of macrophages/microglia during demyelination
.....55

Figure 9 Slightly reduced paramedial cortical thickness after remyelination58

Figure 10 Neuronal density is not altered during de- and remyelination59

Figure 11 Visualization of dendritic branches and spines60

Figure 12 3D analysis of dendritic and spine shapes61

Figure 13 Reduced densities of dendritic spines and branches in chronic MS63/64

LIST OF TABLES

Table 1 Genotyping PCR for EGFP expression35

Table 2 PCR program for EGFP genotyping35

Table 3 MS and control cases.....62

ABBREVIATIONS

2D	Two-dimensional
3D	Three-dimensional
ANOVA	Analysis of variance
APC	Antigen-presenting cell
APS	Ammonium persulfate
BBB	Blood-brain barrier
BiozziABH	Biozzi antibody high
BSA	Bovine serum albumin
bp	Base pair
CC	Corpus callosum
CD	Cluster of differentiation
CCR	C-C chemokine receptor
CFA	Complete Freund's adjuvant
CIS	Clinical isolated syndrome
CNS	Central nervous system
CSF	Cerebrospinal fluid
Cx	Cortex
DAB	3,3'-Diaminobenzidine
DAPI	4',6-diamidino-2-phenylindole
dATP	Deoxyadenosine triphosphate
dCTP	Deoxycytidine triphosphate
dGTP	Deoxyguanosine triphosphate
DNA	Deoxyribonucleic acid
DIR	Double inversion recovery
dNTPs	Deoxynucleotide triphosphates
dTTP	Deoxythymidine triphosphate
DTT	Dithiothreitol
EAE	Experimental autoimmune encephalomyelitis
EBV	Epstein-Barr virus
E.coli	Escherichia coli
EDTA	Ethylenediaminetetraacetic acid
EGFP	Enhanced green fluorescent protein

ABBREVIATIONS

ELISA	Enzyme-linked immunosorbent assay
F1	Filial 1
FBS	Fetal bovine serum
GM	Grey matter
HLA	Human leukocyte antigen
i.c.	Intracortical
IFA	Incomplete Freund's adjuvant
IFN	Interferon
Ig	Immunoglobulin
IL	Interleukin
i.p.	Intraperitoneal
IPTG	Isopropylthio- β -galactoside
LDAO	N,N-Dimethyldodecylamine-N-oxide
MHC	Major histocompatibility complex
MBP	Myelin basic protein
MOG	Myelin oligodendrocyte glycoprotein
MRI	Magnetic resonance imaging
MS	Multiple sclerosis
MSIF	Multiple Sclerosis International Federation
NAA	N-acetyl aspartate
NF	Neurofilament
NAGM	Normal appearing grey matter
NAWM	Normal appearing white matter
OD ₆₀₀	Optical density measured at 600 nm
OPC	Oligodendrocyte precursor cell
PAGE	Polyacrylamide gel electrophoresis
PBS	Phosphate buffered saline
PCR	Polymerase chain reaction
PFA	Paraformaldehyde
PLP	Proteolipid protein
PPMS	Primary progressive multiple sclerosis
psi	Pounds per square inch (pressure unit)
RRMS	Relapsing-remitting multiple sclerosis
s.c.	Subcutaneous

ABBREVIATIONS

SD	Standard deviation
SDS	Sodiumdodecyl sulfate
SEM	Standard error of the mean
SPMS	Secondary progressive multiple sclerosis
TCR	T cell receptor
TE	Tris-EDTA
TEMED	Tetramethylethylenediamine
Tfh	Follicular helper T cells
TGF	Transforming growth factor
Th	T helper
TNF	Tumor necrosis factor
Tregs	Regulatory T cells
VEGF	Vascular endothelial growth factor
WHO	World Health Organization
WM	White matter

1 INTRODUCTION

Multiple sclerosis (MS) is a chronic inflammatory demyelinating disease of the central nervous system (CNS) typically starting in young adults between 20 and 40 years of age (Compston and Coles, 2008; Noseworthy et al., 2000). MS, also known as *encephalomyelitis disseminata*, is the leading cause of nontraumatic permanent neurologic disability in this age group in the United States and Europe (Dutta and Trapp, 2007).

The prevalence of MS varies around the world and is highest in Europe (WHO and MSIF, 2008). The World Health Organization (WHO) and Multiple Sclerosis International Federation (MSIF) estimated in 2008 a total number of people diagnosed with MS of approximately 1.3 million worldwide (WHO and MSIF, 2008). Germany belongs to the countries with the highest estimated prevalences of MS and in 2008, 122'000 people suffered from MS (MSIF).

The potentially first patient's description widely accepted representing MS originated from the patient's diaries. From 1822-1848, Sir Augustus d'Este, grandson of King George III, described in detail his periodic symptoms including recurring impaired vision, diplopia, weakness of the legs, ataxia, spasms, and paralysis (Pearce, 2005). From the early 19th century many scientists and physicians studied on the still unnamed nervous disease and contributed to the advanced understanding. Working independently Robert Carswell and Jean Cruveilhier discovered damage to the CNS in pathological studies (Pearce, 2005). In 1868, the Parisian Jean-Martin Charcot first described multiple sclerosis as an independent disease and correlated clinical symptoms with pathology of the CNS. He termed the disease "*sclérose en plaques*" (Charcot, 1868). MS is an unpredictable complex disease with diverse clinical, immunological and pathological phenotypes. Despite extensive research on this heterogeneous disorder the main cause of MS remained undiscovered. Studies in humans and animal models reflecting key features of the pathology found in MS patients contributed to our understanding resulting to the idea of a CD4⁺ T cell-mediated autoimmune disease evolving in genetically susceptible individuals exposed to an environmental trigger. The broadening understanding in the recent years that neurodegeneration detrimentally affected individuals with MS and the modification of the concept, that MS is not only restricted to the white matter (WM) but also involves frequently and extensively the grey matter (GM) yielded additional focuses in MS research.

1.1 Multiple sclerosis

1.1.1 Etiology of MS

The cause of MS has not yet been identified and the reason for the global varying prevalence is still unknown. However, evidences exist that MS occurs in genetically high-risk individuals exposed to an environmental agent.

A role for a genetic factor in disease susceptibility is supported by the familiar recurrence risk of MS that varied depending on the relatedness to the patient. First-degree relatives of MS patients have an approximately 15-25 fold higher risk (recurrence risk of 3-5%) to develop MS compared to the general population (lifetime prevalence 0.2%). In twin studies it was shown that there is a higher concordance rate in monozygotic twins (about 20%) in comparison to dizygotic twins (about 5%) (Dyment et al., 2004).

Furthermore, gene variations have been linked with an increased risk to develop MS. The MHC class II alleles (MHC, major histocompatibility complex, in vertebrates this system is named HLA, human leukocyte antigen) DR15 and DQ6 with the following genotypes DRB1*1501, DRB5*0101, DQA1*0102, and DQB2*0602 were associated with MS especially in Northern Europe. In addition, gene variations in interleukin-2 and interleukin-7 receptor α chains were linked to an increased susceptibility (Compston and Coles, 2008).

The variable global disease distribution of MS with increasing prevalences to the north and south in both hemispheres from the equator suggested an environmental factor contributing to disease manifestation. Moreover, children migrating from high-risk to low-risk regions adopted the decreased risk of developing MS. Reversed migration in childhood is associated with an increased risk (Compston and Coles, 2008).

In addition, clinical infections increased the risk of relapses in MS. Exacerbations that occurred during the period of a systemic infection led more frequently to sustained neurological deficits (Andersen et al., 1993; Buljevac et al., 2002; Sibley et al., 1985). Among putative infectious agents, Epstein-Barr (EBV) virus infection was strongly associated with MS (Ascherio and Munger, 2007a; Haahr and Hollsberg, 2006). It was suggested that EBV infection manifested as infectious mononucleosis in young adulthood is a risk factor for developing MS (Thacker et al., 2006). EBV interference with MS risk might involve mechanisms of molecular mimicry between viral and myelin components (Lang et al., 2002). In autopsy brain tissue of MS patients with different disease courses EBV-infected B lymphocytes/plasma cells were detected in the meninges and perivascular compartment of

INTRODUCTION

WM lesions. MS cases with a secondary progressive disease course even exhibited ectopic B cell follicles in the meninges suggested to represent main sites of EBV persistence (Serafini et al., 2007).

In addition to putative infectious agents, environmental factors like cigarette smoking, low sunlight, deficiency in vitamin D, diet, geomagnetism, air pollutants, radioactive rocks, and toxins have been suggested to trigger the development of MS (Ascherio and Munger, 2007b; Compston and Coles, 2008; Hernan et al., 2005; Mikaeloff et al., 2007).

The female predominance of about 2:1 suggests hormones as nongenetic factor contributing to MS risk. This assumption was supported by the fact that the rate of relapses decreased especially during the third trimester of pregnancy but was increased immediately after birth (Confavreux et al., 1998).

1.1.2 Diagnosis and clinical presentation

The clinical course and response to immunomodulatory therapies of individual MS patients is very heterogenous. Clinical manifestation depends on the affected CNS region and most patients show visual, sensory, motor, and autonomic deficits. The expectancy of life is only slightly reduced. Fatality of MS cases is attributable to about $\frac{2}{3}$ of patients and to the higher risk and complications of infections in progressive diseased individuals. A fulminant and fatal clinical disease course, in which MS patients die within month after disease onset, is rare (Marburg's variant of MS). Impairment in social and work life are side-effects besides depression and suicide that remain a great risk among patients (Compston and Coles, 2008; Noseworthy et al., 2000).

1.1.2.1 Diagnosis

Guidelines for diagnostic criteria for MS have been established and revised (McDonald et al., 2001; Polman et al., 2011; Polman et al., 2005). The basic concept in MS diagnosis is dissemination of lesions in space and time. Clinical, imaging, laboratory and physiologic evidences can contribute to diagnosis such as periods of neurologic dysfunctions, lesions detected in magnetic resonance imaging (MRI), disease progression, positive oligoclonal bands in cerebrospinal fluid (CSF) showing increased intrathecal synthesis of immunoglobulins of restricted specificity and prolonged latency of evoked potentials indicating slowed propagation of action potentials in demyelinated axons (Compston and Coles, 2008).

INTRODUCTION

Neurologic disability in MS patients can be assessed by the Kurtzke Expanded Disability Status Scale (EDSS) (Kurtzke, 1983), a rating system with 10 steps from 0 (normal) to 10 (death due to MS).

1.1.2.2 Clinical disease courses in MS

At disease onset about 80% of patients are affected by a relapsing-remitting disease course (RRMS) characterized by periodic episodes of neurologic deficits (relapses) followed by complete or partial recovery of the symptoms (remission). In about 10% of cases relapses are absent for more than 20 years and MS is considered to be benign. RRMS typically affects young adults in the second and third decade of life and shows a female to male predominance of ~2:1 (Noseworthy et al., 2000). In average ten years after disease onset ~50% of patients who suffered from RRMS enter a disease phase with a steady worsening of clinical symptoms, fewer relapses and incomplete recovery, called secondary progressive MS (SPMS) (Siffrin et al., 2010). About 20% of MS patients manifested a primary progressive disease course (PPMS) that is characterized by a gradually progressive deterioration of clinical symptoms from disease onset and a similar incidence between men and women (Noseworthy et al., 2000).

Regardless of an initial relapsing-remitting or progressive disease course, the age at time of irreversible disability is about 40 years (Confavreux and Vukusic, 2006). In addition, if a clinical threshold of irreversible disability is passed, the following progression of impairments is neither affected by relapses before nor during this phase (Confavreux et al., 2003; Confavreux et al., 2000).

1.1.2.3 Clinical correlates of cortical lesions

MS was typically considered as a white matter (WM) disease but it has become increasingly obvious that the grey matter (GM) is frequently and extensively involved. Lesions in the GM may contribute to the so-called clinico-radiological paradox indicating that the WM pathology cannot explain the complete spectrum of clinical deficits (Barkhof, 2002). As an example, cognitive symptoms and epileptic seizures might be better explained by GM than WM pathology. Cognitive deficits are a common feature in MS affecting 40-65% of patients. These symptoms can affect patients with a RR disease course but is more severe in the progressive forms whereas it seems to be more pronounced in SPMS than PPMS (Amato et al., 2006; Chiaravalloti and DeLuca, 2008; Rinaldi et al., 2010). Imaging studies associated the accumulation of cortical GM lesions with cognitive decline in MS patients (Calabrese et

al., 2009; Roosendaal et al., 2009). Additional factors affecting cognitive performance are depression and fatigue that are also common symptoms in many patients with MS (Chiaravalloti and DeLuca, 2008; Feinstein, 2011). Furthermore, MS is linked to an increased risk of epilepsy than the general population (Catenoix et al., 2011; Spatt et al., 2001). It was shown that the accumulation of cortical lesions is higher in epileptic versus non-epileptic RRMS patients and that they exhibit a more severe cortical atrophy, more pronounced cognitive impairment and higher physical disability (Calabrese et al., 2008; Calabrese et al., 2012b). An association of physical disability and the accumulation of cortical lesions has been confirmed in further MRI acquisition studies (Calabrese et al., 2012c; Calabrese et al., 2010b). Interestingly, cortical lesions have even been detected in some patients a long time before MRI showed inflammatory lesions in the WM, which suggests that cortical demyelination could represent the initial pathological event in MS (Calabrese and Gallo, 2009; Popescu et al., 2011).

Treatment studies in RRMS patients showed an effect of disease-modifying drugs on cortical pathology in MRI over two years as assessed by a reduced accumulation of new cortical lesions and reduced progression of cortical atrophy compared to untreated patients (Calabrese et al., 2012a; Rinaldi et al., 2012).

1.2 Myelin and myelin proteins

Myelin or the myelin-forming oligodendrocytes are generally believed to be attacked by an autoimmune response in MS leading to demyelination. Myelin is predominantly present in the WM of CNS tissue and gives these structures macroscopically the white appearance. However, myelin is also a component of the GM, albeit to a lesser extent, and ensheathes many axons originating from or terminating on cortical neurons.

Myelin consists of 75% lipids and 25% proteins. The multilamellar myelin sheath is built by lipid-rich plasma membrane extensions of oligodendrocytes in the CNS, which spirally surround axons and thereby forming myelinated axon segments called internodes. Internodes are periodically interrupted by the so-called *nodes of Ranvier* resulting in short uncovered axon segments enabling saltatory nerve conduction. Thus, myelin functions as an electrical insulator and provides fast and energy-efficient impulse propagation over long distances. The loss of myelin was associated with a conduction block and increased vulnerability to axons and neurons (Franklin and Ffrench-Constant, 2008). In contrast to axons, dendrites do not show myelination.

INTRODUCTION

In the most used animal model of MS research, experimental autoimmune encephalomyelitis (EAE), many myelin proteins like proteolipid protein (PLP), myelin basic protein (MBP), and myelin oligodendrocyte glycoprotein (MOG) have been shown to induce MS-like pathology and disease (Iglesias et al., 2001).

1.2.1 Proteolipid protein (PLP)

PLP is the major integral membrane protein of myelin in the CNS that account for ~50% of the CNS myelin protein mass. Two PLP forms are expressed, the full-length PLP (~30 kDa) and a shorter isoform, the splice variant DM20 (~20 kDa). Both proteins are primarily expressed in the CNS. DM20 can also be detected in the thymus, in which full-length PLP is only hardly detectable. Central tolerance to most epitopes to full-length PLP could be mediated by the higher expression of thymic DM20 (Goverman, 2011; Seamons et al., 2003).

1.2.2 Myelin basic protein (MBP)

MBP was the initial antigen with which CNS autoimmune diseases were elicited. MBP is a component of the central and peripheral myelin. In the CNS myelin MBP is the second most abundant protein (30-40% weight of membrane protein) whereas in the peripheral myelin it is less strongly expressed (5-15%). The MBP gene locus encodes two protein families, classic-MBPs (~21.5 kDa) and golli-MBPs. Classic-MBP proteins are components of the myelin sheath in central and peripheral nervous system. Golli-MBP isoforms are expressed in the nervous system, thymus, peripheral lymphoid tissues. Central tolerance to epitopes from classic MBP could be mediated by the thymic expression of golli-MBP (Goverman, 2011; Seamons et al., 2003).

1.2.3 Myelin oligodendrocyte glycoprotein (MOG)

MOG is a ~28 kDa glycoprotein and highly conserved between species. MOG is quantitatively a minor component of myelin with 0.05-0.1% of the total myelin protein and is expressed on the outermost surface of the myelin sheath containing a single immunoglobulin-like domain exposed to the extracellular environment (Johns and Bernard, 1999). MOG is primarily expressed in the CNS but MOG transcripts have been detected in mouse and human thymus (Derbinski et al., 2001; Pagany et al., 2003).

1.3 Immunology of MS

MS is considered as an autoimmune, CD4⁺ T cell-mediated disease of the CNS. In this current concept, autoaggressive myelin-specific T cells attack the myelin sheath thereby triggering

the formation of inflammatory demyelinated lesions, which lead to the manifestation of MS. A role for an autoreactive T cell response was supported by the findings that myelin-specific T cells have been isolated from MS patients although they also have been shown to exist in healthy individuals (Burns et al., 1983; Olsson et al., 1990; Pette et al., 1990; Richert et al., 1983) and naïve animals (Anderson et al., 2000; Schluesener and Wekerle, 1985). Furthermore, in the widely used EAE model, MS-like diseases can be induced by active immunization with myelin antigens inducing a CD4⁺ T cell response or by adoptive transfer of activated myelin-specific CD4⁺ T cells in naïve recipients (Gold et al., 2006). Additionally, spontaneous EAE has been observed in mice expressing a transgenic myelin-specific T cell receptor (TCR) (Goverman et al., 1993; Pollinger et al., 2009; Waldner et al., 2000). Insights into disease pathomechanisms in MS were gained mostly from animal models and primarily from studies on EAE.

1.3.1 Concept of autoimmune T cell responses

The initiation of CNS inflammation required the presence of autoreactive CNS-specific T cells in the peripheral circulation that escaped central and peripheral tolerance mechanisms. Central tolerance in thymus can be escaped by autoreactive thymocytes with low avidity to the cognate antigen presented by antigen-presenting cells (APCs) or may be circumvented due to the limited number of thymic APCs presenting the self-antigen. In the periphery self-tolerance might be maintained by regulatory T cells (Tregs) (Goverman, 2011).

Before migration into the CNS peripheral myelin-specific T cells have to be activated. According to this, myelin epitopes have to be presented by APCs in the context of MHC class II (e.g. dendritic cells) but these conditions are still not understood (Goverman, 2009). Alternative mechanisms for autoreactive T cell activation could be molecular mimicry (Fujinami and Oldstone, 1985), a mechanism in which pathogens and self-antigens share cross-reactive epitopes, or bystander activation (Deshpande et al., 2001), a mechanism in which an unrelated infection might lead to the activation of pre-existing autoraggressive T cells (McCoy et al., 2006). Among other investigations, two important EAE studies performed by Reboldi et al., 2009 and Bartholomaeus et al., 2009 shed light on the beginning of CNS inflammation (Ransohoff, 2009). Peripheral activated effector T cells migrate to and enter the still uninflamed CNS in a first wave by crossing the blood-cerebrospinal fluid (CSF) barrier in the choroid plexus in a C-C chemokine-receptor 6 (CCR6)-dependent manner and enter the subarachnoid space. Then, a second wave of T cells enter the CNS by crossing activated parenchymal blood vessels (blood-brain barrier, BBB) in a CCR6-independent

INTRODUCTION

manner (Reboldi et al., 2009). In the first wave, T cell reactivation in the subarachnoid space has been shown to occur by interaction of T cells with MHC class II APCs (Kivisakk et al., 2009), which lead to the activation of subpially and then distally microglial cells and blood vessels (Goverman, 2009). During the second wave of T cell entry, activated T cells arrested at and scanned activated blood vessels, crawled preferentially against the blood flow, crossed the blood vessel into the subarachnoid space and continued their scan. Encountering their specific antigen led to production of proinflammatory cytokines and CNS inflammation (Bartholomaeus et al., 2009). Furthermore, these events led to activation/recruitment of macrophages/microglia and tissue damage such as demyelination and neurodegeneration. Activated macrophages/microglia might be the responsible cells for axonal damage because their number correlates with disease severity and they can secrete harmful soluble factors (Gold et al., 2006).

1.3.2 Role of CD4⁺ T cell effector subsets

The differentiation of naïve CD4⁺ T cells into effector T cells with a distinct phenotype is induced by stimulation with cognate antigen presented on MHC class II molecules on professional APCs in the presence of co-stimulatory signals and a distinct cytokine milieu. Several CD4⁺ lineages such as T helper (Th) cells, subdivided in type 1 (Th1), type 2 (Th2), type 17 (Th17), regulatory T cells (Tregs) and follicular helper T cells (Tfh) have been described. Tfh cells mediate B cell help for antibody production in germinal centers. Tregs derived from positively selected thymic CD4⁺ T cells with higher affinity to self-antigens than normal and are thought to suppress autoimmunity. The first classified Th cells were Th1 and Th2 cells. Th1 differentiation required interleukin (IL)-12 and the main effector cytokine is IFN- γ whereas Th2 cells differentiate in the presence of and secrete IL-4. Later, additional subsets were identified such as the IL-17, IL-21, and IL22-secreting Th17 cells that are stimulated by transforming growth factor (TGF)- β and IL-6 (Fletcher et al., 2010; Petermann and Korn, 2011; Zhu et al., 2010).

IFN- γ -producing Th1 effector cells have been originally considered as the major pathogenic T cell in EAE and MS. The Th1 disease hypothesis was concluded from studies performed in IL-12p40 deficient mice that were resistant to EAE (Gran et al., 2002), adoptive transfer experiments in which myelin-specific Th1 cells induced EAE (Baron et al., 1993), observations that IFN- γ treatment exacerbated disease in MS (Panitch et al., 1987) and detection of IFN- γ in active MS lesions (Traugott and Lebon, 1988). However, this concept was revisited when it was shown, that mice, deficient of important factors in the Th1 pathway

INTRODUCTION

(IFN- γ deficient mice, IFN- γ receptor deficient mice and IL-12p35 deficient mice) were highly susceptible to EAE (Becher et al., 2002; Ferber et al., 1996; Gran et al., 2002; Willenborg et al., 1996). IL-12 is composed of the subunits p35 and p40. But p40 forms with the subunit p19 another cytokine IL-23 (Oppmann et al., 2000). IL-23 drives the differentiation of effector Th17 cells and it was shown, that adoptively transferred Th17 cells can induce EAE (Langrish et al., 2005). Both, IL-12 and IL-23 polarized Th1 and Th17 cells were pathogenic and induced similar EAE disease courses in mice but showed different expression patterns of CNS chemokines, composition and localization of infiltrating cells and responsiveness to immunomodulatory treatments (Kroenke et al., 2008). A relevant role for Th17 cells in MS was suggested by several observations. Th17 cells have been detected in CSF of patients with RRMS and interestingly, frequencies of Th17 cells were increased during relapses compared to patients in remission (Brucklacher-Waldert et al., 2009). Furthermore, IL-17 positive cells were detected in MS brain (Kebir et al., 2007; Tzartos et al., 2008) and *in vitro* experiments showed that Th17 lymphocytes crossed more efficiently the BBB compared to Th1 cells (Kebir et al., 2007).

1.3.3 Role of CD8⁺ T cells

A putative involvement of CD8⁺ T cells in MS arose in gene association studies in HLA class I regions, which suggested a predisposition by the HLA-A3 allele (HLA-A*0301) and protection by the HLA-A2 allele (HLA-A*0201) (Friese and Fugger, 2009). In addition, histological studies showed a predominance of CD8⁺ T cells compared to CD4⁺ T cells and a clonal expansion of these CD8⁺ T cells in the MS lesions (Babbe et al., 2000; Frischer et al., 2009). The recent described cortical GM lesions in early-stage MS patients also showed CD8⁺ T cell infiltrates (Lucchinetti et al., 2011). Furthermore, the extent of axonal damage was correlated with the number of CD8⁺ T cells in MS lesions (Bitsch et al., 2000; Kuhlmann et al., 2002) and *in vitro* experiments showed that neurites can be damaged by cytotoxic CD8⁺ T cells (Medana et al., 2001). Due to the deficiency of CD8⁺ T cell-driven EAE models, only few studies could assess the role of these effector cells (Willing and Friese, 2012) that might exert pathogenic (Huseby et al., 2001) and regulatory functions (York et al., 2010).

1.3.4 Role of antibodies and B cells

MS research primarily focused on the role of T cells, however, the involvement of B cells and antibodies also attracted investigators in the recent years. Not only the presence of oligoclonal bands in CSF of MS patients (Kabat et al., 1942), which are important paraclinical diagnostic markers (Freedman et al., 2005), but also the detection of abundant deposition of

INTRODUCTION

immunoglobulins (Ig) and components of the complement in many MS lesions (designated as pattern II) (Lucchinetti et al., 2000) and responsiveness of patients exhibiting such lesion pattern II to plasma exchange (Keegan et al., 2005) confirmed an involvement of humoral factors like antibodies in MS. The myelin surface protein MOG was characterized by the particular ability to induce a demyelinating autoantibody response in parallel to an encephalitogenic T cell response (Gold et al., 2006). MOG-induced EAE in rats shared important aspects of the pathology in MS (Adelmann et al., 1995; Johns et al., 1995) and a direct pathogenic role for a MOG-specific monoclonal antibody was shown by the augmentation of demyelination *in vivo* in rat EAE models (Lassmann et al., 1988; Linington et al., 1988; Schluesener et al., 1987). Even serum obtained from MS patients with high anti-MOG autoantibody titers enhanced demyelination and axonal damage in rats with EAE (Zhou et al., 2006). Moreover, MOG autoantibodies have been detected in WM lesions in EAE and MS and were associated with myelin damage (Genain et al., 1999; Raine et al., 1999). Additionally, an autoantibody response against the potassium channel KIR4.1 expressed on glial cells was shown in a proportion of MS patients (Srivastava et al., 2012). However, the epitope(s) recognized by specific pathogenic antibodies is still unknown (Iglesias et al., 2001). In contrast to pathogenic IgG antibodies showed IgM antibodies beneficial effects and have been shown to promote remyelination in animal models of MS (Bieber et al., 2002; Miller et al., 1994; Warrington et al., 2007).

B cells and plasma cells are involved in antibody production and secretion. In recent studies an involvement of B cells in MS was suggested as depletion of circulating B cell populations by administration of rituximab, a chimeric monoclonal antibody specific for CD20⁺ B cell (not plasma cells), decreased brain lesions and relapses in RRMS (Bar-Or et al., 2008; Hauser et al., 2008). In contrast, atacicept, a human recombinant fusion protein containing binding sites for two important cytokine regulators of B cell maturation, function and survival, that selective impair mature B cells and antibody-secreting plasma cells was shown to increase disease activity in MS (Hartung and Kieseier, 2010). B cells might contribute to disease independent of antibodies. In EAE it was shown that the time-dependant depletion of B cells influenced EAE outcome (Matsushita et al., 2008) and interleukin 6 secreting B cells might drive pathogenesis in T cell mediated autoimmune disease (Barr et al., 2012).

1.4 Pathology of MS

Inflammation, de- and remyelination, neurodegeneration and glial scar formation are pathological characteristics occurring in the brain and spinal cord of MS patients. Tissue damage can occur in a focal or global diffuse manner and is disease-stage dependent. Both, WM and GM areas can be affected, whereas the GM in the cerebral cortex is extensively involved (Kidd et al., 1999; Lassmann et al., 2007; Lassmann et al., 2012; Peterson et al., 2001).

1.4.1 Immunopathology

Primarily active lesions, which are most frequent in patients with acute disease or RRMS, are accompanied by inflammatory infiltrates composed of T cells, B cells, plasma cells and activated macrophages/microglia in which CD8⁺ T cells outnumber CD4⁺ T cells (Babbe et al., 2000; Friese and Fugger, 2009; Frischer et al., 2009; Lucchinetti et al., 2000). In early active stage demyelinated lesions in the WM, identified by myelin destruction and macrophages/activated microglia containing intracytoplasmic myelin products, four different patterns have been described. Pattern I and II lesions described early active demyelination with a T cell- and macrophage-dominated inflammation. Pattern II lesions showed additional deposition of immunoglobulins (mainly IgG) and complement C9neo. The other two patterns III and IV were thought to arise through a primary oligodendrocyte dystrophy. Lesion patterns were homogeneous within multiple early active lesions from the same patient but heterogeneous between different patients (Lucchinetti et al., 2000). Inflammation in WM lesions might be associated with damage to the BBB as shown by gadolinium-enhanced lesions in MRI (Miller et al., 1988). Slowly expanding lesions, inactive and remyelinated lesions showed less inflammation (Lassmann et al., 2012).

Cortical demyelinated lesions in early MS disease-stage have been described very recently and were identified as inflammatory and strongly associated with meningeal inflammation. Cortical lesions were composed of macrophages/microglia, CD3⁺ and CD8⁺ T cells as well as but to a lesser extent B cells (Lucchinetti et al., 2011; Popescu et al., 2011). As the patient presented by Popescu et al., in 2011 showed an inflammatory cortical lesion linked to gadolinium enhancement in MRI it was suggested that inflammation induced damage of the BBB in cortical lesions.

Chronic cortical lesions in late-stage disease were found to be less inflammatory than early cortical lesions (Bo et al., 2003a; Peterson et al., 2001) probably due to long intervals between lesion formation and autopsy. However, profound meningeal inflammation has been

identified in progressive MS (Magliozzi et al., 2007; Serafini et al., 2004) that were associated with subpial demyelination (Kutzelnigg et al., 2005). Moreover, the severity of meningeal inflammation correlated with GM demyelination and neurite loss (Choi et al., 2012; Howell et al., 2011). In immunohistological studies it was suggested that the BBB integrity is relatively preserved in intracortical GM lesions due to the lack of markers for BBB disruption or astrogliosis (van Horssen et al., 2007). Furthermore, in cortical GM lesions some complement deposition was found (Brink et al., 2005; Schwab and McGeer, 2002) probably shedding light on a possible pathomechanism mediated by humoral factors.

1.4.2 Demyelination

Plaques of focal demyelination are characteristic hallmarks of all MS disease stages and they can be classified depending on the activity into classic active lesions, slowly expanding lesions, inactive lesions or remyelinated shadow plaques by the level of inflammatory activity, axon loss or remyelination status (Lassmann et al., 2012).

WM lesions showed variable densities of oligodendrocytes at all stages of demyelinating activity between nearly complete loss and numbers exceeding densities in the periplaque WM (Lucchinetti et al., 1999).

Although the early description of cortical demyelination by Charcot in the late 18th century (Popescu and Lucchinetti, 2012) and other neuropathologists later on (Brownell and Hughes, 1962; Dinkler, 1904; Lumsden, 1970; Sander, 1898; Taylor, 1892) remained cortical lesions understudied over a long time period until improved immunohistological staining techniques led to a histopathological reinvestigation of GM pathology (Bo et al., 2003a; Bo et al., 2003b; Giaccone et al., 2012; Kidd et al., 1999; Peterson et al., 2001; Vercellino et al., 2005). Cortical demyelination was thought to occur in part independently to pathologic WM changes (Bo et al., 2007; Giaccone et al., 2012; Kutzelnigg et al., 2005) and may represent an early or initial target of MS (Calabrese and Gallo, 2009; Popescu et al., 2011).

Currently, cortical lesions are classified into four types depending on their localization (Bo, 2009; Calabrese et al., 2010a; Popescu and Lucchinetti, 2012) based on the system used in Kidd et al., 1999, simplified in Peterson et al., 2001 and modified by Bo et al., 2003b. Accordingly, leukocortical lesions extending through both WM and GM were assigned to lesion type I. Purely intracortical lesions that neither extend to the pial surface nor to the subcortical WM were defined as lesion type II. Cortical lesions of type III classified subpial lesions that often affect several adjacent gyri. Lesions extending throughout the full width of

the cortex without affecting the subcortical WM were assigned to lesion type IV. Type III and IV lesions were both classified as subpial lesions.

Very recently, extensive and well-demarcated cortical demyelinating lesions have been described in early disease-stage MS patients with the most common lesion type located leukocortical followed by subpial and intracortical lesions. Lesions were primarily classified as active and contained often foamy, myelin-laden macrophages indicative for ongoing demyelination. Additionally, in a subset of lesions a reduction of oligodendrocyte density was observed in comparison to nearby myelinated cortex (Lucchinetti et al., 2011; Popescu et al., 2011).

Although already present in RRMS and acute MS, cortical demyelination was most prominent and extensive in patients with a progressive disease stage (Kutzelnigg et al., 2005) and the most common lesion type was subpial (Albert et al., 2007; Bo et al., 2003b; Kutzelnigg et al., 2005; Peterson et al., 2001; Vercellino et al., 2005). Chronic cortical lesions also showed well-demarcated area of demyelination and oligodendrocyte/glial cell loss (Albert et al., 2007; Bo et al., 2003a; Bo et al., 2003b; Peterson et al., 2001; Wegner et al., 2006).

The degree of cortical demyelination varied regionally with the most affected brain areas in the cingulate gyrus (17-44%) followed by the temporal and frontal cortices (17-28%). Less damage occurs in the paracentral lobule (11.5%), occipital lobe (8%) and primary motor cortex (3.5%) (Bo, 2009).

1.4.3 Remyelination

Remyelination is a regenerative repair mechanism in demyelinated plaques that restores the lost myelin sheath (Franklin and Ffrench-Constant, 2008). It was shown that remyelination prevented axonal loss after demyelination (Irvine and Blakemore, 2008) and played a role in functional recovery (Liebetanz and Merkler, 2006; Manrique-Hoyos et al., 2012; Merkler et al., 2009). Histologically, variable degree of remyelination can be noted, which was most extensive in the so-called shadow plaques. Characteristic for remyelinated plaques was the reduced myelin density in comparison to the surrounding normal appearing brain matter due to a thinner myelin sheath thickness (Bruck et al., 2003). Extensive remyelination can be observed in the WM in RRMS and MS patients in progressive disease stages (Patani et al., 2007; Patrikios et al., 2006). However, remyelination is often incomplete or absent although oligodendrocyte precursor cells (OPCs) have been shown to be present in chronic lesions but it seemed that they failed to proliferate and differentiate (Wolswijk, 1998). Differentiation of OPCs to mature oligodendrocytes is a prerequisite for myelin regeneration.

Remyelinating capacity has also been observed in cortical GM lesions and was even more extensive in cortical lesions in comparison to WM lesions (Albert et al., 2007). Remyelinated plaques contained an increased number of oligodendroglia at the lesion border compared to the demyelinated center of lesions or control cortex (Albert et al., 2007). Furthermore, remyelination has also been observed in the cerebral cortex of animal models after a demyelinating event (Merkler et al., 2006b; Merkler et al., 2009; Skripuletz et al., 2008).

1.4.4 Neurodegeneration and atrophy

Axonal damage, transection and loss (Ferguson et al., 1997; Lovas et al., 2000; Trapp et al., 1998), progressive brain atrophy (Fisher et al., 2002; Rudick et al., 1999), decrease of the neuronal marker N-acetyl aspartate (NAA) (Bjartmar et al., 2000) and neuronal loss (Papadopoulos et al., 2009; Wegner et al., 2006) have been associated with MS (Trapp and Nave, 2008). Progressive axon degeneration is considered as the main cause of gradually worsening of irreversible neurologic deficits in MS (Trapp and Nave, 2008). In MS lesions, acute axonal damage is mostly prominent in early disease stages, correlated with inflammation and decreased over time (Kuhlmann et al., 2002). Diffuse axonal injury was also detected in normal appearing WM (NAWM) but more pronounced in progressive disease compared to acute or RRMS (Kutzelnigg et al., 2005). Demyelination is not a prerequisite for axon damage, which can be reversible (Nikic et al., 2011). Mechanisms leading to axon damage in acute lesions may include vulnerability of demyelinated axons to the inflammatory environment, glutamate-mediated excitotoxicity or cytotoxic CD8⁺ T cells (Trapp and Nave, 2008). In addition to neuronal pathology in the WM the neuronal compartment in the GM was also affected.

In early-stage MS, it was shown that several cortical demyelinated lesions showed neuritic swellings indicative for acute damage. However, the majority of lesions showed relative preservation of neurites. In rare cases, focal neuritic loss was observed (Lucchinetti et al., 2011).

Chronic cortical lesions showed neuronal damage as indicated by apoptosis, a mild to moderate neuronal loss, smaller neuronal sizes and transected axons and dendrites in the demyelinated cortex (Choi et al., 2012; Magliozzi et al., 2010; Peterson et al., 2001; Vercellino et al., 2005; Wegner et al., 2006). Neuronal loss was not restricted to lesions as it was also observed in normal appearing GM (NAGM) (Choi et al., 2012; Magliozzi et al., 2010). Loss and injury of thalamic and cortical neurons by measuring NAA levels has also been suggested (Cifelli et al., 2002; Kapeller et al., 2001; Wylezinska et al., 2003). In

addition, synaptic loss was detected in leukocortical lesions (Wegner et al., 2006). However, another study found no reduction in synaptic density (Vercellino et al., 2005).

GM atrophy was also shown to be a pathologic hallmark of MS. GM atrophy can occur early in the disease, increased with disease stage and was related to disease progression (De Stefano et al., 2003; Fisher et al., 2008; Rudick et al., 2009). As additional parameter thinning of cortical thickness was detected in MS patients in MRI studies (Chen et al., 2004; Sailer et al., 2003) and in a histological study (Wegner et al., 2006).

Permanent deficits in MS may occur when axonal loss exceeds a threshold that CNS mechanisms cannot compensate for (Bjartmar et al., 2003; Dutta and Trapp, 2007). Compensatory processes may include axonal remodeling leading to restoration of damaged axonal connections as it was shown in MS-like lesions in rats (Kerschensteiner et al., 2004a).

1.5 Animal models of MS

Animal models have been very useful tools to investigate putative pathomechanisms and test therapeutic approaches in inflammatory, demyelinating diseases like MS. Depending on the needs, immune-mediated, toxic, viral and genetic models have been established (Ransohoff, 2012).

1.5.1 Experimental autoimmune encephalomyelitis (EAE)

The most used animal model in MS research is EAE, which is an immune-mediated disease leading to inflammatory demyelinated lesion in the CNS. The view, that MS is a T cell-mediated autoimmune disease and most of our current knowledge concerning CNS inflammation derived from studies on EAE.

EAE was first described by Thomas Rivers in the early 1930s (Rivers et al., 1933). Rivers and colleagues repeatedly injected intramuscularly rabbit brain homogenates in rhesus monkeys and observed in two out of eight treated animals clinical signs (ataxia, weakness, paresis). Tissue sections revealed inflammation and demyelination in the CNS. From the date EAE was elicited in various species including marmoset monkeys, guinea pigs, rats and mice by either immunization with CNS tissue or myelin-derived antigens, usually emulsified in complete Freund's adjuvant (CFA) or adoptive transfer of activated autoaggressive T cells, and led to the establishment of well-characterized animal models reflecting specific features of the immunopathology in MS. CFA is a mineral oil-based solution containing components of heat-inactivated mycobacteria tuberculosis that stimulated induction of EAE (Gold et al., 2006). Nowadays, most studies were performed in C57BL/6 mice in which EAE is induced by

INTRODUCTION

subcutaneous active immunization with MOG-peptide (amino acids 35-55) emulsified in CFA and additional injection of pertussis toxin to augment disease induction. This ‘conventional’ EAE was reproducible and benefits from the diversity of transgenic and knockout mice available on a C57BL/6 background. Unfortunately this EAE displayed only a chronic monophasic disease course (without recurring disease bouts), elicit primarily a CD4⁺ T cell response and predominantly affected the spinal cord leading to the classic symptoms of ascending paralysis (Ransohoff, 2012). EAE can also be induced by immunization with MOG₁₋₁₂₅ (amino acids 1-125) in CFA in C57BL/6 leading to a similar chronic-progressive disease course. Another standard EAE mouse model eliciting a relapsing-remitting disease course was induced in SJL mice by immunization with PLP-peptide (amino acids 139-151) emulsified in CFA (Gold et al., 2006). BiozziABH mice represent another mouse strain also highly susceptible to EAE. These mice exhibited a chronic relapsing-remitting disease course upon immunization with homologous spinal cord homogenate, myelin containing full-length ‘native’ MOG or myelin antigens such as MOG₁₋₁₂₅ in adjuvant among other CNS antigens. Inflammation and demyelination are particular evident during the relapse/chronic disease phase (Amor et al., 1994; Amor et al., 2005; Baker et al., 1990; Smith et al., 2005). Additionally to active immunization schemes, EAE can be elicited by adoptively transferred activated myelin-specific T cells in different species (Ben-Nun et al., 1981; Zamvil et al., 1985).

1.5.2 Targeted EAE models

In the above mentioned ‘conventional’ rodent EAE models, inflammation primarily targets the spinal cord leading to disseminated spinal lesions in space and time. An animal EAE model showing demyelinated inflammatory lesions randomly distributed in the cerebral cortex similar to those in MS has been described in marmoset monkeys (Merkler et al., 2006a; Pomeroy et al., 2008; Pomeroy et al., 2005). Later, ‘conventionally’ MOG₁₋₁₂₅-immunized rats (LEW.1W and LEW.1AR1 rat strains) showed extensive cortical demyelination distributed in the forebrain (Storch et al., 2006). In active immunized mice (MOG₃₅₋₅₅ in mice on a C57BL/6 background, PLP₁₃₉₋₁₅₁ in SJL/J mice) cortical lesions were detected by a decreased or absent intensity of myelin staining (Girolamo et al., 2011; Mangiardi et al., 2011; Rasmussen et al., 2007). Unfortunately, lesions that occur randomly in anatomical localization are difficult to study precisely. These limitations were overcome by the introduction of localized EAE models targeting a predetermined area. The first inflammatory targeted EAE model was established in rat spinal cord. Stereotactic injection of

INTRODUCTION

proinflammatory cytokines in a predetermined spinal region led to local inflammation, focal demyelinated lesions and axonal damage in this area sharing similarities with MS lesions (Kerschensteiner et al., 2004b). In 2006, the targeted spinal cord EAE was transferred to the cerebral cortex as a model reflecting human GM pathology was still missing. Merkler and colleagues adjusted the protocol from the targeted spinal cord EAE (from Kerschensteiner et al., 2004b) and developed a focal EAE rat model for cortical demyelination reflecting key features of cortical MS lesions. They stereotactically injected a mixture of proinflammatory cytokines into the cortex and triggered local demyelinated lesions. These lesions showed cortical inflammation (T cells and activated macrophages/microglia) as early, transient and rapidly resolving phenomenon, deposition of complement C9, rapid remyelination, acute axonal damage but no apparent loss thereafter and sporadic irreversible neuronal damage (Merkler et al., 2006b). This model also shed light on an association between cortical demyelination and cortical function. By measuring the propagation velocity of a wave of depolarization of neurons and glia cells in GM (cortical spreading depression) it was shown that the velocity of this propagating wave inversely correlated with the myelin content (Merkler et al., 2009). Unfortunately, further mechanistic studies on cortical pathology were hampered by the lack of useful transgenic rat strains.

2 AIM OF THE STUDY

The increasing association between inflammatory demyelinated lesions within the cerebral cortex and clinical impairments in MS patients demonstrated the urgent need for a suitable mouse model to study cortical pathology. The present project aimed to establish and characterize a mouse model that reflects key pathological features of cortical MS lesions. In order to facilitate studies on cortical pathology a targeted model was sought, in which lesions were induced in a predetermined cortical area in a defined time window by an inflammatory stimulus. MS patients in early disease-stages showed cortical lesions with demyelination and inflammation, therefore, the modeled cortical lesions should be accompanied by infiltrates composed of T cells and activated macrophages/microglia and loss of myelin. Furthermore, the next step of the project was to elucidate neuronal pathology as measured by axonal density and neuronal numbers since some extent of neuronal injury was detected in lesions of early MS patients but is most prominent in late-stage disease. Furthermore, a method allowing detailed studies on dendritic pathology in mice should be established. In addition, dendritic pathology was assessed in the cerebral cortex of chronic MS patients.

Following specific aims were addressed in this doctoral thesis:

- 1) Establishment of a targeted EAE mouse model showing cortical demyelinated lesions triggered by an inflammatory stimulus.
- 2) Characterization of targeted cortical EAE with regard to the extent of demyelination, capacity for remyelination and inflammation (T cells, activated macrophages and microglia) and neuronal pathology (axonal and neuronal densities).
- 3) Establishment of three-dimensional (3D) reconstruction and analysis of dendritic processes in the cerebral cortex of mice.
- 4) Assessment of abnormalities in dendritic branch pattern and number of dendritic spines in cortical GM of progressive MS patients.

3 MATERIAL AND METHODS

3.1 Material

3.1.1 Reagents

Reagent	Company	Catalog number
<i>Animal experimentation</i>		
Aqua ad iniectabilia	BBraun	#353 5665
Dulbecco's Phosphate Buffered Saline (DPBS), 1x	Gibco	#14190-094
Esconarkon	StreuliPharma AG	#55815002
Freund's Adjuvant Incomplete	Sigma-Aldrich	#F5506
Isoflurane	Nicholas Piramal (I) Limited	
Ketasol-100 (Ketamine)	Graeub	#668.51
Monastral Blue (Copper(II)phthalocyanine-tetrasulfonic acid tetrasodium salt)	Sigma-Aldrich	#274011
Mouse VEGF (164aa)	MACS MiltenyiBiotec	#130-094-087
Mycobacterium Tuberculosis H37Ra	Difco	#231141
Paraformaldehyde (PFA)	AppliChem	#A3813
Pertussis toxin	Sigma	#P2980
Phenol red	Sigma-Aldrich	#32661
Prequillan (Acepromazine)	Fatro	#56 719
Recombinant Mouse TNF- α aa 80-235	R&D Systems	#410-MT/CF
Recombinant Murine IFN- γ	PeproTech GmbH	#315-05
Rompun 2% (Xylazine)	Bayer HealthCare	#35 464
Sodium azide	Sigma-Aldrich	#S2002
<i>Proteinbiochemistry</i>		
Acetic acid (glacial) 100%	Merck	#1.00063.2500
Acrylamide/Bis Solution 29:1, 40%	Bio-Rad	#161-0146
Agar, granulated	Difco	#214530
Ammonium Persulfate	Amersham	#171311-01
β -Mercapthoethanol	PlusOne	#17131701

MATERIAL AND METHODS

BSA Standard	Bio-Rad	#500-0206
Bradford Protein Assay, 1x Dye Reagent	Bio-Rad	#500-0205
Bromophenol Blue	Bio-Rad	#161-0404
Complete protease inhibitor cocktail tablets	Roche	#04693116001
Coomassie Brilliant Blue R 250	Sigma	#27816
DNAse I	Roche	#04716728001
DL-Dithiothreitol (DTT)	Sigma	#D9779
EDTA	Fluka	#03680
Glycerol for molecular biology, 99%	Sigma	#G5516
Glycine	Bio-Rad	#161-0718
Imidazole	Sigma	#56748
IPTG	Invitrogen	#15529-019
Javel water 13/14%	Reactolab	#10200-150
Kanamycin	Roth	#T832.1
LDAO	Sigma	#40236
Lysozyme	AppliChem	#A3711
Protein Standard Dual Color	Bio-Rad	#161-0374
SDS, 20% Solution	AppliChem	#A3942
Sodiumacetate	Fluka	#71185
Sodium chloride	Acros Organics	#207790050
Sodium dihydrogen phosphate monohydrate	Fluka	#71506
Sodium phosphate dibasic dihydrate	Sigma-Aldrich	#30435
Sodium phosphate dibasic heptahydrate	Sigma-Aldrich	#S9390
Talon Metal Affinity Resin	Clontech	#635503
TEMED	Sigma	#T7024
Tris (MW121g/mol)	Bio-Rad	#161-0719
Tryptone	BD Bacto	#211705
Urea	Sigma	#51456
Yeast Extract	BD Bacto	#212750

DNA isolation and genotyping PCR

Agarose	Promega	#V3125
dATP	Fermentas	#R0141
dCTP	Fermentas	#R0151

MATERIAL AND METHODS

dGTP	Fermentas	#R0161
dTTP	Fermentas	#R0171
GeneRuler 100bp DNA Ladder	ThermoScientific	#SM0321
Green GoTaq reaction buffer, 5x (M791A)	Promega	#M3175
GoTaq DNA Polymerase (M830B)	Promega	#M3175
QuickExtract DNA Extraction Solution	epicenter	#QE09050
SybrSafe DNA gel stain	Invitrogen	#S33102
Water Molecular biology grade	AppliChem	#A7398

Primer	Sequence	Company
GFP-geno Fwd	5'-AAG TTC ATC TGC ACC ACC G-3'	Microsynth
GFP-geno Rev	5'-TCC TTG AAG AAG ATG GTG CG-3'	Microsynth
GFP-intctrl Fwd	5'-CTA GGC CAC AGA ATT GAA AGA TCT-3'	Microsynth
GFP-intctrl Rev	5'-GTA GGT GGA AAT TCT AGC ATC ATC C-3'	Microsynth

ELISA

BSA (Albumin – Fraction V)	AppliChem	#A1391,0100
FBS Superior	Biochrom AG	#S0615
Sulfuric acid 95-97%, p.a.	Merck	#731
TMB	Moss, Inc.	#TMBUS-1000
Tween 20	Sigma-Aldrich	#P9416

Histology and immunohistochemistry

Acetone	Acros Organics	#176800025
Alcohol absolutus 2% MEK (Ethanol)	Brenntag	#13229-307
Ammonium hydroxide, 32%	Merck	#1.05426
Calcium carbonate	Merck	#5286707
Citric acid monohydrate	Merck	#1.00244
Chromium(III) potassium sulfate dodecahydrate	Sigma-Aldrich	#243361
DAB chromogen + substrate buffer	Dako	#K3468/K5001
Dako Real antibody diluent	Dako	#S2022
Dako Real peroxidase blocking solution	Dako	#S2023
Dako wash buffer, 10x	Dako	#S3006

MATERIAL AND METHODS

DAPI (Dilactate)	Invitrogen	#D3571
Formalin (Formaldehyde solution min 37%)	Merck	#1.04003.1000
Fluoprep	bioMérieux	#75 521
Gelatin from porcine skin	Fluka	#48722
Isopentane (2-Methylbutane)	Merck	#106056
MayersHemalaun	Merck	#1.09249.0500
Mercury chloride	Merck	#4419
Methanol	Acros Organics	#176840025
Nitric acid, 65%	Merck	#100456
Paraffin (Embedding System)	H-Plast	#95100.00
Paraffin (Tissue Processor)	Brenntag	#12270-331
Potassium chromate	Sigma-Aldrich	#216615
Potassium dichromate	Sigma-Aldrich	#60188
Silver nitrate	Roth	#9370.2
Sodium carbonate	Sigma	#S2127
Sodium dihydrogen phosphate monohydrate	Fluka	#71506
Sodium hydroxide	Fluka	#71690
Sodium phosphate dibasic heptahydrate	Sigma-Aldrich	#S9390
Sodium thiosulfate pentahydrate	Merck	#106516
Sucrose	Fluka	#84097
Tissue-Tek O.C.T. compound	Sakura	#4583
Triton X-100	Fluka	#93418
UltraClear	J.T.Baker	#3905
Ultrakitt (mounting medium)	J.T.Baker	#3921

3.1.2 Antibodies

Antigen	Isotype	Clone	Company	Catalog number
<i>Primary antibodies for immunohistochemistry</i>				
MBP	Rabbit IgG	polyclonal	Dako	#A0623
Mac-3 (CD107b)	RatIgG1	M3/84	BioLegend	#108501
NeuN	Mouse IgG1	A60	Millipore	#MAB377
CD3	Rat IgG1	CD3-12	AbD Serotec	#MCA1477

MATERIAL AND METHODS

Secondary antibodies for immunohistochemistry

Alexa Fluor 555 Goat-anti-Rabbit IgG (H+L)	Invitrogen	#A21429
Fab Fragment Goat-anti-mouse IgG (H+L)	JacksonImmunoRes.	#115-007-003
Dako EnVision HRP labeled polymer anti-rabbit	Dako	#K4003
Dako EnVision HRP labeled polymer anti-mouse	Dako	#K4001
Polyclonal Rabbit Anti-Rat Immunoglobulins/Biotinylated	Dako	#E0468
Dako Real Streptavidin Peroxidase (HRP)	Dako	#K5001

Antibody for ELISA

Anti-Mouse IgG-Peroxidase Conjugate	Sigma-Aldrich	#A8924
-------------------------------------	---------------	--------

3.1.3 Buffers and solutions

Animal experimentation

Monastral Blue, 3%

Monastral Blue	0.03g
Sterile PBS	1ml

Paraformaldehyde (PFA), 8%:

PFA	80g
10 M sodium hydroxide	~ 5 drops
10x PBS	100ml
Distilled water	fill up to 1000ml
Adjust to pH = 7.3 and filter	
Store at -20°C	

PFA, 4%:

8% PFA	500ml
1x PBS	500ml
Store at 4°C	

MATERIAL AND METHODS

Phosphate buffered saline (PBS), 10x

Sodium phosphate dibasic dihydrate	12.8g
Sodium dihydrogen phosphate monohydrate	3.86g
Sodium chloride	85g
Distilled water	fill up to 1000ml

PBS-sodium azide, 0.02%

10x PBS	10ml
Sodium azide	0.02g
Distilled water	fill up to 100ml

Proteinbiochemistry

APS, 10%

APS	0.1g
Distilled water	1ml

Coomassie destain solution

100% acetic acid (glacial)	10%
Methanol	10%
In distilled water	

Coomassie stain solution, 0.1%

Coomassie R250	1g
Methanol	400ml
Distilled water	500ml
100% acetic acid (glacial)	100ml

Dialysis buffer, 1x

Sodium acetate	4.1 g (10 mM)
Distilled water	fill up to 5l
100% acetic acid (glacial)	2.875ml
Adjust to pH = 3	

MATERIAL AND METHODS

Imidazol, 1M

Imidazol	3.404g
8 M urea	fill up to 50ml
Store at 4°C	

Imidazol, 40mM

1 M imidazol	2400µl
8 M urea	fill up to 60ml

Imidazol, 5mM

1 M imidazol	175µl
8 M urea	fill up to 35ml

IPTG, 1M

IPTG	1g
Aqua ad iniectabilia	4.2ml

Kanamycin

Kanamycin	40mg
Aqua ad iniectabilia	1ml

LB agar

Tryptone	10g
Yeast Extract	5g
Sodium chloride	10g
Agar	15g
Distilled water	fill up to 1l
Adjust to pH 7	
Treat by autoclave	
40 mg/ml Kanamycin	1ml

MATERIAL AND METHODS

LB Medium

Tryptone	10g
Yeast Extract	5g
Sodium chloride	10g
Distilled water	fill up to 1l
Adjust to pH 7.4	
Treat by autoclave	
40 mg/ml Kanamycin	1ml

Sample loading buffer, 5x

Tris, pH = 6.8	0.25M
Glycerol	50%
SDS	5%
DTT	0.5M
Bromophenol Blue	0.02%
In distilled water	

SDS running buffer, 10x

Tris	250mM
Glycine	2.5M
SDS	1%
In distilled water	

Separation buffer, 2x

Tris, pH = 8.8	0.75M
SDS	0.2%
In distilled water	

Separation gel, 15%

2x separation buffer	5ml
40% Acrylamide/Bis Solution 29:1	3.75ml
Distilled water	1.25ml
TEMED	5 μ l
10% APS	50 μ l

MATERIAL AND METHODS

Solubilisation buffer

8 M urea	10ml
β-Mercapthoethanol	14μl (20 mM)

Sonication buffer

Sodiumchloride	17.53g (300 mM)
Sodiumphosphatedibasicheptahydrate	6.7g (25 mM)
Sodiumdihydrogenphosphatemonohydrate	3.45g (25 mM)

Stacking buffer, 2x

Tris, pH = 6.8	0.25M
SDS	0.2%
In distilled water	

Stacking gel, 4%

Stacking buffer 2x	1ml
40% Acrylamide/Bis Solution 29:1	200μl
Distilled water	800μl
TEMED	5μl
10% APS	50μl

TAE buffer, 1x

Tris	0.04M
Glacial acetic acid	0.04M
EDTA	0.002M
In distilled water	

TE buffer, 1x

Tris	10mM
EDTA	1mM
In distilled water	
Adjust to pH = 7	

MATERIAL AND METHODS

Tris stock solution, 1M

Tris	121g
Distilled water	fill up to 1l
Adjust to pH = 6.8 or pH = 8.8	

Urea, 8M

Urea	480.48g
Distilled water	fill up to 1l

Wash buffer

LDAO	8.5ml
Soni buffer	fill up to 500ml

ELISA

Sulfuric acid, 2N

95-97% sulfuric acid	51.12ml
Distilled water	448.9ml

Sulfuric acid, 1N

2N sulfuric acid	100ml
Distilled water	100ml

PBS-T_{0.05%}

1x PBS	1l
Tween 20	0.5ml

PBS-T_{0.05%}/10%FBS

1x PBS	10ml
Tween 20	0.005ml
100% FBS	1ml

MATERIAL AND METHODS

Histology

Citrate buffer, 10x (0.1M), pH = 6

Citric acid monohydrate	21g
Distilled water	fill up to 1l
Adjust to pH = 6	

Citrate buffer, 1x (0.01M), pH = 6

Citrate buffer 10x	100ml
Distilled water	900ml

Developer solution (Bielschowsky's silver staining)

Formalin	20ml
Distilled water	100ml
Citric acid monohydrate	0.5g
Nitric acid	2 drops

Formalin, 10%

Formalin neutral	100ml
Distilled water	900ml

Formalin neutral

Formalin	1l
Calcium carbonate	add until saturation
Filter	

Formalin with salt

Formalin	1l
Sodium dihydrogen phosphate monohydrate	40g
Sodium phosphate dibasic heptahydrate	60g
Tap water	fill up to 10l

MATERIAL AND METHODS

Gelatin solution for coating slides (0.5%)

Gelatin	0,25g
Chromium (III) Potassium Sulfate Dodeca-H	0,05g
Distilled water	fill up to 50ml

Sorensen's phosphate buffer, 0,4M

Sodium phosphate dibasic heptahydrate	87.92g
Sodium dihydrogen phosphate monohydrate	9.94g
Distilled water	fill up to 1l
Adjust to pH = 7.4	

3.1.4 Laboratory animals

BiozziABH/RijHsd (referred to as BiozziABH) inbred mice were purchased from Harlan Laboratories (Order code: 937). EGFP-M mice (B6.Cg-Tg(Thy1-EGFP)MJrs/J on a C57BL6/J background), in which EGFP is expressed by the *thy1* sequence in less than 10% of cortical neurons (Feng et al., 2000), were obtained from The Jackson Laboratory (Stock number: 007788). Male BiozziABH mice were bred with female EGFP-M mice to obtain F1 BiozziABH x GFP-M hybrids (referred to as F1 hybrids).

3.1.5 Human brain samples

For histopathological analysis of multiple sclerosis tissue, human brain autopsies of male and female individuals with multiple sclerosis were obtained from the collection of the Department of Neuropathology at the Georg-August University, Göttingen, Germany. The use of the brain samples for scientific purposes was in accordance with the guidelines of the Ethics Committee of the Georg-August University, Göttingen, Germany.

3.1.6 Equipment

Animal experimentation

Changing station CS5 Type: 9CS53	Tecniplast S.P.A.	
Drill (K5plus Anlage)	Kavo	#4965/4911
Drilling head	Gebr. Brassler GmbH&CoKG	#H141A104 014
Ear bars (Mouse) 60° Tip	David Kopf Instruments	#922

MATERIAL AND METHODS

Ear puncher, KN-292B, 2.0	Napox	
Forceps, 12cm	F.S.T	#11002-12
Forceps, 2AM-SA	rubis, Switzerland	
Forceps	Aesculap	#BD043R
Homogenizer pistil for 1,5ml tubes	neoLab	#6-1060
Iris Scissors STR S/S 120MM	Aesculap	#BC064R
Isoflurane system for anesthesia	tem sega	
Laminar flow Hera Safe Type: HS18	Heraeus	#50054579
Micro knife	F.S.T	#10055-12
Micro scissors, curved, 15,5cm, 6"	KLS martin group	#11-773-01
Mouse Adaptor	Stoelting	#51624
Needle holder, durogrip TC, 145mm	Aesculap	#BM015R
Peristaltic pump Type: MC-MS/CA-4/8	Ismatec	
Scale PL602-S	Mettler Toledo	
Scissors	F.S.T	#14060-11
Scissors	Hermle	#521
Scissors	F.S.T	#14013-17
Scissors	Hermle	#501
Scissors	Hermle	#511
Shaver	Tondeo	#100766
Stereo microscope M60	Leica	
Stereotaxic device	Stoelting	#51600
Tissue Forceps Slim – 1x2 Teeth	F.S.T	#11023-10
TUB PTFE 2XHUBadaptor <small>Ga24x20mm length</small>	Chromatographie Service GmbH	#06586510
Warming plate	MedaxHaska AG	

Proteinbiochemistry

3-D Shaker GyroTwister	Labnet	
Centrifuge Tubes, 50ml	KendroSorvall	#03146
Circular mixer RM 5	Assistent	#348
Electrophoresis Power Supply E802	Consort	
Homogenizer motor Type HS-30E Set	witeg	#DH.WOS01011
Homogenizer + PTFE pistil, 40ml, cylindric	schuett-biotec GmbH	#3.213 402

MATERIAL AND METHODS

Lab-Shaker RS-306 Type AG20	Infors AG HT	
Lab-Shaker Type LSR-V	Adolf Kühner AG	
Magnetic Stirrer RH basic 2	IKA	#3339000
Mini-Protean 3 Cell Electrophoresis System	Bio-Rad	
Nalgene Centrifuge Bottles, 250ml	Thermo Scientific	#3141-0250
NanoDrop 2000c	Thermo Scientific	#ND-2000C
Sonic Ruptor 400 Ultrasonic Homogenizer	Omni International	#18-000-115
Superspeed centrifuge Sorvall RC-5B	Sorvall	#RC-5B
Superspeed centrifuge Sorvall RC-5B Plus	Sorvall	#RC-5B Plus
Vaccum pump N86KN.18	KNF Lab Neuberger	
VMax Kinetic Microplate reader	Molecular Devices	

Histology and immunohistochemistry

CryostatCryoStar NX70	ThermoScientific	#957070
Microscope, confocal LSM510Meta	Zeiss	
Microscope, light, CX41	Olympus	
Microscope, fluorescence, Axioskop 2	Zeiss	
Microtome, rotary HM 340 E	Thermo Scientific	#904090A
Mirax Midi slide scanner	Zeiss	
Pascal pressure chamber, model S2800	Dako	
Tissue Embedding System TES 99	Medite	#TES99
Tissue Processor Tissue-Tek VIP	Sakura	
Vibratome series 1000, Sectioning system	TPI	#050418

Others

Centrifuge, benchtop, 5415R	Eppendorf	
Centrifuge, benchtop, Model 4-16K	Sigma	#10475
Freezer -20°C	Liebherr ProfiLine	
Fridge	LiebherrProfiLine	
Laminar flow MSC-Advantage 1.8	Thermo Scientific	#51026370
Laminar flow BH 2006-D 195	Faster	
PCR 96 well Fast Thermal Cycler, Veriti	Applied Biosystems	
Pipettes	Gilson	
Electrophoresis system, Sub-Cell GT	BioRad	#170-4401

MATERIAL AND METHODS

Electrophoresis system power supply	BioRad
ThermoMixer, MKR 13	HLC BioTech
Ultra-low Temp. Freezer Forma 900 Series	Thermo Scientific
UV gel documentation	witec ag

3.1.7 Consumables

Animal experimentation

Animal Lancet 5mm	Goldenrod	
BD Microtainer SST Tubes	BD	# 365951
Butterfly	BD Valu-Set	#387425
Capillaries	HirschmannLaborgeräte	#903 02 08
Glass capillaries	BlaubrandintraMark	#7087 07
Insulin syringe 0,3ml	BD Micro-Fine	#320837
Insulin syringe 0,5ml	BD Micro-Fine	#320812
Insulin syringe 1ml	BD Micro-Fine	#324811
LuerLock syringes 3ml	BBraunOmnifix	#4617022V
LuerLock syringes 5ml	BBraunOmnifix	#4617053V
Needles 26G x $\frac{3}{8}$ (0,45mm x 10mm)	BD Microlance	3 #300300
Needles 18G x $1\frac{1}{2}$ (1,2mm x 40mm)	BD Microlance 3	#304622
Scalpels, surgical disposable	B. Braun	#5518075
Sugi	Kettenbach	#31602
Suture material	Ethicon	#6683H
Syringe filter 0,22 μ m	TPP	#99722

Proteinbiochemistry

Cuvettes	Sarstedt	#67.742
Dialysis Cassette, Slide-A-Lyzer 3,5	Pierce	#66 110
F96Maxisorp immunoplate	Nunc	#442404
Poly-Prep Chromatography Columns, 5ml	BioRad	#731-1550
PP Centrifuge and Test Tubes, 14ml	BD	#352059

MATERIAL AND METHODS

Histology and immunohistochemistry

24 well cell culture plate, cellstar	Greiner bio-one	#662 160
Embedding cassette, Uni-Cassette Biopsy green	Sakura	#4174
Microscope cover glasses, 22x22mm	VWR	#631-1570
Microscope cover glasses, 24x50mm	VWR	#631-1574
Microscope slides, Superfrost Plus	Menzel GmbH	#J1800AMNZ
Microtome blade	Feather	#S35
Razor blade, stainless steel, uncoated	GEM	#62-0167
Superglue, Cyanolit universal classic	3M	#241-D
Tubes for cryo asservation	Semadeni	#1661

Others

Combitips Plus 1.0ml	Eppendorf	#0030 069.234
Combitips Plus 5.0ml	Eppendorf	#0030 069.250
Eppendorf tubes, safe lock, 1.5ml	Eppendorf	#0030 120.086
Eppendorf tubes, safe lock, 2.0ml	Eppendorf	#0030 120.094
Falcon tubes, 15ml	Nunc	#366052
Falcon tubes, 50ml	BD	#352070
Micro Amp Fast reaction tubes	Applied Biosystems	#4358293
Protein LoBind Tubes 0.5ml	Eppendorf	#022431064

3.1.8 Software

Fiji open source image processing software	http://fiji.sc/ ; Schindelin <i>et al.</i> , 2012
GraphPadPrism 5.01	GraphPad Software, Inc.
Huygens Essential	Scientific Volume Imaging
LSM Image Browser Version 4.2.0.121	Zeiss
LSM 510 Version 4.0 SP2	Zeiss
NeuronStudio (Beta) Version 0.9.92	CNIC: http://research.mssm.edu/cnic/tools-ns.html
Pannoramic Viewer 1.15 RTM	3D Histech Ltd
Tissue Studio Version 2.0.4	Definiens Developer XD 64

MATERIAL AND METHODS

3.2 Methods

3.2.1 Genotyping of EGFP-M positive animals

Expression of *EGFP* in cortical neurons was determined by PCR. DNA was extracted from ear stamps with QuickExtract DNA Extraction Solution. The biopsy was roughly mixed in 50 μ l QuickExtract DNA Extraction Solution and incubated shaking for 15 min at 65°C followed by an incubation step at 98°C for 2 min. 1.5 μ l extracted DNA from the supernatant was used as template for genotyping PCR (see Table 1 Genotyping PCR for EGFP expression and Table 2 PCR program for EGFP genotyping).

The Primers GFP-geno Fwd and GFP-geno Rev (see all primer sequences in materials) were used for expression of the target sequence that results in a 173 bp PCR product. The Primers GFP-intctrl Fwd and GFP-intctrl Rev served as internal positive PCR control and result in a 324 bp amplicon. EGFP positive animals showed a strong DNA band at 173 bp and a weak control amplicon at 324 bp, whereas EGFP negative animals showed only a strong DNA band at 324 bp.

PCR products were separated by electrophoresis on a 2% agarose gel stained with SybrSafe DNA gel stain (1:10000). PCR products were visualized using ultraviolet light.

Table 1 Genotyping PCR for EGFP expression

Reagents	Volume (12.5 μ l)
Green GoTaq reaction buffer ,5 x	2.5 μ l
dNTPs (10 mM, each 2.5 mM)	0.5 μ l
Primers (10 μ M)	each 0.5 μ l
GoTaq DNA Polymerase	0.1 μ l
Water Molecular biology grade	5.9 μ l
DNA	1.5 μ l

Table 2 PCR program for EGFP genotyping

Temperature (°C)	Time (sec)	Replication
94	180	1x
94	30	35x
60	60	
72	60	
72	600	1x
4	indefinite	

3.2.2 Expression and purification of recombinant rat MOG₁₋₁₂₅

The N-terminal sequence of recombinant rat MOG₁₋₁₂₅ (amino acids 1-125) was produced as previously described (Adelmann et al., 1995). His-tagged MOG₁₋₁₂₅ was expressed in *Escherichia coli* (*E.coli*) strain BL21 and purified using Ni-NTA columns. A small amount of the bacterial glycerol stock was streaked onto a LB agar plate containing 40 µg/ml Kanamycin and grown at 37°C overnight. A preparatory culture of 6 ml LB Medium (40 µg/ml Kanamycin) was inoculated with a single colony of MOG₁₋₁₂₅ expressing *E.coli* and incubated for 12 h at 37°C. A large-scale expression was performed in 2 l LB-Media (40 µg/ml Kanamycin) inoculated with 4 ml of the preparatory culture. Bacteria were incubated at 37°C until they reached an OD₆₀₀ of 1. Then protein over expression was induced by addition of 1 mM IPTG and cultures were incubated for further 4 h at 37°C. Bacteria were harvested at 6000 rpm for 15 min at 4°C and dry pellets were stored at -20°C overnight.

All purification steps (including centrifugations) were performed at 4°C. After resuspension of each bacteria pellet in 10 ml sonication buffer containing lysozyme, DNase I and protease inhibitor cocktail tablet (e.g. 70 ml sonication buffer + knife point lysozyme + 70 µl DNase I + 1 Complete protease inhibitor cocktail tablet), cells were lysed by pulsed sonication. Sonication (1 puls/second) was performed six times for 1 min at intensity between 40-45%. Lysed bacteria suspensions were centrifuged at 11000 rpm and pellets were resolved in wash buffer. Further preparation and extraction of insoluble MOG₁₋₁₂₅ present in inclusion bodies was performed using a homogenizer with a motorized pistil at 500 revolutions per minute. Suspensions were homogenized three times in wash buffer and one time in sonication buffer. After every homogenizing step suspensions were centrifuged at 14000 rpm. After the last step pellets were stored at -20°C.

Each MOG₁₋₁₂₅ pellet was resolved in 11 ml solubilisation buffer on a circular mixer for several hours and purified as follows. Nickel-NTA-columns contained 5 ml Talon Metal Affinity Resin that was equilibrated successively in 2 M, 4 M, 6 M urea solutions prepared in sonication buffer and finally in 8 M urea. In each equilibration step the resin was resolved in urea solution, mixed on a circular mixer for 20 min and centrifuged at 1000 rpm for 4 min. Supernatants were discarded. The resuspended MOG₁₋₁₂₅ was loaded on the equilibrated resin and incubated for 2 h on a circular mixer. After loading, the resin was washed three times with 8 M urea for 20 min on a circular mixer and filled into the Poly-Prep Chromatography Columns. MOG₁₋₁₂₅-loaded resin was washed further two times with 8 M urea and 5 ml 5 mM imidazole. MOG was eluted by addition of 40 mM imidazole. 1 ml fractions were collected

MATERIAL AND METHODS

and MOG₁₋₁₂₅ containing fractions were pooled (measured by a colour change using Bradford Protein Assay 1x Dye Reagent).

Purified MOG₁₋₁₂₅ was dialysed two times against 10 mM acetate buffer for 24 h. MOG₁₋₁₂₅ concentration was determined by a Bradford assay using Bradford Protein Assay 1x Dye Reagent and BSA standard protein dilutions. Protein degradation was analyzed by SDS-PAGE and Coomassie staining. Finally MOG₁₋₁₂₅ was diluted in water to a final concentration of 3 µg/µl and stored in aliquots at -80°C.

3.2.3 SDS-PAGE

SDS-PAGE was performed using a 4% stacking gel and 15% separation gel. A maximum of 24 µg MOG₁₋₁₂₅ were dissolved in TE buffer containing 1x sample loading buffer. MOG samples were heated at 95°C for 5 min and loaded into the stacking gel. A protein standard was used as molecular weight marker. The gel was initially run at 150 V in SDS running buffer until the lanes were parallel. Subsequently voltage was increased to 200 V for the separation.

After electrophoresis gel was stained by 0.1% Coomassie stain solution for 5 min and washed several times with Coomassie destain solution until the lanes were visible.

3.2.4 Animal experiments

Animal experiments were performed in the Department of Neuropathology, University of Göttingen and the animal facility of the University Medical Center Göttingen in accordance with the guidelines and approved by the corresponding authorities in Niedersachsen (Germany) and in the Department of Pathology and Immunology, University of Geneva and in the animal facility of the University Medical Center Geneva in accordance with the guidelines and approved by the corresponding authorities in Geneva (Switzerland).

Animals were kept in a 12:12 h light/dark cycle with food and water *ad libitum*.

3.2.5 Blood sampling

Animals were anaesthetized by inhalation of isoflurane and blood samples were taken by puncturing the submandibular vein on the day of immunization and the second and the fifth week after immunization. Animals were fixed tight at the head and a lancet was pricked into

MATERIAL AND METHODS

the vein. Blood (~5 drops) was collected in a BD Microtainer tube. After 30 min of coagulating tubes were centrifuged at 15000 g for 1.5 min and stored at -20°C.

3.2.6 Induction of EAE

EAE was induced in eight to ten week old male and female BiozziABH mice and F1 hybrids of BiozziABH and EGFP-M mice. Animals were anesthetized by inhalation of isoflurane and immunized subcutaneously in all four flanks with 50 µg recombinant rat MOG₁₋₁₂₅ emulsified in incomplete Freund's adjuvant (IFA) supplemented with 10 mg/ml *Mycobacterium Tuberculosis* H37Ra in a total volume of 200 µl. Immunization was repeated one week later. Additionally 200 ng Pertussis toxin was administered intraperitoneally on both days of immunization and also the following day. Control animals were treated in an analogous manner but emulsions did not contain MOG. Clinical signs and weight were monitored daily from the tenth day.

Clinical presentation was classified by an EAE scoring system ranging from score 0 to 5 (0: no overt clinical signs; 0.5: paresis of the tip of the tail; 1: complete tail paralysis; 1.5: difficulties to straighten up from a dorsal position; 2: hind limb paresis; 2.5: partial hind limb paralysis; 3: complete hind limb paralysis; 3.5: partial fore limb paralysis; 4: complete fore limb paralysis; 5: moribund).

3.2.7 Intracerebral stereotactic injection

Cortical lesions were induced by injection of 0.5 µg recombinant mouse TNF- α and 1500 U recombinant murine IFN- γ into the cortex three or five weeks after EAE induction as indicated in figure legends. For the surgical procedure animals were anesthetized using ketamine and xylazine containing acepromazine.

BiozziABH mice with a clinical score or those who have been developed a clinical score were anesthetized by intraperitoneal (i.p.) injection of 67.5 mg/kg body weight ketamine followed by an injection of a mixture consisting of 8.8 mg/kg body weight xylazine and 1.35 mg/kg body weight acepromazine. BiozziABH mice without any clinical sign were anesthetized by i.p. injection of 75 mg/kg body weight ketamine followed by an injection of a mixture consisting of 9.75 mg/kg body weight xylazine and 1.5 mg/kg body weight acepromazine.

F1 hybrids were anesthetized by i.p. injection of 90 mg/kg body weight ketamine followed by an injection of a mixture consisting of 11.7 mg/kg body weight xylazine and 1.8 mg/kg body

MATERIAL AND METHODS

weight acepromazine. Anesthesia was administered in sterile PBS to maintain normal hydration during the surgical procedure.

After loss of consciousness, mice were mounted on a stereotaxic device equipped with a mouse adaptor and mouse ear bars to hold the head fixed. The scalp was opened and a fine hole was drilled into the skull 0.6 mm caudal to the bregma and 2.2 mm lateral to the sagittal suture (Figure 1A). To avoid damage of the brain, the last part of the skull was removed carefully with a surgical micro knife giving access to the surface of the brain. A fine drawn glass capillary (outer diameter $\sim 25\ \mu\text{m}$) was inserted 1.2 mm in an angle of 60° into the cortex (Figure 1B). These coordinates allow a targeted cytokine injection 0.6 mm caudal to the bregma, 1.2 mm lateral to the sagittal suture in a depth of 0.8 mm in the cortex. The addition of a blue marker dye (Monastral Blue) to the cytokine mixture allowed tracing of the lesion site. The cytokine mixture of $0.5\ \mu\text{g}$ TNF- α and 1500 U IFN- γ was dissolved in sterile PBS and a total volume of $2\ \mu\text{l}$ cytokine mixture was injected over a time period of 5 min. After the surgical procedure the skull was sealed by suturing the scalp and animals were kept warm until they woke up. In order to exclude tissue damage due to the penetration of the glass capillary, sterile PBS containing the blue marker dye was injected in MOG-immunized animals.

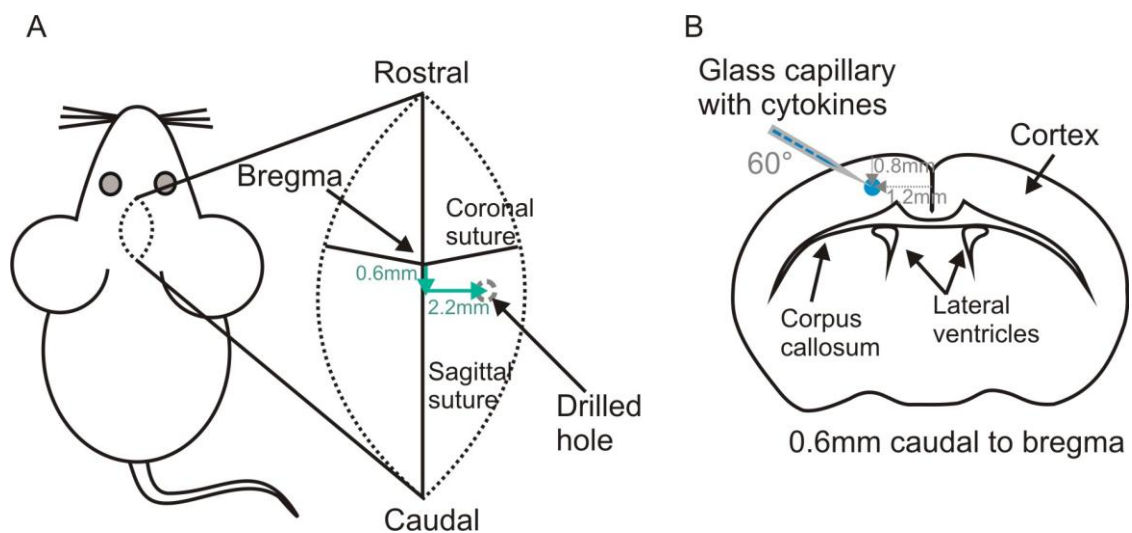


Figure 1 Strategy of targeted cortical EAE

Defined coordinates for intracerebral stereotactic injection are shown. (A) Schematic representation of the anatomical features after opening the scalp. The bregma is used as reference point for setting the stereotactic coordinates. A hole was drilled 0.6 mm caudal to the bregma and 2.2 mm lateral to the sagittal suture. (B) The glass capillary was inserted 1.2 mm in an angle of 60° into the cortex. These coordinates allowed the injection of the cytokines 1.2 mm lateral to the sagittal suture in a depth of 0.8 mm. The cytokine mixture contained a blue marker dye allowing tracing of the lesion site.

3.2.8 Enzyme-linked immunosorbent assay (ELISA)

Anti-MOG autoantibody titers were measured in naïve mice and two and five weeks after EAE induction. Each well of a 96-well Nunc plate was coated with 0.4 µg recombinant rat MOG₁₋₁₂₅ in 1x PBS overnight at 4°C. Wells were blocked with 5% BSA in 1x PBS for 1 h at room temperature and washed three times with 1x PBS. Sera were prediluted 100-fold in PBS-T_{0.05%}/10% FBS. Beginning with the 100-fold sera dilution antibody titers were titrated in 3-fold dilutions in 11 steps in PBS-T_{0.05%}/10% FBS and incubated for 2 h at room temperature in the well plate. Autoantibodies were detected by a goat-anti-mouse IgG-peroxidase conjugate (1:10000) for 1 h at room temperature and developed with 50 µl TMB-US per well for 5 min. The reaction was stopped by addition of 50 µl 1 N sulfuric acid and the optical density was measured at 450 nm. After both antibody incubation steps plates were washed at least four times with PBS-T_{0.05%}. Threshold for seropositivity was defined as an absorption value higher than a control animal achieved in a 300-fold dilution.

3.2.9 Histology of mouse brain tissue

3.2.9.1 Tissue processing

3.2.9.1.1 Perfusion and sectioning

Tissue was analyzed histologically three days and three weeks after intracortical cytokine injection. For this purpose, animals were anaesthetized intraperitoneally with a lethal dose of Esconarkon. After loss of consciousness mice were perfused transcardially with 15 ml ice-cold 1x PBS followed by 50 ml 4% ice-cold paraformaldehyde over 10 min (perfusion velocity ~6.5 ml/min) using a peristaltic pump. Brains were carefully dissected from the skull and postfixed in 4% paraformaldehyde for 24 h at 4°C. Brain tissue was then transferred into 1x PBS. Coronal slices of ~3 mm containing the injection site (Figure 2) were cut out and either embedded in paraffin using an automated tissue processor (gradually dehydration to paraffin) or cryoprotected in Tissue-Tek and stored at -20°C or -80°C. Tissue obtained from BiozziABH or EGFP-negative F1 hybrids was embedded in paraffin whereas tissue from EGFP-positive F1 hybrids was cryoprotected. Paraffin-embedded tissue was trimmed until the injection site (recognized by the blue marker dye within the tissue) and then 1-2 µm thin coronal sections containing the lesion were mounted on microscope slides. Sectioning was performed using a rotary microtome. Tissue slices obtained from EGFP-positive F1 hybrids

MATERIAL AND METHODS

were incubated in 30% sucrose for 3 days at 4°C, embedded in Tissue-Tek and stored at -20°C. Cryosections of 30 µm thickness were cut directly before staining using a cryostat.

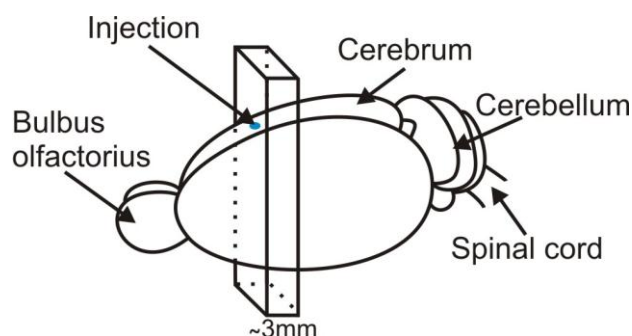


Figure 2 Coronal sectioning of the injection site

A coronal slice including the injection site of about 3 mm thickness was carefully cut out from the fixed brain as shown in the scheme. The exact injection site was visible on the surface of the brain due to the blue marker dye. The coronal slice was either embedded in paraffin or cryoprotected for further trimming to the lesion and obtaining slices for histological analyses.

3.2.9.1.2 Deparaffinization and rehydration

Paraffin-embedded tissue sections were incubated in a dry oven at 55-60°C overnight. Deparaffinization was performed successive in four bath of Ultraclear for 10 min respectively and rehydrated by incubating the slides twice in 100% ethanol, one time in 90% ethanol, one time in 70% ethanol and one time in 50% ethanol in water for 5 min respectively and finally washed in distilled water.

For dehydration tissue sections were incubated in the same bath in a reversed order for 5 min respectively, mounted in Ultrakitt and coverslipped.

3.2.9.2 Histochemistry

3.2.9.2.1 Bielschowsky's silver staining

Axon density was determined by Bielschowsky silver staining. Deparaffinized tissue sections were washed with distilled water and afterwards incubated in 20% silver nitrate solution for 20 min. Following washing in distilled water, sections were incubated in 20% silver nitrate solution containing 5% ammonium hydroxide for 15 min protected from light. Sections were transferred in 0.6% ammonium hydroxide and swayed. 1/35 volume of the developer solution was added to the 20% silver nitrate solution containing 5% ammonium hydroxide while stirring. Subsequently the sections were transferred into the solution and developed until the

MATERIAL AND METHODS

colour of the sections turned brown. Following washing in distilled water, sections were incubated in 2% sodium thiosulfate solution for 2 min. Finally sections were washed with tap water, dehydrated (as described above), mounted in Ultrakitt and coverslipped.

3.2.9.3 Immunohistochemistry

3.2.9.3.1 Antigen retrieval for CD3, Mac-3, NeuN in paraffin-embedded sections

Immunostainings for some antigens required an antigen retrieval step in order to unmask antigenic sites that were masked during fixation

Rehydrated tissue sections were treated for 30 sec at 125°C under pressure (20-22 psi) in 1x citrate buffer (pH = 6) in a Pascal pressure chamber. Antigen retrieved sections were allowed to cool down, washed in distilled water and subsequently stained.

3.2.9.3.2 Immunohistochemistry for MBP and NeuN in paraffin-embedded sections

Antigens in paraffin-embedded sections that were recognized by a primary mouse or rabbit antibody were stained using the Dako EnVision System. All staining steps were performed at room temperature in a humid chamber. Sections were washed in 1x Dako wash buffer for 2 min and blocked with Dako Real peroxidase blocking solution for 5 min. After two washing steps in 1x Dako wash buffer for 5 min, sections were treated with the primary antibody diluted in Dako Real antibody diluent for 1 h. Primary antibody dilutions are as follows: 1:1000 for MBP and 1:50 for NeuN.

After washing with 1x Dako wash buffer for 2 min, Dako EnVision HRP labeled polymer anti-rabbit or anti-mouse IgG secondary antibody was added for 30 min. After that, sections were washed twice with 1x Dako wash buffer for 5 min and developed with DAB-containing developer solution (20 µl DAB chromogen + 1 ml DAB substrate buffer). Tissue sections were washed with tap water followed by counterstaining with Mayer's Hämalaun. Finally, sections were dehydrated (as described above), mounted in Ultrakitt and coverslipped. NeuN-staining required additionally a Fab blocking and FBS blocking step before primary antibody treatment. Fab blocking was performed by incubating the sections with Fab Fragment Goat-anti-mouse IgG diluted 1:50 in Dako Real antibody diluent after peroxidase blocking for 1 h. Subsequently sections were blocked with 10% FBS diluted in Dako Real antibody diluents for 20 min and stained with the primary antibody thereafter. NeuN sections were not counterstained.

3.2.9.3.3 Immunohistochemistry for Mac-3 and CD3 in paraffin embedded sections

Antigens in paraffin-embedded sections that were recognized by a primary rat antibody were stained using a Biotin-Streptavidin System from Dako. All staining steps were performed at room temperature in a humid chamber. Peroxidase blocking and incubation with primary antibodies was performed as described above. Primary antibody dilutions are as follows: 1:100 for CD3 and 1:200 for Mac-3.

After washing with 1x Dako wash buffer for 2 min, tissue sections were incubated with a biotinylated Rabbit Anti-Rat antibody diluted 1:250 in Dako Real antibody diluent for 15 min. After two washing steps with 1x Dako wash buffer for 5 min, Dako Real Streptavidin Peroxidase (HRP) was added for 15 min. Subsequently the sections were washed twice with 1x Dako wash buffer for 5 min and developed with DAB-containing developer solution as described above. Tissue sections were washed with tap water followed by counterstaining with Mayer's Hämalaun. Finally, sections were dehydrated (as described above), mounted in Ultrakitt and coverslipped.

3.2.9.3.4 Immunohistochemistry for MBP in EGFP positive cryosections

Cryosections (40 µm) were cut and directly transferred in a 24 well cell culture plate containing 1x PBS. Sections were stained free-floating (protected from light) at room temperature on a shaker if not indicated otherwise. Sections were washed three times with 1x PBS for 10 min, treated for 15 min with cooled methanol at -20°C and washed three times with 1x PBS for 15 min. Sections were blocked in 1x PBS containing 10% FBS and 0,5% Triton X-100 for 1 h and treated with the primary antibody diluted in 1x PBS containing 1% FBS and 0.5% Triton X-100 overnight. Primary antibody dilution was 1:200 for MBP. After washing three times in 1x PBS for 10 min, sections were treated with the secondary fluorescence labeled (Alexa Fluor 555) goat-anti-rabbit IgG (H+L) antibody diluted 1:200 in 1x PBS containing 1% FBS and 0.5% Triton X-100 for 3 h. Sections were washed three times with 1x PBS for 30 min. DAPI was stained 1:10000 in 1x PBS for 15 min and sections were washed three times with 1x PBS for 10 min. Sections were stretched in distilled water containing 0.1% gelatin and 10% ethanol and put on slides, mounted in Fluoprep and coverslipped.

3.2.10 Histology of human brain tissue

3.2.10.1 Human tissue collection

Tissue samples were collected from four autopsy cases with multiple sclerosis and three control autopsy cases without neurologic disease. Brains were stored immediately after death in 4% formalin with salt for one to two month. Brain tissue containing the cortex was dissected at one topographic area, namely frontotemporal lobe, of both hemispheres. Tissue blocks were split into two parts and one part was embedded in paraffin and stained for MBP to assess cortical demyelination (MBP staining was performed according to the MBP staining protocol for mice with the exception, that human sections required the above mentioned antigen retrieval in 1x citrate buffer using a Pascal pressure chamber). The second part of the block was processed for Golgi-Cox impregnation to study cortical dendritic pathology.

3.2.10.2 Golgi-Cox impregnation

In order to assess dendritic pathology in human brain tissue a Golgi-Cox impregnation was performed. Formalin-fixed tissue blocks were washed three times with 0.4 M Soerensen phosphate buffer (pH = 7,4) at room temperature for washing out the fixative. Subsequently the blocks were incubated afloat in a solution consisting of 5% potassium dichromate, 5% mercury chloride and 5% potassium chromate for three weeks protected from light at room temperature. After postfixation in 10% formalin for 1 h at 37°C, tissue blocks were cut in 70 µm sections using a vibratome. Tissue slices were treated with 5% sodium carbonate for 2 min at room temperature, washed with distilled water and mounted on gelatin-coated slides. Sections were mounted in Ultrakitt and coverslipped for further analyses.

3.2.11 Image acquisition, processing and analyses of histological tissue sections

Brightfield histological slides were scanned in an automated mode with a Mirax Midi slide scanner equipped with a Plan-Apochromat 20x/0.8 objective and detected with a Marlin F-146C IRF Medical camera. Images were either analyzed manually using Pannoramic Viewer 1.15 or automatically in Tissue Studio Version 2.0.4.

Cortical de- and remyelination was analyzed in scanned MBP-stained paraffin sections on the ipsilateral (injected) hemisphere using Pannoramic Viewer 1.15 by measuring the area of demyelination and the length of subpial demyelination.

MATERIAL AND METHODS

Axonal density was analyzed on the ipsilateral hemisphere in Bielschowsky's silver-stained tissue sections. Myelin density was determined in adjacent MBP-stained sections. Axon and myelin density was measured in cortical layer I and II (depth of 150 μ m from the pial surface into the cortex) with a counting grid under a light microscope at 40x magnification. Intersections of axons and myelin with the counting grid were counted in four visual fields alongside the pial surface. One visual field encompassed an area of 200 μ m x 150 μ m.

Inflammatory T cell infiltrates were determined in scanned CD3-stained paraffin sections, total activated, round/oval-shaped and foamy macrophages/microglia were assessed respectively in scanned Mac-3-stained sections on the ipsilateral hemisphere using Panoramic Viewer 1.15. The number of cells was counted in different cortical layers, namely cortical layers I+II, layer III+IV and V of at least 0.15mm² respectively or in the combined cortical layers I-V of at least 0.45mm².

Cortical thickness was measured paramedially in scanned NeuN-stained paraffin sections on both hemispheres using Panoramic Viewer 1.15.

Neuronal density was analyzed in scanned paraffin sections stained for neuronal nuclei (NeuN) on the ipsilateral and contralateral hemisphere in cortical layers II, III+IV and V as well as in combined cortical layers II-V using Tissue Studio Version 2.0.4 in comparable area sizes as described above for inflammatory infiltrates. Tissue Studio counted NeuN⁺ neurons automatically by detection of DAB-stained, brown nuclei and perikarya in marked regions of interest.

Dendrites and dendritic spines in mice were visualized in MBP-stained cryosections of EGFP positive F1 hybrids. Segments of the main dendritic branch extending upright to the surface of the brain of neurons in cortical layer V-VI were imaged in distinct distances from the soma. Images of 44 μ m x 44 μ m were acquired using a confocal laser scanning microscope (LSM510Meta) equipped with an upright Zeiss Axio Imager Z1 microscope. Images were captured with a Plan Apochromat 63x 1.4 Oil DIC objective using an Argon/2 laser (488 nm) in a coupled detector. EGFP-expressing neurons were detected by emitted fluorescence. To achieve ideal sampling for image processing (deconvolution) confocal stacks were scanned in z-direction in an interval of 200 nm to obtain an overlap of 75%. Each frame was scanned four times and averaged. Voxel sizes of 75 nm x 75 nm x 200 nm were obtained using a 3x zoom. Images were deconvolved using Huygens Essential to improve resolution laterally and

MATERIAL AND METHODS

axially. Dendrites and dendritic spines were analyzed using NeuronStudio (Beta) Version 0.9.92. Dendritic shaft radii, general spine densities, spine densities of specific spine shapes and spine head volumes were computed. Spines were classified according to their morphologic characteristics into mushroom, stubby or thin by using the default values in NeuronStudio (Beta) Version 0.9.92 (CNIC). In detail, spines that have a head to neck diameter ratio greater than 1.1 were classified as thin or mushroom. Spines that meet that criteria and have a head diameter greater than or equal to 0.35 μm were classified as mushroom, otherwise as thin. Spines that have a head to neck diameter ratio smaller than or equal to 1.1 and a spine length to head diameter ratio greater than 2.5 were classified as thin, otherwise as stubby. Changing radii were measured by the sum of slopes between radii from two adjacent nodes divided by the dendritic length meaning the more irregularly the dendrite the more variable is the radius and the higher the sum of slopes for an imaged dendritic segment.

Dendritic pathology in MS cases was investigated in Golgi-Cox-impregnated sections. Dendrites were classified to be located within the lesion, at the lesion border or in the NAGM according to the MBP staining on adjacent sections and localization of the neuronal soma. Dendrites of cortical layer IV-VI neurons were imaged. In detail, basal segments of the main dendritic branch extending upright to the surface of the brain were studied in 50 μm successive distances from the soma. Image acquisition was performed as described above. Golgi-Cox-impregnated structures were detected by the reflected laser light. For this purpose, the microscope was set up only with a 80/20 beam splitter. Image sampling and processing (deconvolution) was performed as described above. Dendritic spines and branches per dendritic length were counted and dendritic width was measured using Fiji software.

3.2.12 Statistical analyses

Data illustration and statistical analysis was performed using Prism 5.01 (GraphPad).

4 RESULTS

4.1 Development of a targeted EAE model of cortical demyelination

EAE was induced in BiozziABH mice and F1 hybrids generated from BiozziABH and EGFP-M mice. Animals were immunized twice against recombinant MOG₁₋₁₂₅ in CFA. Controls were treated with CFA alone. Cortical demyelination was elicited five and three weeks after the first immunization in BiozziABH and F1 hybrids respectively by the intracortical injection of TNF- α and IFN- γ as described above (Figure 1). Control mice were treated equally. Brain tissue was collected three days and three weeks after lesion induction for histological analyses (Figure 2). Injection site was recognized by a blue marker dye. Clinical EAE scores (if occurred) are not shown as they reflect lesions affecting the spinal cord but not the here investigated cortical GM.

4.2 Immunization with MOG₁₋₁₂₅ leads to high antibody titers in serum

Myelin-specific autoantibodies may play a crucial role in triggering demyelination in the cerebral cortex. Therefore, mice were immunized with recombinant MOG₁₋₁₂₅ instead of MOG-peptide. Autoantibody titers against MOG₁₋₁₂₅ were measured two and five weeks after immunization in sera of BiozziABH and F1 hybrids using ELISA (Figure 3). MOG-immunized BiozziABH (Figure 3A) and F1 hybrids (Figure 3B) developed autoantibody titers from week two after the first immunization that increased slightly in BiozziABH and remained stable in F1 mice to week five. In naïve mice and control animals that were treated with CFA alone autoantibodies against MOG were not detected (nd).

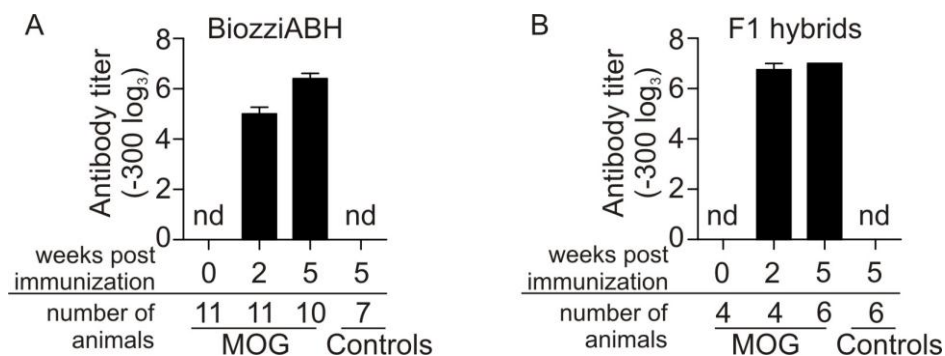


Figure 3 MOG₁₋₁₂₅-immunization induces high autoantibody titers

Autoantibody titers against MOG₁₋₁₂₅ were measured at indicated timepoints after immunization in (A) BiozziABH and (B) F1 hybrids. Data are shown as mean + SEM. nd = not detected.

4.3 Cortical demyelination is primarily located at subpial areas, reveals partial remyelination and mimics cortical MS lesions

Demyelinated lesions were induced by intracortical (i.c.) injection of the proinflammatory cytokines TNF- α and IFN- γ five weeks and three weeks after immunization against MOG₁₋₁₂₅ in BiozziABH and F1 hybrids respectively. Cortical demyelination as well as remyelination were assessed on MBP-stained paraffin sections on the injected (ipsilateral) hemisphere three days and three weeks after cytokine injection respectively. Induced cortical plaques could be classified as active lesions three days after cytokine injection as evidenced by the presence of myelin-laden cells (Figure 4). These cells, corresponding to macrophages/microglia, phagocytosed myelin debris as indicated by cytoplasmic colocalization of MBP⁺ fragments at the lesion border of demyelinated cerebral cortex. Generally, MBP-laden macrophages/microglia are indicative for active demyelination.

Furthermore, cortical demyelination was detected in MOG-immunized BiozziABH as well as F1 hybrids three days after lesion induction but not in controls (Figure 5). Both experimental groups showed capacity for widespread remyelination three weeks after lesion induction (Figure 5).

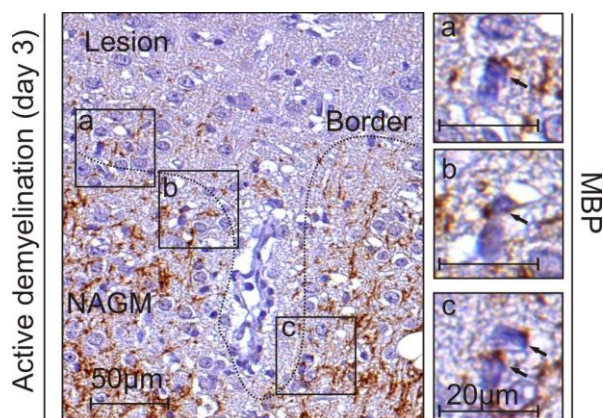


Figure 4 Active demyelination can be observed three days after cytokine injection

A representative picture of a cortical lesion border (marked by the dotted line) showing demyelination at the top and the surrounding NAGM at the bottom in a MBP-stained section. Note at the lesion border phagocytes containing MBP⁺ fragments can be observed (boxes a, b, and c, arrows in the higher magnification of boxes a, b, and c on the right-hand side) indicating ongoing demyelination.

RESULTS

Topologically, lesions primarily affected subpial areas with demyelination extending from the pial surface mostly to cortical layer II (Figure 5). These lesions spread laterally as band-like demyelinated area. Similar cortical lesion types were seen primarily in chronic MS patients and were reminiscent of the described lesion type III affecting subpial areas (Bo et al., 2003b; Peterson et al., 2001). Purely intracortical lesions could as well be detected and were observed as small round-shaped demyelinated areas, centered on blood vessels (Figure 5). This lesion type was less frequently observed than subpial demyelination and accounted for only 1% of the total demyelinated area in BiozziABH mice and 4% of the total demyelinated area in F1 hybrids.

Targeted cortical demyelination was quantified as the area of demyelination (subpial as well as intracortical) in MOG-immunized BiozziABH and F1 hybrids three days and three weeks after cytokine injection (Figure 5). The extent of demyelination was similar between BiozziABH ($0.51 \pm 0.09 \text{ mm}^2$, Figure 5A) and F1 hybrids ($0.49 \pm 0.11 \text{ mm}^2$, Figure 5B) at day three. Three weeks after cytokine injection both experimental groups showed a significant reduction in demyelinated area and a partial restoration of myelin in the ipsilateral cortex, indicating a transient cortical demyelination (Biozzi: $0.02 \pm 0.003 \text{ mm}^2$, F1 hybrids: $0.10 \pm 0.02 \text{ mm}^2$, Figure 5A and B). The residual area of demyelination at week three was significantly smaller in BiozziABH mice compared to F1 hybrids ($p = 0.0159$, statistical evaluation was performed as indicated in the legend of Figure 5). Therefore, remyelination in BiozziABH mice is more efficient than in F1 hybrid mice. The intracerebral injection of PBS alone led to no signs of demyelination in a MOG-immunized animal (data not shown).

In addition to the demyelinated area the length of subpial demyelination was analyzed on the same MBP-stained sections. The lateral extension of subpial demyelination was comparable in BiozziABH ($3.60 \pm 0.51 \text{ mm}$, Figure 5A) and F1 hybrids ($3.52 \pm 0.31 \text{ mm}$, Figure 5B) three days after intracortical cytokine injection. According to the reduced area of demyelination the length of subpial demyelination was also significantly reduced in both animal strains three weeks after lesion induction. Again BiozziABH showed a significant more efficient regeneration (BiozziABH $0.14 \pm 0.01 \text{ mm}$ and F1 hybrids $0.81 \pm 0.14 \text{ mm}$, $p = 0.0159$, statistical evaluation was performed as indicated in the legend of Figure 5A and B).

Since similar extents of cortical demyelination were observed in BiozziABH and F1 hybrids and the intercross with C57BL6/J animals could allow the use of transgenic animals as e.g. reporter strains in F1 hybrids, this work further focused on the analysis of the effects of de- and remyelination in F1 hybrids.

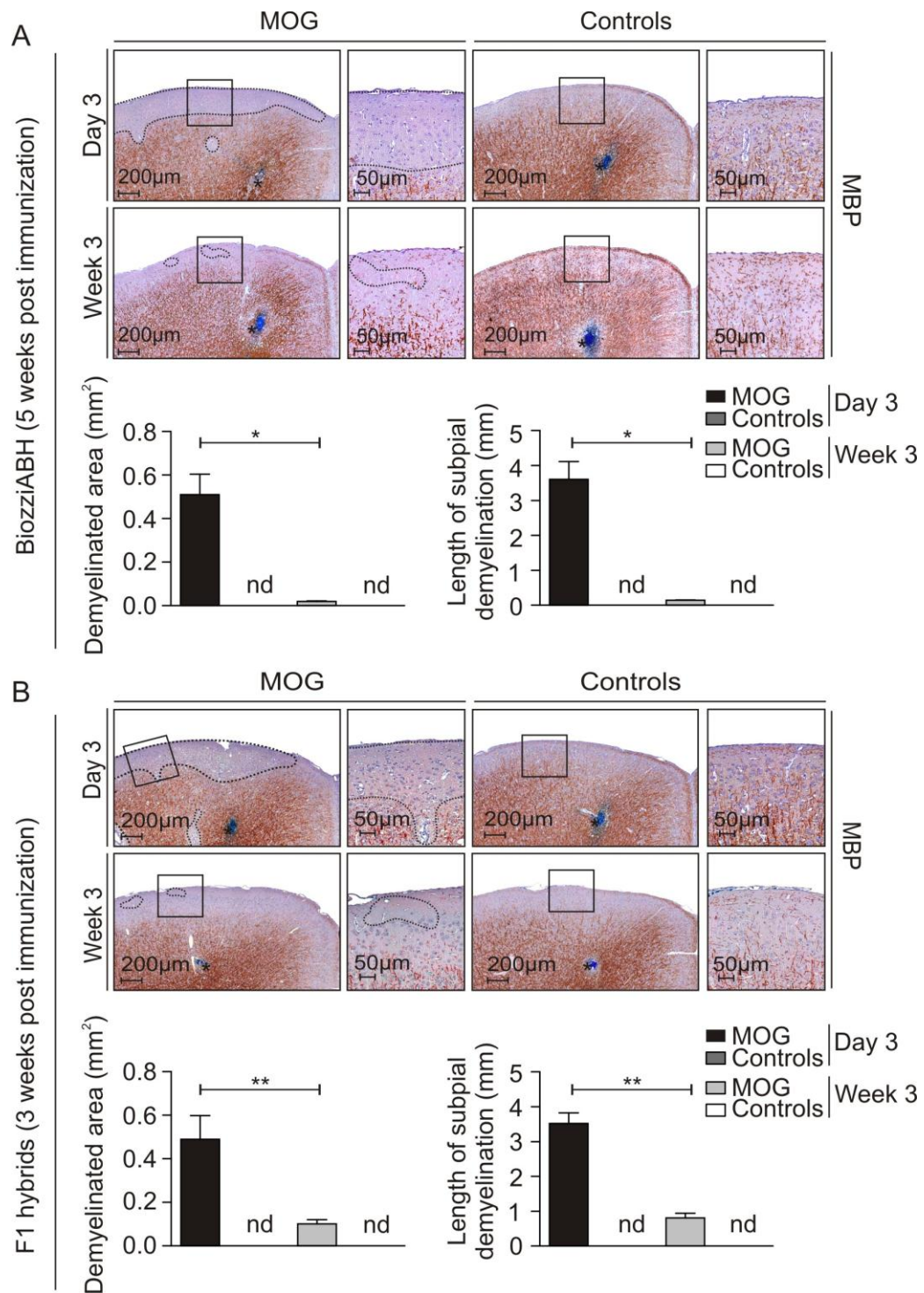


Figure 5 Targeted cortical demyelination is followed by partial remyelination

Representative pictures and quantification of demyelination (area and subplial length) in (A) BiozziABH (n = 4 animals per group) and (B) F1 hybrids (n = 5 animals per group) at indicated time points after cytokine injection revealed widespread cortical demyelination (indicated by the dotted line) at three days followed by partial remyelination at three weeks. Injection site is marked by an asterisk. Data are shown as mean + SEM. Statistical evaluation was performed by a Mann-Whitney test. * indicates statistical significance (* = p<0.05, ** = p<0.01). nd = not detected.

4.4 Axonal preservation but incomplete remyelination in targeted cortical demyelinated lesions

Although remyelination occurred within three weeks after cytokine injection this process remained incomplete as seen by a less dense myelin staining compared to controls (Figure 6) and residual small demyelinated areas (Figure 5). In order to investigate whether the partial remyelination may be due to axonal loss, axonal density was determined in Bielschowsky-stained paraffin sections in F1 hybrids in cortical layer I-II during de- and remyelination on the ipsilateral hemisphere (Figure 6C). Furthermore myelin density was assessed equally in de- and remyelinated cortex in adjacent MBP-stained paraffin sections (Figure 6A). Afterwards, the proportion of myelinated axons was determined by calculating the ratio of myelin intersections to axon intersections (Figure 6E). Corroborating the previous analyses of the extent of demyelination, during ongoing demyelination three days after cytokine injection subpial myelin density in cortical layer I-II was significantly reduced in MOG-immunized F1 hybrids (10.35 ± 2.94 MBP⁺ intersections/field) compared to control animals (39.90 ± 3.15 MBP⁺ intersections/field). Three weeks after cytokine injection myelin density significantly regenerated in MOG-immunized animals (22.35 ± 3.35 MBP⁺ intersections/field) compared to demyelinated animals. However, the density of myelin was still significantly decreased compared to control animals (42.00 ± 1.50 MBP⁺ intersections/field) similar to the above-described results (Figure 6A and B). The axon density was comparable in MOG-immunized and control F1 hybrids at all timepoints with 104.10 ± 1.15 axon intersections/field in MOG-immunized F1 hybrids in comparison to 107.70 ± 4.68 axon intersections/field in controls at three days after cytokine injection. Three weeks after lesion induction MOG-sensitized F1 hybrids revealed 98.95 ± 6.01 axon intersections/field compared to 97.15 ± 3.84 axon intersections/field in controls (Figure 6C and D), clearly demonstrating that no significant axonal degeneration occurred during de- and remyelination. Accordingly, the proportion of myelinated axons in demyelinated cortex ($8.49 \pm 3.13\%$) is significantly decreased compared to controls at day three ($37.49 \pm 3.91\%$) and to remyelinated cortex ($22.79 \pm 3.58\%$) three weeks after cytokine injection. Nevertheless, the proportion of myelinated axons is still significantly reduced in remyelinated cortex in comparison to controls ($43.36 \pm 1.44\%$) at three weeks after lesion induction (Figure 6E), indicating that only approximately 50% of demyelinated axons got remyelinated during the observed period of three weeks.

RESULTS

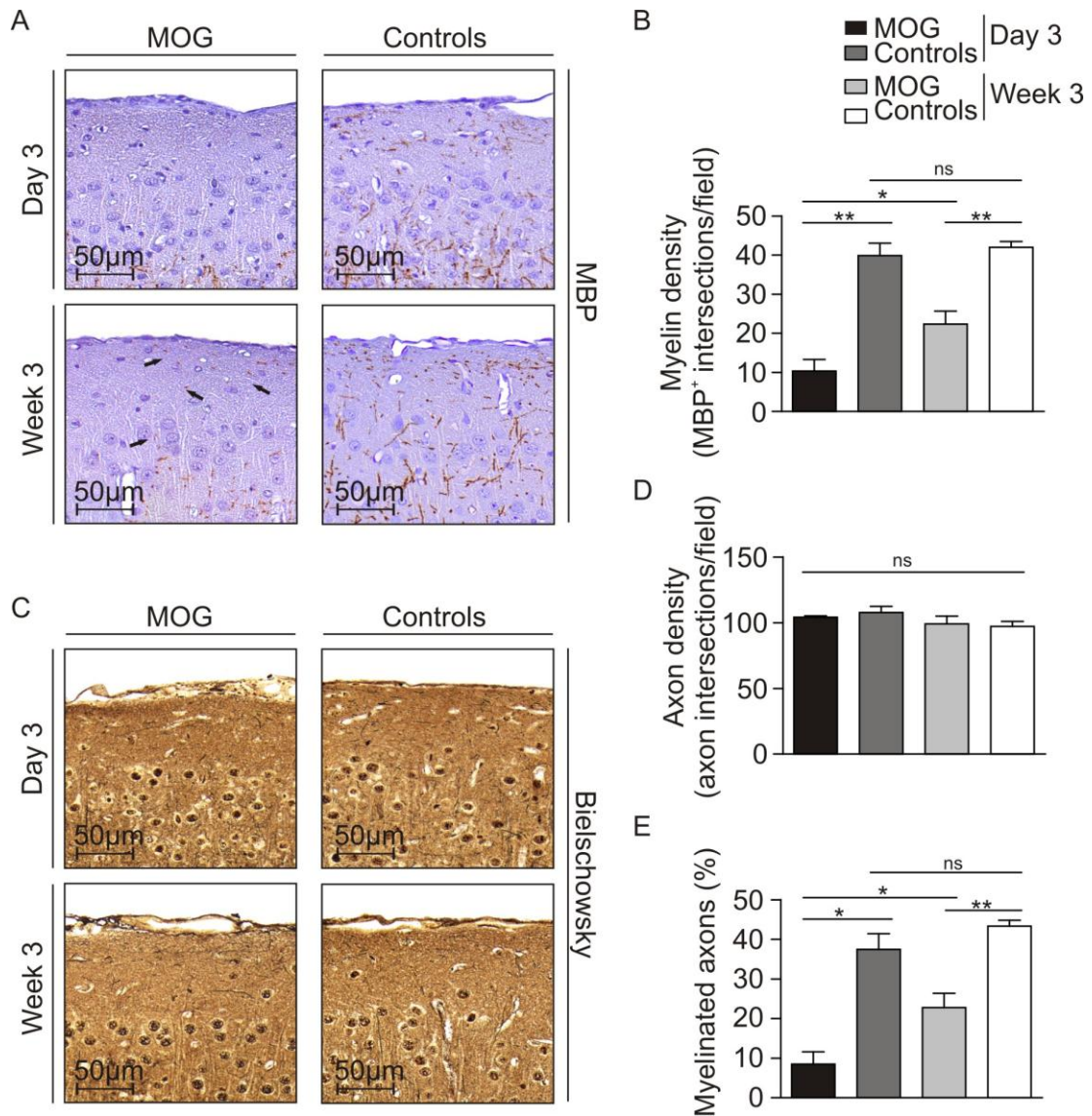


Figure 6 Axonal preservation in incomplete remyelinated lesions

Representative pictures of (A) MBP- and (C) Bielschowsky-stained sections are depicted at indicated time points after cytokine injection in F1 hybrids. Quantification of myelin density (B), axonal density (D), and proportion of myelinated axons (E) in subpial areas revealed demyelination at three days followed by incomplete remyelination (arrows in A) at three weeks and preservation of axons at all indicated time points after lesion induction. All groups included $n = 5$ animals except for the MOG day 3 group of axon density and myelinated fraction ($n = 4$ animals). Data are represented as mean + SEM. Statistical evaluation was performed by a Mann-Whitney test. * indicates statistical significance ($* = p < 0.05$, $** = p < 0.01$).

4.5 Cortical inflammation is transient after lesion induction

4.5.1 Infiltration of T cells during demyelination

Active cortical demyelination was shown to occur on a background of inflammation in MS patients (Lucchinetti et al., 2011) as well as in rats (Merkler et al., 2006b). Therefore, inflammatory infiltrates of T cells were assessed in CD3-stained paraffin sections in different cortical areas in the injected hemisphere three days and three weeks after intracortical cytokine injection (Figure 7). Cortical areas comprising cortical layer I+II, III+IV and V were analyzed separately and combined (cortical layer I-V). Infiltrating T cells were readily detectable in all analyzed cortical layers three days after cytokine injection and a small number of T cells was still visible at three weeks (Figure 7A, cortical layer I+II are shown). Quantitative analysis of cortical layers I-V proved the number of infiltrating T cells significantly increased in MOG-immunized F1 hybrids (47.58 ± 8.24 Total CD3⁺ T cells/mm²) in comparison to controls (21.82 ± 2.06 Total CD3⁺ T cells/mm²) at day three (Figure 7B). Three weeks later the T cell number significantly decreased in MOG-sensitized animals (6.33 ± 0.95 Total CD3⁺ T cells/mm²) and controls (0.32 ± 0.32 Total CD3⁺ T cells/mm²) (Figure 7B). Subanalysis investigating distinct cortical layers showed no overt increase of T cells in MOG-immunized mice in the cortical layer I+II (41.75 ± 18.93 CD3⁺ T cells/mm²), where demyelination is mostly prominent, compared to other cortical layers (layer III+IV 51.48 ± 24.08 CD3⁺ T cells/mm² and layer V 49.51 ± 22.85 CD3⁺ T cells/mm²). However, T cell numbers were significantly higher in all analyzed cortical areas in MOG-immunized animals compared to controls at day three (layer I+II: 21.67 ± 5.05 CD3⁺ T cells/mm², layer III+IV: 22.32 ± 9.81 CD3⁺ T cells/mm², layer V: 21.47 ± 9.23 CD3⁺ T cells/mm²) and to animals at three weeks (layer I+II: 11.34 ± 6.09 CD3⁺ T cells/mm², layer III+IV: 4.82 ± 5.85 CD3⁺ T cells/mm², layer V: 2.85 ± 2.6 CD3⁺ T cells/mm² for MOG-immunized animals and layer I+II: not detectable CD3⁺ T cells/mm², layer III+IV: 0.95 ± 2.13 CD3⁺ T cells/mm², layer V: not detectable CD3⁺ T cells/mm² for controls) (Figure 7C). Intracerebral injection of PBS alone in a MOG-immunized mouse led to infiltration of a low number of T cells around the injection site and the needle track at three days (data not shown). Thus, cortical demyelination was accompanied by a transient T cell infiltration and T cells distribute almost equally throughout the whole ipsilateral cortex three days after lesion induction.

RESULTS

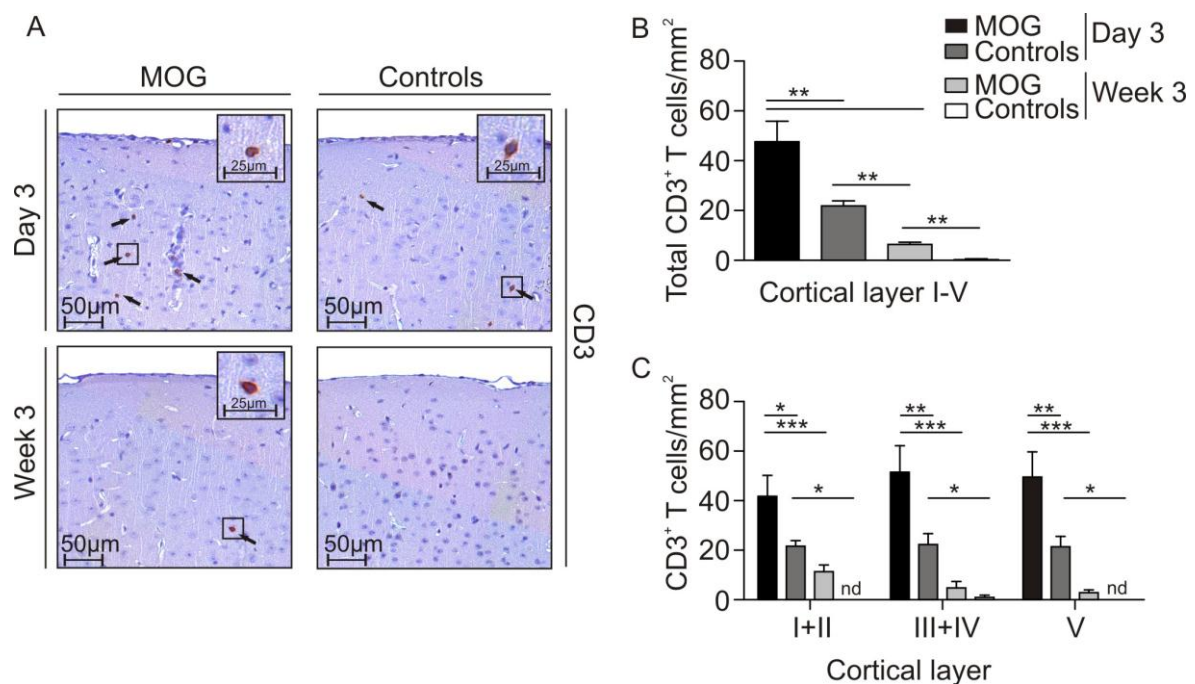


Figure 7 Transient CD3⁺ T cell infiltration during demyelination

(A) Representative pictures of CD3-stained T cells (marked by arrows) in F1 hybrids are depicted at indicated time points after lesion induction. Quantification of the number of T cells in cortical layer I-V (B) and specific cortical layers (C) revealed a transient increase of T cells throughout the ipsilateral hemisphere in MOG-sensitized mice at day three after lesion induction. (B) Data are shown as mean + SEM (n = 5 animals per group). For statistical evaluation a Mann-Whitney test was performed. * indicates statistical significance (** = p<0.01). (C) Data are expressed as mean + SD (n = 5 animals per group). A two-way ANOVA followed by a Bonferroni post hoc analysis was performed for statistical analysis. * indicates statistical significance (* = p<0.05, ** = p<0.01, *** = p<0.001). nd = not detected.

4.5.2 Different morphological phenotypes of macrophages/microglia are present in demyelinated cortex

The presence of different morphological activated macrophages/microglia phenotypes might represent functional variety. A hallmark for ongoing demyelination is the presence of myelin-phagocytosing and foamy macrophages. Therefore, total numbers of activated macrophages/microglia as well as morphologic round-shaped and foamy macrophage/microglia phenotypes were analyzed respectively in Mac-3-stained paraffin sections in distinct cortical layers of the ipsilateral hemisphere three days and three weeks after lesion induction as described above (Figure 8). The Mac-3 antigen is expressed on the surface of activated macrophages/microglia but much less on restint microglia. Different reactive phenotypes are depicted in Figure 8A on the right-hand side.

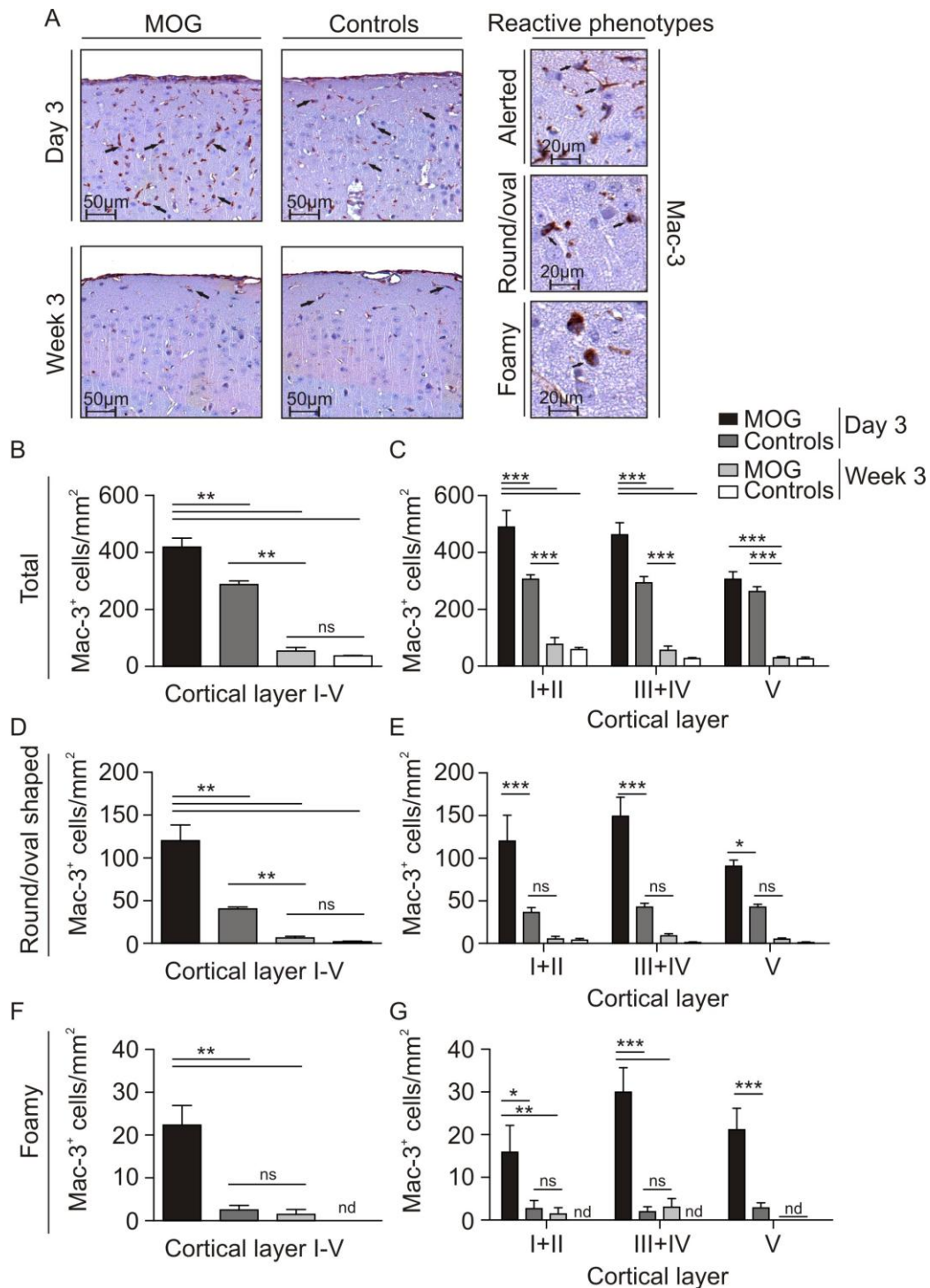


Figure 8 Different morphological phenotypes of macrophages/microglia during demyelination

(A) Representative pictures of Mac-3⁺ activated macrophages/microglia in subpial areas (left) and different reactive phenotypes (right). Quantification of total activated macrophages/microglia (B, C) and subdivision into round/oval-shaped (D, E) and foamy (F, G) phenotypes in cortical layer I-V or indicated cortical layers. Note the number of activated macrophages/microglia and especially round/oval-shaped and foamy phenotypes was increased during demyelination in MOG-immunized F1 hybrids at day three. (B, D, F) Data are shown as mean + SEM (n = 5 animals per group). For statistical evaluation a Mann-Whitney test was performed. * indicates statistical significance (** = p < 0.01). (C, E, G) Data are expressed as mean + SD (n = 5 animals per group). A two-way ANOVA followed by a Bonferroni post hoc analysis was performed. * indicates statistical significance (* = p < 0.05, ** = p < 0.01, *** = p < 0.001). nd = not detected.

RESULTS

High numbers of activated macrophages/microglia were detectable in the cortex of MOG-immunized mice and controls three days after cytokine injection which then decreased at three weeks (Figure 8A). Quantitative analysis revealed significantly more numbers of activated macrophages/microglia in cortical layers I-V of MOG-sensitized F1 hybrids (418.3 ± 31.21 Mac-3⁺ cells/mm²) compared to controls (286.6 ± 13.17 Mac-3⁺ cells/mm²) at day three and in comparison to both experimental groups three weeks after lesion induction (MOG: 53.91 ± 12.41 Mac-3⁺ cells/mm², Controls: 37.01 ± 1.94 Mac-3⁺ cells/mm²) (Figure 8B). Analyses of distinct cortical areas showed that the number of total activated macrophages/microglia was significantly higher in MOG-immunized mice in cortical layer I+II (488.27 ± 130.83 Mac-3⁺ cells/mm²) and III+IV (461.04 ± 96.23 Mac-3⁺ cells/mm²) in comparison to controls (I+II: 305.22 ± 34.89 Mac-3⁺ cells/mm², III+IV: 292.40 ± 50.03 Mac-3⁺ cells/mm²) three days after cytokine injection. In cortical layer V comparable numbers of activated macrophages/microglia were detected in MOG-immunized animals (305.45 ± 58.06 Mac-3⁺ cells/mm²) and controls (262.22 ± 37.94 Mac-3⁺ cells/mm²) (Figure 8C). Considering round/oval-shaped activated macrophages/microglia similar results were obtained. In cortical layer I-V significantly more round/oval-shaped activated macrophages/microglia were detected in MOG-immunized animals (119.8 ± 18.61 Mac-3⁺ cells/mm²) compared to controls (40.34 ± 2.06 Mac-3⁺ cells/mm²) during demyelination. Only a few round/oval-shaped activated macrophages/microglia remained in the cortex within three weeks in MOG-immunized mice (6.26 ± 1.95 Mac-3⁺ cells/mm²) but were almost absent in controls (1.95 ± 0.72 Mac-3⁺ cells/mm²) (Figure 8D). In all distinct cortical layers round/oval shaped macrophages/microglia were significantly more present but primarily in layer I+II (119.83 ± 67.55 Mac-3⁺ cells/mm²) and III+IV (148.90 ± 50.09 Mac-3⁺ cells/mm²), slightly less in V (90.67 ± 15.36 Mac-3⁺ cells/mm²) but still significantly increased compared to controls (I+II: 36.22 ± 12.97 Mac-3⁺ cells/mm², III+IV: 42.42 ± 10.43 Mac-3⁺ cells/mm², V: 42.39 ± 7.60 Mac-3⁺ cells/mm²) three days after lesion induction (Figure 8E). Foamy macrophages/microglia that were indicative for phagocytosing myelin debris thereby representing ongoing demyelination were mostly seen in MOG-immunized F1 hybrids three days after cytokine injection in cortical layers I-V. This group showed significantly higher numbers of foamy cells (22.35 ± 4.44 Mac-3⁺ cells/mm²) compared to controls (2.49 ± 1.10 Mac-3⁺ cells/mm²) at three days and to both experimental groups at three weeks after lesion induction, in which foamy macrophages/microglia are nearly not present (MOG: 1.49 ± 1.13 Mac-3⁺ cells/mm², Controls: not detected) (Figure 8F). Detailed analyses regarding distinct cortical layers revealed significantly higher numbers of foamy macrophages/microglia in all

RESULTS

cortical areas but primarily in cortical layer III+IV (30.00 ± 12.66 Mac-3⁺ cells/mm²) and V (21.16 ± 11.29 Mac-3⁺ cells/mm²) and slightly less in cortical layer I+II (15.88 ± 14.11 Mac-3⁺ cells/mm²). In all other experimental groups they were nearly completely absent (Figure 8G). The intracerebral injection of PBS alone in a MOG-sensitized mouse revealed a few activated macrophages/microglia close to the injection site and needle track three days later (data not shown). Due to the injection of proinflammatory cytokines in control mice, macrophages/microglia were on alert and expressed the activation marker Mac-3. However, since round/oval-shaped and foamy phenotypes are virtually not present in control animals this indicated that these cells are differentially activated. Round/oval-shaped and especially foamy macrophages seemed to contribute to demyelination.

4.6 Cortical EAE reveals no neuronal loss

4.6.1 Cortical thickness is slightly reduced after remyelination

Cortical thinning is a general sign for cortical atrophy. Cortical thickness was measured paramedially in NeuN-stained paraffin sections in the ipsi- and contralateral hemisphere of F1 hybrids as indicated (Figure 9A). MOG-immunized F1 hybrids showed a statistical trend for a reduced paramedial cortical thickness three weeks after lesion induction on the ipsilateral (1191 ± 70.59 μm , $p = 0.056$ compared to MOG day three) and contralateral (1267 ± 60.19 μm , $p = 0.15$ compared to MOG day three) hemisphere compared to both hemispheres in MOG-immunized mice at day three (ipsilateral: 1416 ± 30.33 μm , contralateral: 1395 ± 12.09 μm). Controls revealed comparable cortical thicknesses three days (ipsilateral: 1341 ± 54.61 μm , contralateral: 1368 ± 73.04 μm) and three weeks (ipsilateral: 1328 ± 62.04 μm , contralateral: 1359 ± 46.99 μm) after cytokine injection in comparison to F1 hybrids three days after lesion induction (Figure 9B).

RESULTS

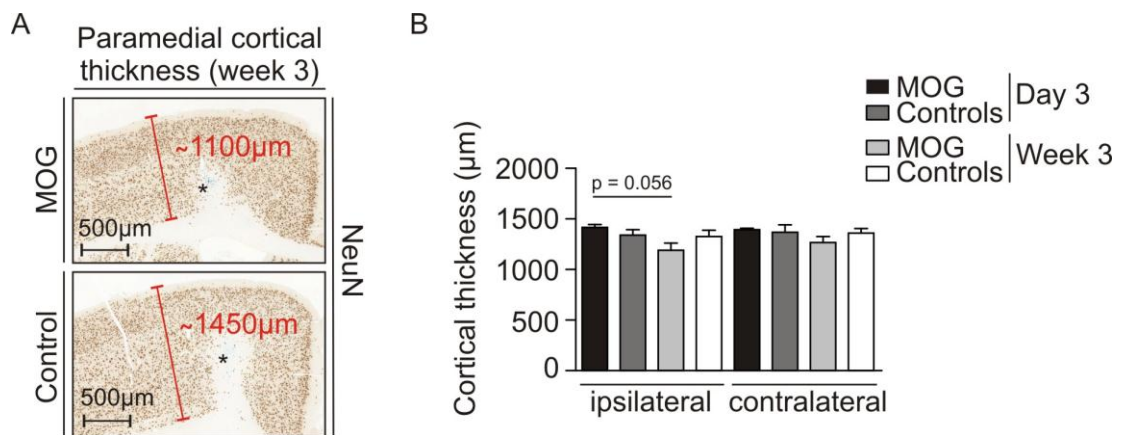


Figure 9 Slightly reduced paramedial cortical thickness after remyelination

(A) Representative pictures of NeuN-stained tissue sections and measurement of paramedial cortical thickness in F1 hybrids. Injection site is marked by the asterisk. (B) Quantitative analysis revealed a trend for reduced cortical thickness in MOG-immunized mice three weeks after cytokine injection on the ipsilateral hemisphere. Data are expressed as mean + SEM (n = 5 animals per group).

4.6.2 Neuronal density is not reduced in targeted EAE

Evaluation of a potential loss of cortical neurons was assessed by counting the number of cortical NeuN⁺ neuronal nuclei automatically in paraffin sections on both hemispheres. Neurons were counted in cortical layers II, III+IV and V respectively and combined (cortical layer II-V) and neuron detection was performed as shown in Figure 10A. MOG-immunized animals did not reveal a loss of cortical neurons in any analyzed cortical area at all time points (data not shown). Depicted is the neuronal density of cortical layer II-V. According to the absence of axonal degeneration in MOG-immunized mice, no loss of neurons on both hemispheres could be observed three weeks after cytokine injection (ipsilateral: 1953 ± 128.2 NeuN⁺ cells/mm², contralateral: 1915 ± 102.7 NeuN⁺ cells/mm²) compared to MOG-immunized mice (ipsilateral: 1924 ± 58.31 NeuN⁺ cells/mm², contralateral: 2055 ± 53.74 NeuN⁺ cells/mm²) and controls (ipsilateral: 1902 ± 73.97 NeuN⁺ cells/mm², contralateral: 2141 ± 69.32 NeuN⁺ cells/mm²) three days after intracortical injection and to controls three weeks (ipsilateral: 1936 ± 46.18 NeuN⁺ cells/mm², contralateral: 1880 ± 59.43 NeuN⁺ cells/mm²) after lesion induction (Figure 10B).

RESULTS

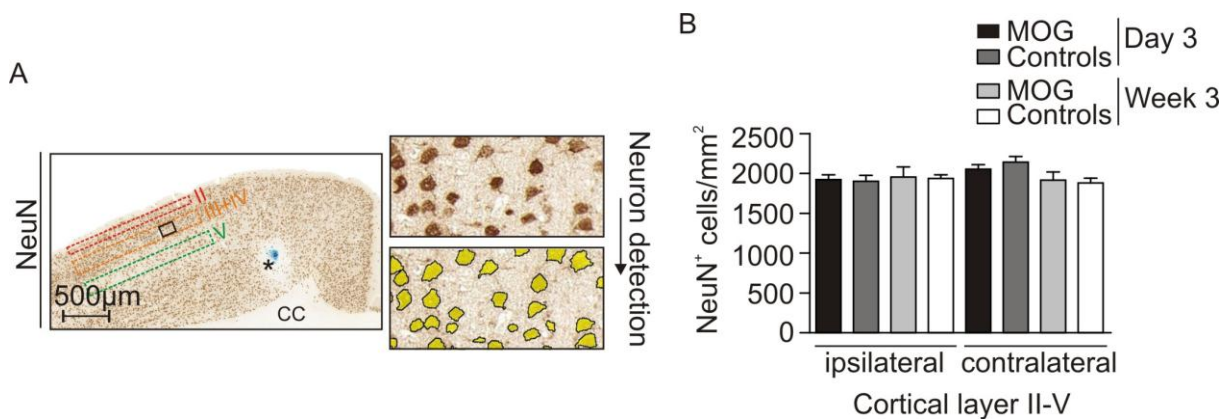


Figure 10 Neuronal density is not altered during de- and remyelination

(A) Neuronal density was analyzed by counting NeuN⁺ cells automatically in the ipsi- and contralateral hemisphere in areas of cortical layers II-V. (B) Neuronal cell counts revealed comparable numbers of NeuN⁺ cells in both hemispheres at all indicated timepoints and groups. Data are shown as mean + SEM (n = 5 animals per group).

4.7 Visualization and shape analysis of dendrites and spines in the cerebral cortex of mice

Neurons receive signaling input via their dendrites and spines. During neurodegenerative processes loss of synaptic transmission therefore alter the functional properties of neurons. Previous studies showed that in MS patients loss of synaptic density in demyelinated hippocampi (Dutta et al., 2011) and leukocortical lesions (Wegner et al., 2006) can occur. However, it remains still unclear at which cellular level such alterations affect dendrites and spines. The primary aim of this work was, therefore, to establish a method that would enable to study alterations in neuronal structures as dendrites and dendritic spines in the cerebral cortex at subcellular level with high spatial resolution. In this approach a computational assisted method was used with which neuronal structures can be reconstructed and alterations in spine densities, shapes or dendritic irregularities can be detected. In order to visualize dendrites and dendritic spines, tissue from EGFP⁺ F1 hybrids was analyzed since these mice expressed EGFP in less than 10% of cortical neurons allowing the tracking and reconstruction of distinct cortical dendrites with high spatial resolution (Feng et al., 2000). Main dendritic branches of neurons located in the cortical layer V-VI were imaged in distinct distances from the soma using a confocal laser scanning microscope and images were deconvolved (Figure 11). High-resolution imaging revealed detailed dendritic structures like dendritic branches (Figure 11B) and spines (Figure 11C and D). Zooming in allowed even the detection of single dendritic spines (Figure 11E-G).

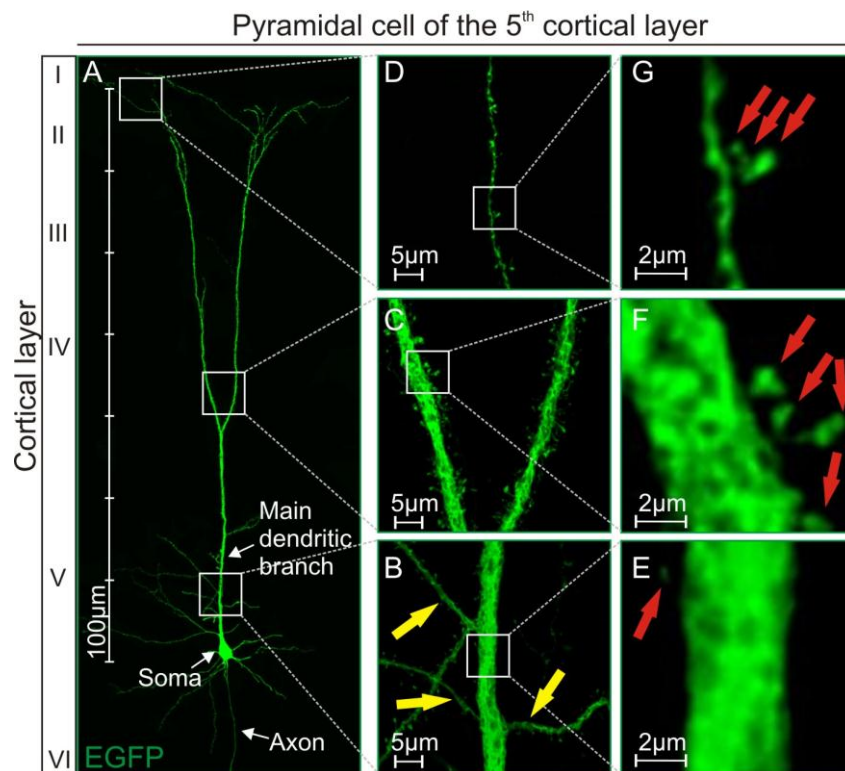


Figure 11 Visualization of dendritic branches and spines

(A) Confocal image of an EGFP⁺ cortical neuron with the main dendritic branch extending upright to the brain surface. (B-D) High resolution images revealed dendritic branches (yellow arrows) and spines. (E-G) Zooming in allowed detection of single spines (red arrows).

Three-dimensional (3D) reconstruction of such neuronal processes was performed using NeuronStudio (CNIC) (Figure 12). NeuronStudio allowed automated tracing of the main dendritic branch and detection as well as classification of dendritic spines (Figure 12A-C, E) using the so-called Rayburst sampling algorithm (Rodriguez et al., 2008; Rodriguez et al., 2006). Rayburst sampling used multidirectional rays casting from the center of mass of a 3D object to its surface in order to compute precisely diameters, volumes and surface areas (Dumitriu et al., 2011; Rodriguez et al., 2008; Rodriguez et al., 2006). Spine volumetric measurements like spine head volumes (Figure 12F) used a 3D Rayburst algorithm (Rodriguez et al., 2006). Two-dimensional (2D) Rayburst algorithms were used to analyze dendritic shaft diameter at each node (Rodriguez et al., 2006; Wearne et al., 2005), which is useful to estimate irregularities in branch diameters (Figure 12D), and to perform spine shape classifications (Rodriguez et al., 2008) (Figure 12E). Spines were classified according to the default values set in NeuronStudio (CNIC) into mushroom, stubby or thin (Figure 12B). Generally, spine density was a function of distance to the soma (Figure 12C), different spine

RESULTS

shapes were distributed along the dendrite (Figure 12E and F) and basal dendritic segments were more regularly shaped in contrary to more distal parts, which showed some fluctuations as indicated by increased changes in radii per dendritic length (Figure 12D). Using this computational approach clearly showed, that precise detection of dendrites and spines and shape analyses was performable. Ongoing measurements will assess dendritic and spine alterations within demyelinated cerebral cortex.

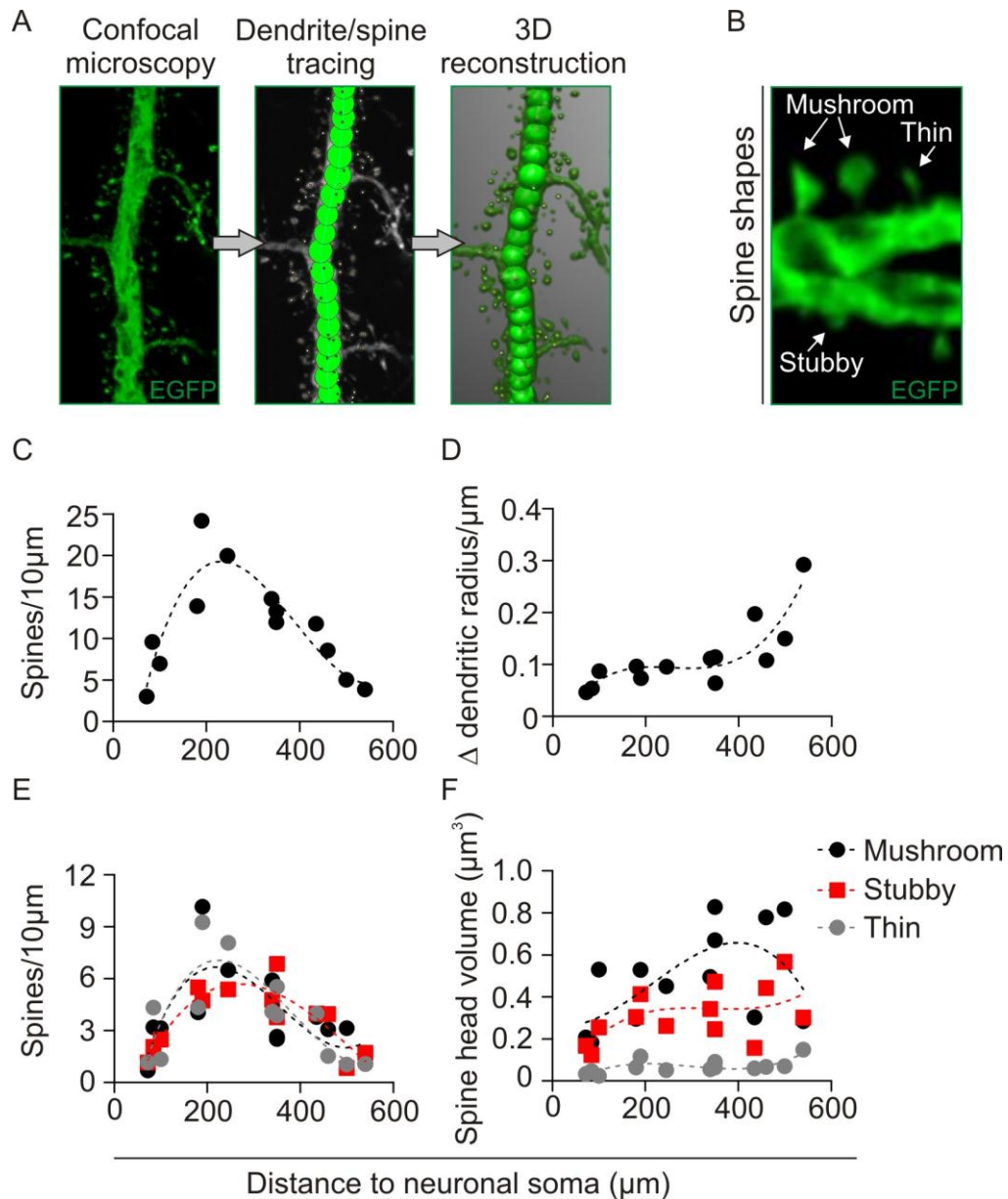


Figure 12 3D analysis of dendritic and spine shapes

(A) Tracing of dendrites (green nodes) and spines (colored small circles) in deconvolved confocal images led to 3D reconstruction and analysis of spine density (C) and fluctuations in dendritic shaft radius (D) as function of distance to the soma using NeuronStudio. (B) Shape classification of spines and their densities (E) and head volumes (F) were automatically computed in NeuronStudio. Data represent measurements obtained from 3 dendrites.

RESULTS

4.8 Loss of dendritic spines and branches in the cortex of progressive MS cases

Since synaptic loss has been shown in leukocortical lesions (Wegner et al., 2006), cortical dendrites were analyzed in autopsy specimen from chronic MS patients with a late disease-stage focussing on the number of dendritic spines and branches and compared to dendrites in healthy controls (Figure 13). MS autopsy cases and controls are summarized in Table 3. Brain tissue containing cerebral cortex was dissected from the frontotemporal lobe (F2-3) of both hemispheres and tissue blocks were split into two parts and either processed for MBP staining to assess cortical demyelination or Golgi-Cox staining to study cortical dendrites (Figure 13A). In two out of four MS patients cortical demyelinated lesions could be detected in the frontotemporal cortex specimen. A representative picture of such a human cortical lesion in comparison to NAGM and GM in healthy controls is shown in Figure 13B. On the basis of the adjacent MBP-stained sections, cortical neurons were classified as located within the lesion, at the lesion border or in NAGM. In Golgi-Cox impregnated sections neurons of the cortical layer IV-VI were chosen for image acquisition with a confocal laser scanning microscope (Figure 13C). Spines and branches were counted on 50 μm successive basal dendritic segments of the main dendritic branch from the neuronal soma in MS cases and healthy controls. Individual case spine counts are depicted in Figure 13D. Similar to the distribution of spine densities detected in mice, control specimen showed that the number of spines increased in relation to the distance to the soma with a continuous increase in spine number to distances of 150 μm to 200 μm from the soma and a slight reduction in longer distances.

Table 3 MS and control cases

MS cases	Sex	Age at death	Disease duration	Storage in 4% formalin
1	female	44 years	unknown	1 month
2	female	51 years	over 10 years (RRMS)	2 month
3	male	55 years	over 10 years	1.5 month
4	male	51 years	over 10 years	1.5 month
		Mean age at death: 50.3 years		Mean storage period: 1.5 month
Controls				
1	male	62 years	no neurologic disease	2 month
2	female	68 years	no neurologic disease	1 month
3	male	64 years	no neurologic disease	1 month
		Mean age at death: 64.7 years		Mean storage period: 1.5 month

RESULTS

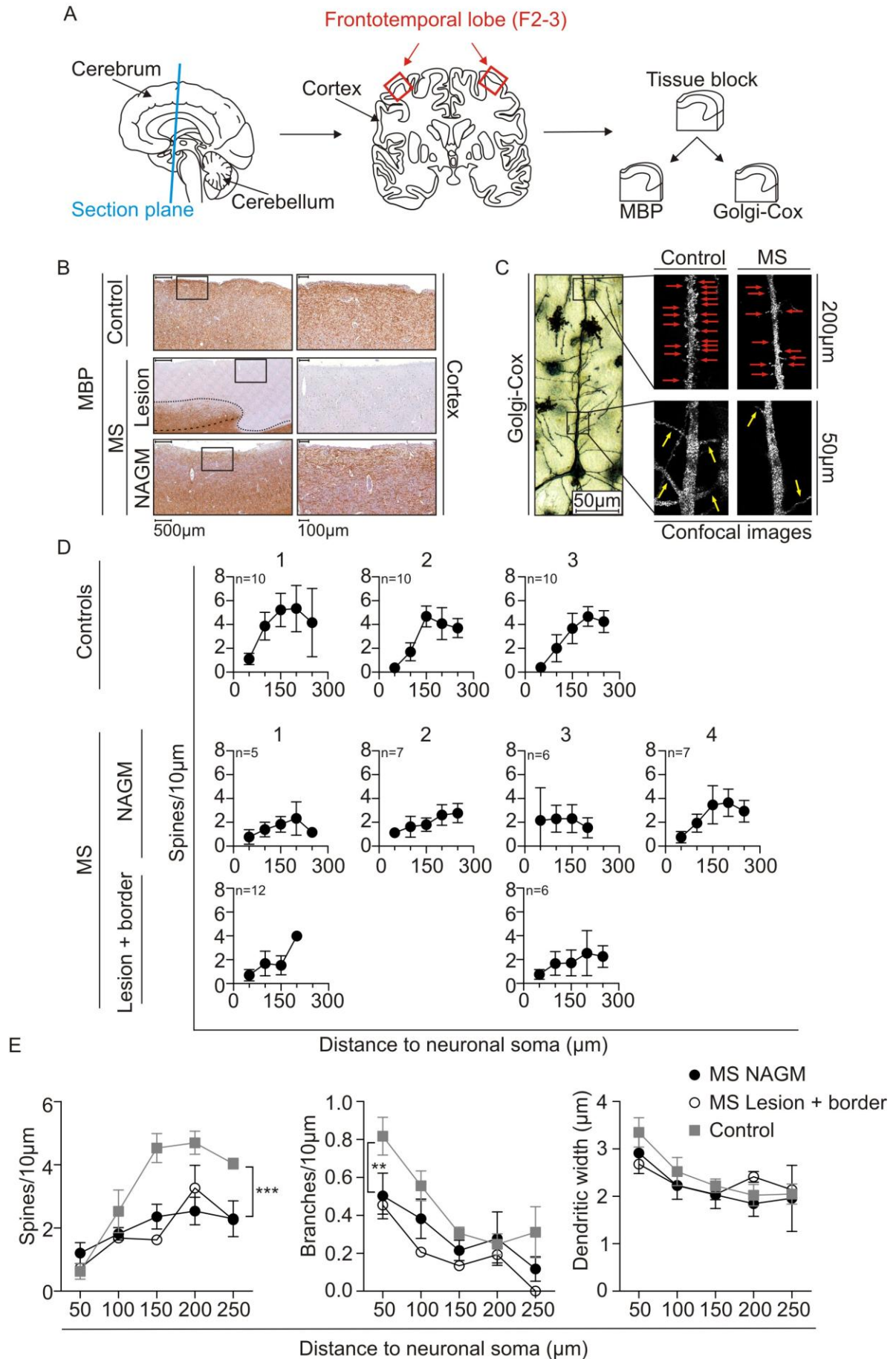
Quantification of spine counts in MS patients revealed a decreased number of dendritic spines predominantly at longer distances to the soma in comparison to controls and the reduction in spine number was irrespective of neuronal localization within a demyelinated lesion including the lesion border or in NAGM. An analysis of combined data of all MS cases and controls indicated a significant reduction in the number of dendritic spines within cortical lesions or NAGM compared to controls in a two-way ANOVA (Figure 13E). The number of dendritic branches showed a significant trend for reduced branch numbers in a two-way ANOVA (post hoc test not significant) primary in shorter distances to the soma in MS patients. In all cases, the investigated dendrites had comparable dendritic width excluding varying spine numbers due to different dendritic sizes (Figure 13E). These results demonstrated a pronounced global dendritic pathology in progressive MS formed by reduced dendritic spine densities in neurons of the lower cortical layers in chronically demyelinated lesions as well as the surrounding NAGM.

Figure 13 Reduced densities of dendritic spines and branches in chronic MS

(A) Autopsy tissue from MS patients and healthy controls was dissected as indicated and processed for MBP staining (B) or Golgi-Cox impregnation (C). (B) Note the cortical lesion in MS (lesion border is indicated by the dotted line, border between GM and WM is marked by the dashed line). (D) Quantification of the number of dendritic spines (red arrows in (C)) and branches (yellow arrows in (C)) in individual cases (analyzed number of dendrites per case is indicated in the graph). (E) Combined individual spine counts revealed a significant reduction in spine and branch density in MS but comparable dendritic width to controls. (D) Data are expressed as mean \pm SD. (E) Data are shown as mean \pm SEM (n = 3 controls, n = 4 MS NAGM, n = 2 MS lesion + border). For statistical analyses a two-way ANOVA was performed. * indicates statistical significance (** = p<0.01, *** = p<0.001).

RESULTS

Figure 13



5 DISCUSSION

5.1 Targeted cortical EAE in mice allows reproducible lesion induction within a defined anatomical area

In the presented work an EAE mouse model targeting the cerebral cortex was established. The intracortical injection of a proinflammatory cytokine cocktail composed of TNF- α and IFN- γ in MOG-immunized BiozziABH and F1 hybrids generated from BiozziABH and mice on a C57BL6/J background triggered the formation of confluent demyelinated lesions in the cortical GM in a predetermined anatomical area, in a temporally well-defined manner and with reproducibility.

Therefore, this model allows the precise investigation of pathomechanisms involved in lesion formation in the cortical GM which is in contrast to ‘conventional’ disseminated EAE models that rarely affect the brain or lesions occur randomly distributed in the GM (Girolamo et al., 2011; Mangiardi et al., 2011; Merkler et al., 2006a; Pomeroy et al., 2008; Pomeroy et al., 2005; Rasmussen et al., 2007; Storch et al., 2006). Moreover, the confluent demyelination with well-demarcated lesion borders induced in the here described model is in contrast to the myelin loss in cerebral cortices of ‘conventional’ EAE mice as demyelination is exemplified by reduced myelin density but confluent demyelinated areas are not measured (Girolamo et al., 2011; Mangiardi et al., 2011). Although cortical lesions were induced artificially, they reproduced the immunopathological nature characteristic for MS lesions. This is in contrast to toxin-induced models like the systemic administration of the copper chelator cuprizone. Cuprizone treatment lead to demyelination in defined anatomical areas like the cerebral cortex (Merkler et al., 2009; Skripuletz et al., 2008), however, this model triggers primarily the death of mature oligodendrocytes and does not mimic the complex immunopathology of MS lesions (Skripuletz et al., 2011; Torkildsen et al., 2008). An important aspect of the here described targeted cortical EAE model was the functionality in BiozziABH mice and their F1 offsprings intercrossed with mice on a C57BL6/J background. Intercrossing of transgenic mice allows the use of reporter strains like the used mice that express EGFP in a subset of cortical neurons in this work. A striking phenomenon was the reproducible induction of primarily subpial lesions in the targeted cortical EAE mouse model sharing pathological hallmarks with MS. EAE lesions spread laterally as band-like demyelination extending from the pial surface of the brain mostly to cortical layer II and exhibited a well-demarcated lesion border. This induced subpial lesion type is reminiscent to lesion type III described in early-stage MS patients

(Lucchinetti et al., 2011) and chronic MS patients (Bo et al., 2003b; Peterson et al., 2001) as well as in the targeted cortical EAE rat model (Merkler et al., 2006b). Subpial lesions were the second most common cortical lesion type (accounted for a considerably proportion of about 34%) in early MS (Lucchinetti et al., 2011) and the most common cortical lesion type in chronic MS (Albert et al., 2007; Bo et al., 2003b; Giaccone et al., 2012; Kutzelnigg et al., 2005; Peterson et al., 2001; Vercellino et al., 2005). The occurrence of almost only subpial lesions and nearly no intracortical or leukocortical lesions would be in favor for an intrinsic cortical demyelinating disease that can occur independently to WM lesions (Giaccone et al., 2012; Kutzelnigg et al., 2005). The lesion distribution preferentially at subpial areas might also be explained by a reflow of intracerebral injected cytokines back through the injection trace to the surface of the brain, which can sometimes be observed during the stereotactic injection of the animals or during mechanical retraction of the capillary. Furthermore, it has been shown that intraparenchymal injected tracer spread along perivascular spaces to the surface of the brain and leaked into the CSF (Abbott, 2004), intracortical injected cytokines could diffuse equally. After reaching subpial areas, the cytokines might activate the BBB and affect BBB integrity to allow activated T cells and autoantibodies to enter the CNS parenchyma and lead to a localized inflammatory lesion in this area. Moreover, cortical demyelination is associated with meningeal inflammation (Choi et al., 2012; Howell et al., 2011; Kutzelnigg et al., 2005; Lucchinetti et al., 2011; Magliozzi et al., 2007). Diffusion of pro-inflammatory cytokines from inflamed meninges could support cortical GM pathology from the surface of the brain (Magliozzi et al., 2010). Since the targeted EAE mouse model also showed meningeal inflammation (data not shown) cortical demyelination might be induced from cytokines released from the meninges. However, since control mice also showed meningeal inflammation, a sole cytokine-mediated mechanism from the meninges seems to be insufficient to induce demyelination.

5.2 Active cortical demyelination and inflammation are transient and do not induce neuronal or axonal loss

The induction of confluent demyelinated lesions in the cerebral cortex of MOG-immunized mice was accompanied by the development of anti-MOG autoantibody titers in sera and widespread but temporarily infiltration of T cells and activated macrophages/microglia in the ipsilateral hemisphere that was subjected to the lesion induction.

DISCUSSION

The inflammatory character and composition of the here described cortical EAE lesions in mice reflect the highly inflammatory nature of cortical demyelinated lesions in early-stage MS patients, which also consists of activated microglia and a strong T cell inflammation (Lucchinetti et al., 2011). Furthermore, these findings are also in line with observations in the targeted cortical EAE rat model. Cortical demyelination accompanies a transient parenchymal T cell infiltration in a comparable range to the here presented model but exhibit 25% less activated macrophages/microglia three days after lesion induction. Inflammation resolves afterwards within two weeks (Merkler et al., 2006b). The profound clearance of inflammation in the targeted EAE mouse model might explain the differences in early disease-stage cortical lesions in MS patients, which are highly inflammatory (Lucchinetti et al., 2011), in comparison to chronic lesions in late-stage MS, which are less inflammatory (Bo et al., 2003a; Peterson et al., 2001). This demonstrates that the targeted EAE mouse model reflects cortical lesions observed in early-stage MS patients and is useful to study underlying pathomechanisms.

A striking aspect between the cytokine-injected cortices of EAE mice exhibiting demyelination and control mice without demyelination was the difference in reactive macrophage/microglia phenotypes. Generally, entire cortical hemispheres subjected to a lesion showed higher numbers of reactive macrophages/microglia with remarkable more round/oval-shaped and especially foamy macrophages/microglia compared to control cortices. Particular the presence of foamy macrophages/microglia in NAGM in the lower cortical layers indicate ongoing demyelination since these cells are associated with ingestion of myelin debris. According to this model, myelin-laden macrophages/microglia are described in the targeted cortical EAE of rats (Merkler et al., 2006b) and in active cortical lesions in early MS (Lucchinetti et al., 2011). Furthermore, the parenchymal distribution of particular round/oval-shaped macrophages/microglia and T cells in affected cortices may indicate an interaction between these cells. Infiltrating activated macrophages and reactive microglia could function as APC thereby triggering local reactivation of infiltrating MOG-specific T cells and propagation of the immune response. In turn, T cells could secrete soluble factors that stimulate macrophages/microglia and also exaggerate the disease (Jack et al., 2005). The presence of round/oval-shaped and foamy macrophages/microglia in lesioned hemispheres might indicate that these cells trigger the observed demyelination. Moreover, all reactive phenotypes could trigger tissue damage by production of toxic mediators or reactive oxygen or nitric oxide species (Jack et al., 2005). Next steps would be to further characterize the cell type that is directly involved in demyelination.

DISCUSSION

In addition to initiate CNS inflammation, encephalitogenic T cells are also required to disrupt the BBB allowing humoral immune factors like antibodies to penetrate the CNS parenchyma (Genain et al., 1995; Iglesias et al., 2001).

In this work, mice were immunized with recombinant MOG₁₋₁₂₅ instead of MOG-peptide in order to elicit a strong MOG-specific antibody response. Peripheral immune priming against MOG was clearly required for the induction of cortical demyelinated lesions in the targeted EAE since mice treated with CFA alone did not reveal signs of cortical demyelination although they were subjected to an intracortical cytokine injection.

Antibody and complement-mediated mechanisms in demyelination have been suggested in active MS lesions by the identification of immunoglobulin and complement deposition in a proportion of patients (Lucchinetti et al., 2000) and by detecting MOG autoantibodies in WM lesions of EAE and MS and their association with myelin damage (Genain et al., 1999; Raine et al., 1999). Furthermore, *in vivo* studies demonstrate that passively transferred MOG-specific monoclonal autoantibodies enhance demyelination in rats that were previously treated with either MBP-specific T cells or MBP/CFA (Lassmann et al., 1988; Linington et al., 1988; Schluesener et al., 1987) and BiozziABH immunized with spinal cord homogenate (Morris-Downes et al., 2002). These findings, together with the detection of high anti-MOG autoantibody titers as well as complement deposition in cortical lesions in targeted rat EAE (Merkler et al., 2006), suggest that the pathogenic effect observed in the here described model is an interplay between B cell derived MOG-specific autoantibodies, probably followed by complement activation, establishment of an autoaggressive T cell response and activation of macrophages/microglia. Macrophages/microglia might be activated by both, autoantibodies in combination with complement and T cells, which then trigger myelin destruction by secretion of toxic factors and phagocytosis of myelin debris.

In the here described model, cortical lesion formation required in addition to the anti-MOG immune response the injection of the proinflammatory cytokines TNF- α and IFN- γ into the cortex.

Both cytokines have been associated with lesion formation in EAE and MS (Steinman, 2001) and are detectable within active MS lesions (Hofman et al., 1989; Selmaj et al., 1991; Traugott and Lebon, 1988). They can activate cerebral endothelial cells, which are important components of the BBB, to express adhesion molecules in order to trigger T cell arrest and migration into the CNS parenchyma and they can induce damage to the BBB by disorganizing cell-cell junctions (Minagar and Alexander, 2003). Most importantly, both cytokines attract and enhance immune responses locally leading to inflammatory demyelinated lesions in the

DISCUSSION

CNS (Kerschensteiner et al., 2004b; Merkler et al., 2006b). Since the half-life of the locally injected cytokine mixture into the cortex is unclear, the transient nature of the acute inflammatory demyelination observed in the here described model might be attributed to a short-lived effect of these cytokines. Therefore, it might be conceivable to induce chronic demyelinated lesions by continuous intracortical delivery of these cytokines for a distinct time period.

Furthermore, transient cortical demyelination did not result in axonal loss in subpial areas although remyelination was only efficient in about 50% of axons. Moreover, neuronal loss was not observed in the affected hemisphere at day three and week three after lesion induction.

Axonal and neuronal preservation are in line with previous findings that shows indeed acute axonal damage as visualized by the accumulation of amyloid precursor protein in axons in areas of subpial demyelination and around inflamed vessels in rat cortex but this result not in a reduction of axonal density after remyelination and only single apoptotic neurons in demyelinated areas are detectable (Merkler et al., 2006b). Moreover, the majority of cortical lesions in early MS exhibit relative axonal preservation and only several plaques have focal neuronal injury seen by pyknotic neurons (Lucchinetti et al., 2011). Axonal preservation in the here described model might be due to the fast decline of inflammation since axonal pathology correlates with inflammation (Kuhlmann et al., 2002; Trapp et al., 1998).

The future aim of the targeted EAE mouse model is the assessment of dendritic pathologies within demyelinated cortical lesions as well as in the surrounding NAGM. This approach needs high-resolution imaging of dendrites and dendritic spines, deconvolution and a computational 3D reconstruction (Dumitriu et al., 2011; Rodriguez et al., 2008; Rodriguez et al., 2006). The introduction of transgenic mice on a C57BL6/J background with fluorescently labeled single cortical neurons in the here used F1 hybrids allowed high-resolution imaging of dendrites, branches and dendritic spines using confocal laser scanning microscopy. Deconvolution and reconstruction of these neuronal structures allowed detailed analysis of dendritic shaft radii, spine densities and even spine shapes in addition to spine head volumes in an automated manner using NeuronStudio (CNIC). This method provides the basis for detecting even subtle changes as alterations in spine volumes or numbers of specific spine shapes or common changes in spine density. Furthermore, potential dendritic swellings can be analyzed by means of radii analysis along the dendrite. Dendritic alterations might represent pathological hallmarks in cerebral cortices of MS patients since synaptic loss can occur in leukocortical lesions (Wegner et al., 2006). Moreover, dendritic pathology occurs

in 'conventional' EAE rat and mouse models in lumbosacral spinal cord tissue (Bannerman et al., 2005; Zhu et al., 2003) and spine loss is detectable in acute EAE on second dendritic branches of striatal neurons (Rossi et al., 2012). Dendritic abnormalities might contribute to clinical symptoms like neuropsychiatric deficits and therefore have to be studied in detail.

5.3 Widespread but incomplete remyelination

Although active demyelination in the here described model was observed as a transient loss of myelin and occurrence of foamy macrophages/microglia and T cell infiltrates in the range of days after cytokine injection, only partial remyelination could be detected after three weeks although axons remained preserved.

In non-demyelinated cortex, myelin is regularly arranged and the proportion of myelinated axons in the cortical layer I+II detected in the targeted EAE mouse model in this work and cortical layer III in targeted EAE rat model is strikingly similar and is about 40% (Garea Rodriguez, 2010). The pattern of remyelinated fibers was diffuse in comparison to normal myelinated equal areas, which is in line with human remyelinated plaques (Bruck et al., 2003). The extent of remyelination was in a similar range in the mouse model and rat model as about 40-50% of axons got remyelinated after a demyelinating event (Garea Rodriguez, 2010). Although remyelination could be observed, it remained incomplete. The partial regenerative capacity however could not be attributed to axonal loss because axons remained preserved in the targeted EAE mouse model and axonal preservation is in line with findings in the rat (Garea Rodriguez, 2010; Merkler et al., 2006b). Furthermore, electron microscopic analysis reveals a thinner myelin sheath confirming that these fibers are remyelinated (Merkler et al., 2006b).

The incomplete remyelination observed in mice might represent a stage, in which the regenerative process has not finished yet and a complete recovery would require longer time periods. However, the partial remyelination observed in the cortical EAE mouse model is in accordance with incomplete remyelination capacity frequently found in MS patients in WM and cortical GM (Albert et al., 2007; Bruck et al., 2003). Mechanisms involved in remyelination may differ in WM and GM lesions as cortical lesions remyelinate more efficient (Albert et al., 2007; Chang et al., 2012). The here established targeted cortical EAE could be extended to target additionally WM structures in order to compare directly the different regenerative capacities and elucidate underlying mechanisms by intercrossing transgenic mice.

Capacity for endogenous cortical remyelination can be observed in MS irrespective of disease duration or age of the patients (Chang et al., 2012), however, chronic demyelinated lesions usually accumulate with disease progression (Kutzelnigg et al., 2005). Exhaustion of remyelination might be attributed to a lack of oligodendrocyte progenitor cells, failure of precursor cell recruitment including proliferation, migration and repopulation or disturbed differentiation and maturation to myelinating oligodendrocytes which is the best evident (Chang et al., 2002; Franklin and Ffrench-Constant, 2008; Kuhlmann et al., 2008). It would therefore be interesting to investigate in the here described model, whether remyelination efficiency can be promoted by different factors interfering with oligodendrocyte differentiation and maturation. Demyelination in cortical GM of rats shows a transient loss of oligodendrocytes but demyelinated areas are repopulated during remyelination (Merkler et al., 2006b) and existing oligodendrocyte precursor cells show substantial proliferation (Garea Rodriguez, 2010). If this is also the case in the mouse remains unclear at state.

5.4 Global dendritic spine loss in cortices of progressive MS patients

Since the end of the 1990s, MS research has refocused on the pathology affecting neuronal structures in the CNS (Peterson et al., 2001; Trapp et al., 1998; Wegner et al., 2006) that might attributed to CNS atrophy (Siffrin et al., 2010) and irreversible neurologic disability (Trapp and Nave, 2008).

In this work, cortical GM autopsy specimen from the frontotemporal lobe of the cerebrum were obtained from progressive MS patients and investigated for pathologic dendritic alterations. Interestingly, MS cortex showed a global reduction of dendritic spine density of neurons located in lower cortical layers in chronically demyelinated lesions as well as in the NAGM. Furthermore, dendrites in the cortical GM of MS patients were identified to trend for decreased branch numbers primarily in basal dendritic segments.

The detailed spine analysis could be achieved by the combination of the neuronal impregnation technique Golgi-Cox, which is invaluable in its characteristic to stain randomly distributed single neurons in the network of indefinitely neurons on an almost clear background, with laser scanning confocal microscopy, which was applicable due to the reflective capacity of the dense metal particles within the neurons and allowed high-resolution imaging (Mancuso et al., 2012; Spiga et al., 2011; Tredici et al., 1993).

Dendritic spine pathologies can be triggered from many conditions like progressive neurodegenerative diseases, malnutrition, genetic disorders associated with mental

DISCUSSION

retardation, traumatic injury or deafferentation (Fiala et al., 2002). The latter, neuronal deafferentation, induces dendritic spine loss in the adult CNS that can be partially recovered by axonal sprouting and replacement of the lost afferent synaptic input (Cheng et al., 1997; Parnavelas et al., 1974). Therefore, damage or loss of projections, e.g. thalamocortical axons, may result in transsynaptic deafferentation and spine loss on neurons in the cortex. Since the thalamus has been associated with neuronal injury and loss in MS (Cifelli et al., 2002; Wylezinska et al., 2003), the here observed spine loss may in part be explained by neurodegenerative processes in other brain areas like the thalamus. Moreover, since thalamocortical projections connect many cortical areas, spine loss would not be restricted to a focal (lesioned) area, spine pathology would rather occur in a global manner as observed in the investigated chronic MS cortices. In addition, transected and damaged neurites have been described in both, WM and GM structures (Peterson et al., 2001; Trapp et al., 1998) that might contribute to a loss of synaptic transmission. In early disease-stage, damaged or lost connecting pathways might induce sprouting or remodeling of axonal connections (Kerschensteiner et al., 2004a), however, if regenerative capacities were exceeded a decline in spine density would persist.

As mentioned above, spine abnormalities are a common feature in neurodegenerative or neuropsychiatric diseases. Spine densities are reduced on cortical neurons in Alzheimer's disease (Fiala et al., 2002; Mavroudis et al., 2011) and schizophrenia (Garey et al., 1998), but are increased in autism spectrum disorders (Hutsler and Zhang, 2010). Furthermore, a neocortical synapse loss is correlated with cognitive deficits in Alzheimer's disease (Terry et al., 1991). Since cognitive deficits are also commonly seen in MS (Amato et al., 2006), the here identified global dendritic spine pathology may partially account for the neuropsychiatric deficits in progressive MS.

6 SUMMARY AND CONCLUSIONS

In the presented work a targeted cortical EAE mouse model was established and characterized. Furthermore, dendritic pathology was investigated in the cortical GM of chronic MS patients.

Cortical demyelinated lesions were induced in EAE mice by the targeted injection of proinflammatory cytokines into the cerebral cortex. Histological evaluation revealed extensive subpial demyelination and widespread inflammation composed of T cells and activated macrophages/microglia three days after lesion induction. Within three weeks inflammation decreased profoundly and lesions remyelinated to a major extent although myelin density and proportion of myelinated axons did not again reach levels of untreated animals. In this acute model axonal and neuronal loss could not be observed in the affected cortex at three days or three weeks after lesion induction. Furthermore, a method was established that allows precise investigation of abnormalities in dendrites and dendritic spines in mice.

A global reduction of dendritic spines in neurons of the lower cortical layers could be identified as a pathological hallmark of chronically demyelinated lesions as well as the surrounding NAGM in autopsy specimen of progressive MS patients.

Targeted cortical EAE lesion in the mouse shared several pathological hallmarks with active lesions in the cortical GM of early-stage MS patients. Neurodegenerative processes observed in chronic MS lesions or surrounding NAGM were not reflected by this model. Therefore, the targeted cortical EAE mouse model mimics cortical lesions rather in early-stage MS patients and is suitable to study pathomechanisms occurring early in the cerebral cortex.

The global reduction of dendritic spines in the cerebral cortex of progressive MS is a new neurodegenerative feature that might be attributed to neuropsychological deficits and should become a new target for therapies.

7 REFERENCES

- Abbott, N.J. (2004). Evidence for bulk flow of brain interstitial fluid: significance for physiology and pathology. *Neurochemistry international* 45, 545-552.
- Adelmann, M., Wood, J., Benzel, I., Fiori, P., Lassmann, H., Matthieu, J.M., Gardinier, M.V., Dornmair, K., and Linington, C. (1995). The N-terminal domain of the myelin oligodendrocyte glycoprotein (MOG) induces acute demyelinating experimental autoimmune encephalomyelitis in the Lewis rat. *Journal of neuroimmunology* 63, 17-27.
- Albert, M., Antel, J., Bruck, W., and Stadelmann, C. (2007). Extensive cortical remyelination in patients with chronic multiple sclerosis. *Brain pathology* 17, 129-138.
- Amato, M.P., Zipoli, V., and Portaccio, E. (2006). Multiple sclerosis-related cognitive changes: a review of cross-sectional and longitudinal studies. *Journal of the neurological sciences* 245, 41-46.
- Amor, S., Groome, N., Linington, C., Morris, M.M., Dornmair, K., Gardinier, M.V., Matthieu, J.M., and Baker, D. (1994). Identification of epitopes of myelin oligodendrocyte glycoprotein for the induction of experimental allergic encephalomyelitis in SJL and Biozzi AB/H mice. *Journal of immunology* 153, 4349-4356.
- Amor, S., Smith, P.A., Hart, B., and Baker, D. (2005). Biozzi mice: of mice and human neurological diseases. *Journal of neuroimmunology* 165, 1-10.
- Andersen, O., Lygner, P.E., Bergstrom, T., Andersson, M., and Vahlne, A. (1993). Viral infections trigger multiple sclerosis relapses: a prospective seroepidemiological study. *Journal of neurology* 240, 417-422.
- Anderson, A.C., Nicholson, L.B., Legge, K.L., Turchin, V., Zaghoulani, H., and Kuchroo, V.K. (2000). High frequency of autoreactive myelin proteolipid protein-specific T cells in the periphery of naive mice: mechanisms of selection of the self-reactive repertoire. *The Journal of experimental medicine* 191, 761-770.
- Ascherio, A., and Munger, K.L. (2007a). Environmental risk factors for multiple sclerosis. Part I: the role of infection. *Annals of neurology* 61, 288-299.
- Ascherio, A., and Munger, K.L. (2007b). Environmental risk factors for multiple sclerosis. Part II: Noninfectious factors. *Annals of neurology* 61, 504-513.
- Babbe, H., Roers, A., Waisman, A., Lassmann, H., Goebels, N., Hohlfeld, R., Friese, M., Schroder, R., Deckert, M., Schmidt, S., *et al.* (2000). Clonal expansions of CD8(+) T cells dominate the T cell infiltrate in active multiple sclerosis lesions as shown by micromanipulation and single cell polymerase chain reaction. *The Journal of experimental medicine* 192, 393-404.
- Baker, D., O'Neill, J.K., Gschmeissner, S.E., Wilcox, C.E., Butter, C., and Turk, J.L. (1990). Induction of chronic relapsing experimental allergic encephalomyelitis in Biozzi mice. *Journal of neuroimmunology* 28, 261-270.

REFERENCES

- Bannerman, P.G., Hahn, A., Ramirez, S., Morley, M., Bonnemann, C., Yu, S., Zhang, G.X., Rostami, A., and Pleasure, D. (2005). Motor neuron pathology in experimental autoimmune encephalomyelitis: studies in THY1-YFP transgenic mice. *Brain : a journal of neurology* *128*, 1877-1886.
- Bar-Or, A., Calabresi, P.A., Arnold, D., Markowitz, C., Shafer, S., Kasper, L.H., Waubant, E., Gazda, S., Fox, R.J., Panzara, M., *et al.* (2008). Rituximab in relapsing-remitting multiple sclerosis: a 72-week, open-label, phase I trial. *Annals of neurology* *63*, 395-400.
- Barkhof, F. (2002). The clinico-radiological paradox in multiple sclerosis revisited. *Current opinion in neurology* *15*, 239-245.
- Baron, J.L., Madri, J.A., Ruddle, N.H., Hashim, G., and Janeway, C.A., Jr. (1993). Surface expression of alpha 4 integrin by CD4 T cells is required for their entry into brain parenchyma. *The Journal of experimental medicine* *177*, 57-68.
- Barr, T.A., Shen, P., Brown, S., Lampropoulou, V., Roch, T., Lawrie, S., Fan, B., O'Connor, R.A., Anderton, S.M., Bar-Or, A., *et al.* (2012). B cell depletion therapy ameliorates autoimmune disease through ablation of IL-6-producing B cells. *The Journal of experimental medicine* *209*, 1001-1010.
- Bartholomaeus, I., Kawakami, N., Odoardi, F., Schlager, C., Miljkovic, D., Ellwart, J.W., Klinkert, W.E., Flugel-Koch, C., Issekutz, T.B., Wekerle, H., and Flugel, A. (2009). Effector T cell interactions with meningeal vascular structures in nascent autoimmune CNS lesions. *Nature* *462*, 94-98.
- Becher, B., Durell, B.G., and Noelle, R.J. (2002). Experimental autoimmune encephalitis and inflammation in the absence of interleukin-12. *The Journal of clinical investigation* *110*, 493-497.
- Ben-Nun, A., Wekerle, H., and Cohen, I.R. (1981). Vaccination against autoimmune encephalomyelitis with T-lymphocyte line cells reactive against myelin basic protein. *Nature* *292*, 60-61.
- Bieber, A.J., Warrington, A., Asakura, K., Ciric, B., Kaveri, S.V., Pease, L.R., and Rodriguez, M. (2002). Human antibodies accelerate the rate of remyelination following lysolecithin-induced demyelination in mice. *Glia* *37*, 241-249.
- Bitsch, A., Schuchardt, J., Bunkowski, S., Kuhlmann, T., and Bruck, W. (2000). Acute axonal injury in multiple sclerosis. Correlation with demyelination and inflammation. *Brain : a journal of neurology* *123 (Pt 6)*, 1174-1183.
- Bjartmar, C., Kidd, G., Mork, S., Rudick, R., and Trapp, B.D. (2000). Neurological disability correlates with spinal cord axonal loss and reduced N-acetyl aspartate in chronic multiple sclerosis patients. *Annals of neurology* *48*, 893-901.
- Bjartmar, C., Wujek, J.R., and Trapp, B.D. (2003). Axonal loss in the pathology of MS: consequences for understanding the progressive phase of the disease. *Journal of the neurological sciences* *206*, 165-171.
- Bo, L. (2009). The histopathology of grey matter demyelination in multiple sclerosis. *Acta neurologica Scandinavica. Supplementum*, 51-57.

REFERENCES

- Bo, L., Geurts, J.J., van der Valk, P., Polman, C., and Barkhof, F. (2007). Lack of correlation between cortical demyelination and white matter pathologic changes in multiple sclerosis. *Archives of neurology* 64, 76-80.
- Bo, L., Vedeler, C.A., Nyland, H., Trapp, B.D., and Mork, S.J. (2003a). Intracortical multiple sclerosis lesions are not associated with increased lymphocyte infiltration. *Multiple sclerosis* 9, 323-331.
- Bo, L., Vedeler, C.A., Nyland, H.I., Trapp, B.D., and Mork, S.J. (2003b). Subpial demyelination in the cerebral cortex of multiple sclerosis patients. *Journal of neuropathology and experimental neurology* 62, 723-732.
- Brink, B.P., Veerhuis, R., Breij, E.C., van der Valk, P., Dijkstra, C.D., and Bo, L. (2005). The pathology of multiple sclerosis is location-dependent: no significant complement activation is detected in purely cortical lesions. *Journal of neuropathology and experimental neurology* 64, 147-155.
- Brownell, B., and Hughes, J.T. (1962). The distribution of plaques in the cerebrum in multiple sclerosis. *Journal of neurology, neurosurgery, and psychiatry* 25, 315-320.
- Bruck, W., Kuhlmann, T., and Stadelmann, C. (2003). Remyelination in multiple sclerosis. *Journal of the neurological sciences* 206, 181-185.
- Brucklacher-Waldert, V., Stuermer, K., Kolster, M., Wolthausen, J., and Tolosa, E. (2009). Phenotypical and functional characterization of T helper 17 cells in multiple sclerosis. *Brain : a journal of neurology* 132, 3329-3341.
- Buljevac, D., Flach, H.Z., Hop, W.C., Hijdra, D., Laman, J.D., Savelkoul, H.F., van Der Meche, F.G., van Doorn, P.A., and Hintzen, R.Q. (2002). Prospective study on the relationship between infections and multiple sclerosis exacerbations. *Brain : a journal of neurology* 125, 952-960.
- Burns, J., Rosenzweig, A., Zweiman, B., and Lisak, R.P. (1983). Isolation of myelin basic protein-reactive T-cell lines from normal human blood. *Cellular immunology* 81, 435-440.
- Calabrese, M., Agosta, F., Rinaldi, F., Mattisi, I., Grossi, P., Favaretto, A., Atzori, M., Bernardi, V., Barachino, L., Rinaldi, L., *et al.* (2009). Cortical lesions and atrophy associated with cognitive impairment in relapsing-remitting multiple sclerosis. *Archives of neurology* 66, 1144-1150.
- Calabrese, M., Bernardi, V., Atzori, M., Mattisi, I., Favaretto, A., Rinaldi, F., Perini, P., and Gallo, P. (2012a). Effect of disease-modifying drugs on cortical lesions and atrophy in relapsing-remitting multiple sclerosis. *Multiple sclerosis* 18, 418-424.
- Calabrese, M., De Stefano, N., Atzori, M., Bernardi, V., Mattisi, I., Barachino, L., Rinaldi, L., Morra, A., McAuliffe, M.M., Perini, P., *et al.* (2008). Extensive cortical inflammation is associated with epilepsy in multiple sclerosis. *Journal of neurology* 255, 581-586.
- Calabrese, M., Filippi, M., and Gallo, P. (2010a). Cortical lesions in multiple sclerosis. *Nature reviews. Neurology* 6, 438-444.

REFERENCES

- Calabrese, M., and Gallo, P. (2009). Magnetic resonance evidence of cortical onset of multiple sclerosis. *Multiple sclerosis* 15, 933-941.
- Calabrese, M., Grossi, P., Favaretto, A., Romualdi, C., Atzori, M., Rinaldi, F., Perini, P., Saladini, M., and Gallo, P. (2012b). Cortical pathology in multiple sclerosis patients with epilepsy: a 3 year longitudinal study. *Journal of neurology, neurosurgery, and psychiatry* 83, 49-54.
- Calabrese, M., Poretto, V., Favaretto, A., Alessio, S., Bernardi, V., Romualdi, C., Rinaldi, F., Perini, P., and Gallo, P. (2012c). Cortical lesion load associates with progression of disability in multiple sclerosis. *Brain : a journal of neurology* 135, 2952-2961.
- Calabrese, M., Rocca, M.A., Atzori, M., Mattisi, I., Favaretto, A., Perini, P., Gallo, P., and Filippi, M. (2010b). A 3-year magnetic resonance imaging study of cortical lesions in relapse-onset multiple sclerosis. *Annals of neurology* 67, 376-383.
- Catenoix, H., Marignier, R., Ritleng, C., Dufour, M., Mauguier, F., Confavreux, C., and Vukusic, S. (2011). Multiple sclerosis and epileptic seizures. *Multiple sclerosis* 17, 96-102.
- Chang, A., Staugaitis, S.M., Dutta, R., Batt, C.E., Easley, K.E., Chomyk, A.M., Yong, V.W., Fox, R.J., Kidd, G.J., and Trapp, B.D. (2012). Cortical remyelination: a new target for repair therapies in multiple sclerosis. *Annals of neurology* 72, 918-926.
- Chang, A., Tourtellotte, W.W., Rudick, R., and Trapp, B.D. (2002). Premyelinating oligodendrocytes in chronic lesions of multiple sclerosis. *The New England journal of medicine* 346, 165-173.
- Charcot, J.M. (1868). Histologie de la sclérose en plaques. *Hop civils et militaires* 140, 141, 143, 554-555, 557-558, 566.
- Chen, J.T., Narayanan, S., Collins, D.L., Smith, S.M., Matthews, P.M., and Arnold, D.L. (2004). Relating neocortical pathology to disability progression in multiple sclerosis using MRI. *NeuroImage* 23, 1168-1175.
- Cheng, H.W., Rafols, J.A., Goshgarian, H.G., Anavi, Y., Tong, J., and McNeill, T.H. (1997). Differential spine loss and regrowth of striatal neurons following multiple forms of deafferentation: a Golgi study. *Experimental neurology* 147, 287-298.
- Chiaravalloti, N.D., and DeLuca, J. (2008). Cognitive impairment in multiple sclerosis. *Lancet neurology* 7, 1139-1151.
- Choi, S.R., Howell, O.W., Carassiti, D., Magliozzi, R., Gveric, D., Muraro, P.A., Nicholas, R., Roncaroli, F., and Reynolds, R. (2012). Meningeal inflammation plays a role in the pathology of primary progressive multiple sclerosis. *Brain : a journal of neurology* 135, 2925-2937.
- Cifelli, A., Arridge, M., Jezard, P., Esiri, M.M., Palace, J., and Matthews, P.M. (2002). Thalamic neurodegeneration in multiple sclerosis. *Annals of neurology* 52, 650-653.
- CNIC NeuronStudio (Beta) <http://research.mssm.edu/cnic/tools-ns.html>.
- Compston, A., and Coles, A. (2008). Multiple sclerosis. *Lancet* 372, 1502-1517.

REFERENCES

- Confavreux, C., Hutchinson, M., Hours, M.M., Cortinovis-Tourniaire, P., and Moreau, T. (1998). Rate of pregnancy-related relapse in multiple sclerosis. *Pregnancy in Multiple Sclerosis Group. The New England journal of medicine* 339, 285-291.
- Confavreux, C., and Vukusic, S. (2006). Age at disability milestones in multiple sclerosis. *Brain : a journal of neurology* 129, 595-605.
- Confavreux, C., Vukusic, S., and Adeleine, P. (2003). Early clinical predictors and progression of irreversible disability in multiple sclerosis: an amnesic process. *Brain : a journal of neurology* 126, 770-782.
- Confavreux, C., Vukusic, S., Moreau, T., and Adeleine, P. (2000). Relapses and progression of disability in multiple sclerosis. *The New England journal of medicine* 343, 1430-1438.
- De Stefano, N., Matthews, P.M., Filippi, M., Agosta, F., De Luca, M., Bartolozzi, M.L., Guidi, L., Ghezzi, A., Montanari, E., Cifelli, A., *et al.* (2003). Evidence of early cortical atrophy in MS: relevance to white matter changes and disability. *Neurology* 60, 1157-1162.
- Derbinski, J., Schulte, A., Kyewski, B., and Klein, L. (2001). Promiscuous gene expression in medullary thymic epithelial cells mirrors the peripheral self. *Nature immunology* 2, 1032-1039.
- Deshpande, S.P., Lee, S., Zheng, M., Song, B., Knipe, D., Kapp, J.A., and Rouse, B.T. (2001). Herpes simplex virus-induced keratitis: evaluation of the role of molecular mimicry in lesion pathogenesis. *Journal of virology* 75, 3077-3088.
- Dinkler (1904). Zur Kasuistik der multiplen Herdsklerose des Gehirns und Rückenmarks. *Dtsch Z Nervenheilkd* 26, 233-247.
- Dumitriu, D., Rodriguez, A., and Morrison, J.H. (2011). High-throughput, detailed, cell-specific neuroanatomy of dendritic spines using microinjection and confocal microscopy. *Nature protocols* 6, 1391-1411.
- Dutta, R., Chang, A., Doud, M.K., Kidd, G.J., Ribaldo, M.V., Young, E.A., Fox, R.J., Staugaitis, S.M., and Trapp, B.D. (2011). Demyelination causes synaptic alterations in hippocampi from multiple sclerosis patients. *Annals of neurology* 69, 445-454.
- Dutta, R., and Trapp, B.D. (2007). Pathogenesis of axonal and neuronal damage in multiple sclerosis. *Neurology* 68, S22-31; discussion S43-54.
- Dyment, D.A., Ebers, G.C., and Sadovnick, A.D. (2004). Genetics of multiple sclerosis. *Lancet neurology* 3, 104-110.
- Feinstein, A. (2011). Multiple sclerosis and depression. *Multiple sclerosis* 17, 1276-1281.
- Feng, G., Mellor, R.H., Bernstein, M., Keller-Peck, C., Nguyen, Q.T., Wallace, M., Nerbonne, J.M., Lichtman, J.W., and Sanes, J.R. (2000). Imaging neuronal subsets in transgenic mice expressing multiple spectral variants of GFP. *Neuron* 28, 41-51.
- Ferber, I.A., Brocke, S., Taylor-Edwards, C., Ridgway, W., Dinisco, C., Steinman, L., Dalton, D., and Fathman, C.G. (1996). Mice with a disrupted IFN-gamma gene are susceptible to the

REFERENCES

induction of experimental autoimmune encephalomyelitis (EAE). *Journal of immunology* 156, 5-7.

Ferguson, B., Matyszak, M.K., Esiri, M.M., and Perry, V.H. (1997). Axonal damage in acute multiple sclerosis lesions. *Brain : a journal of neurology* 120 (Pt 3), 393-399.

Fiala, J.C., Spacek, J., and Harris, K.M. (2002). Dendritic spine pathology: cause or consequence of neurological disorders? *Brain research. Brain research reviews* 39, 29-54.

Fisher, E., Lee, J.C., Nakamura, K., and Rudick, R.A. (2008). Gray matter atrophy in multiple sclerosis: a longitudinal study. *Annals of neurology* 64, 255-265.

Fisher, E., Rudick, R.A., Simon, J.H., Cutter, G., Baier, M., Lee, J.C., Miller, D., Weinstock-Guttman, B., Mass, M.K., Dougherty, D.S., and Simonian, N.A. (2002). Eight-year follow-up study of brain atrophy in patients with MS. *Neurology* 59, 1412-1420.

Fletcher, J.M., Lalor, S.J., Sweeney, C.M., Tubridy, N., and Mills, K.H. (2010). T cells in multiple sclerosis and experimental autoimmune encephalomyelitis. *Clinical and experimental immunology* 162, 1-11.

Franklin, R.J., and Ffrench-Constant, C. (2008). Remyelination in the CNS: from biology to therapy. *Nature reviews. Neuroscience* 9, 839-855.

Freedman, M.S., Thompson, E.J., Deisenhammer, F., Giovannoni, G., Grimsley, G., Keir, G., Ohman, S., Racke, M.K., Sharief, M., Sindic, C.J., *et al.* (2005). Recommended standard of cerebrospinal fluid analysis in the diagnosis of multiple sclerosis: a consensus statement. *Archives of neurology* 62, 865-870.

Friese, M.A., and Fugger, L. (2009). Pathogenic CD8(+) T cells in multiple sclerosis. *Annals of neurology* 66, 132-141.

Frischer, J.M., Bramow, S., Dal-Bianco, A., Lucchinetti, C.F., Rauschka, H., Schmidbauer, M., Laursen, H., Sorensen, P.S., and Lassmann, H. (2009). The relation between inflammation and neurodegeneration in multiple sclerosis brains. *Brain : a journal of neurology* 132, 1175-1189.

Fujinami, R.S., and Oldstone, M.B. (1985). Amino acid homology between the encephalitogenic site of myelin basic protein and virus: mechanism for autoimmunity. *Science* 230, 1043-1045.

Garea Rodriguez, E. (2010). *Damage and Repair in Experimental Cortical Demyelination*. PhD thesis. (University of Göttingen).

Garey, L.J., Ong, W.Y., Patel, T.S., Kanani, M., Davis, A., Mortimer, A.M., Barnes, T.R., and Hirsch, S.R. (1998). Reduced dendritic spine density on cerebral cortical pyramidal neurons in schizophrenia. *Journal of neurology, neurosurgery, and psychiatry* 65, 446-453.

Genain, C.P., Cannella, B., Hauser, S.L., and Raine, C.S. (1999). Identification of autoantibodies associated with myelin damage in multiple sclerosis. *Nature medicine* 5, 170-175.

REFERENCES

- Genain, C.P., Nguyen, M.H., Letvin, N.L., Pearl, R., Davis, R.L., Adelman, M., Lees, M.B., Linington, C., and Hauser, S.L. (1995). Antibody facilitation of multiple sclerosis-like lesions in a nonhuman primate. *The Journal of clinical investigation* 96, 2966-2974.
- Giaccone, G., Bugiani, O., Ferrero, P., Orsi, L., and Tagliavini, F. (2012). A case of multiple sclerosis with pure, massive superficial demyelination. *Neurology* 79, 384-386.
- Girolamo, F., Ferrara, G., Strippoli, M., Rizzi, M., Errede, M., Trojano, M., Perris, R., Roncali, L., Svelto, M., Mennini, T., and Virgintino, D. (2011). Cerebral cortex demyelination and oligodendrocyte precursor response to experimental autoimmune encephalomyelitis. *Neurobiology of disease* 43, 678-689.
- Gold, R., Linington, C., and Lassmann, H. (2006). Understanding pathogenesis and therapy of multiple sclerosis via animal models: 70 years of merits and culprits in experimental autoimmune encephalomyelitis research. *Brain : a journal of neurology* 129, 1953-1971.
- Goverman, J. (2009). Autoimmune T cell responses in the central nervous system. *Nature reviews. Immunology* 9, 393-407.
- Goverman, J., Woods, A., Larson, L., Weiner, L.P., Hood, L., and Zaller, D.M. (1993). Transgenic mice that express a myelin basic protein-specific T cell receptor develop spontaneous autoimmunity. *Cell* 72, 551-560.
- Goverman, J.M. (2011). Immune tolerance in multiple sclerosis. *Immunological reviews* 241, 228-240.
- Gran, B., Zhang, G.X., Yu, S., Li, J., Chen, X.H., Ventura, E.S., Kamoun, M., and Rostami, A. (2002). IL-12p35-deficient mice are susceptible to experimental autoimmune encephalomyelitis: evidence for redundancy in the IL-12 system in the induction of central nervous system autoimmune demyelination. *Journal of immunology* 169, 7104-7110.
- Haahr, S., and Hollsberg, P. (2006). Multiple sclerosis is linked to Epstein-Barr virus infection. *Reviews in medical virology* 16, 297-310.
- Hartung, H.P., and Kieseier, B.C. (2010). Atacicept: targeting B cells in multiple sclerosis. *Therapeutic advances in neurological disorders* 3, 205-216.
- Hauser, S.L., Waubant, E., Arnold, D.L., Vollmer, T., Antel, J., Fox, R.J., Bar-Or, A., Panzara, M., Sarkar, N., Agarwal, S., *et al.* (2008). B-cell depletion with rituximab in relapsing-remitting multiple sclerosis. *The New England journal of medicine* 358, 676-688.
- Hernan, M.A., Jick, S.S., Logroscino, G., Olek, M.J., Ascherio, A., and Jick, H. (2005). Cigarette smoking and the progression of multiple sclerosis. *Brain : a journal of neurology* 128, 1461-1465.
- Hofman, F.M., Hinton, D.R., Johnson, K., and Merrill, J.E. (1989). Tumor necrosis factor identified in multiple sclerosis brain. *The Journal of experimental medicine* 170, 607-612.
- Howell, O.W., Reeves, C.A., Nicholas, R., Carassiti, D., Radotra, B., Gentleman, S.M., Serafini, B., Aloisi, F., Roncaroli, F., Magliozzi, R., and Reynolds, R. (2011). Meningeal inflammation is widespread and linked to cortical pathology in multiple sclerosis. *Brain : a journal of neurology* 134, 2755-2771.

REFERENCES

- Huseby, E.S., Liggitt, D., Brabb, T., Schnabel, B., Ohlen, C., and Goverman, J. (2001). A pathogenic role for myelin-specific CD8(+) T cells in a model for multiple sclerosis. *The Journal of experimental medicine* *194*, 669-676.
- Hutsler, J.J., and Zhang, H. (2010). Increased dendritic spine densities on cortical projection neurons in autism spectrum disorders. *Brain research* *1309*, 83-94.
- Iglesias, A., Bauer, J., Litzenburger, T., Schubart, A., and Linington, C. (2001). T- and B-cell responses to myelin oligodendrocyte glycoprotein in experimental autoimmune encephalomyelitis and multiple sclerosis. *Glia* *36*, 220-234.
- Irvine, K.A., and Blakemore, W.F. (2008). Remyelination protects axons from demyelination-associated axon degeneration. *Brain : a journal of neurology* *131*, 1464-1477.
- Jack, C., Ruffini, F., Bar-Or, A., and Antel, J.P. (2005). Microglia and multiple sclerosis. *Journal of neuroscience research* *81*, 363-373.
- Johns, T.G., and Bernard, C.C. (1999). The structure and function of myelin oligodendrocyte glycoprotein. *Journal of neurochemistry* *72*, 1-9.
- Johns, T.G., Kerlero de Rosbo, N., Menon, K.K., Abo, S., Gonzales, M.F., and Bernard, C.C. (1995). Myelin oligodendrocyte glycoprotein induces a demyelinating encephalomyelitis resembling multiple sclerosis. *Journal of immunology* *154*, 5536-5541.
- Kabat, E.A., Moore, D.H., and Landow, H. (1942). An Electrophoretic Study of the Protein Components in Cerebrospinal Fluid and Their Relationship to the Serum Proteins. *The Journal of clinical investigation* *21*, 571-577.
- Kapeller, P., McLean, M.A., Griffin, C.M., Chard, D., Parker, G.J., Barker, G.J., Thompson, A.J., and Miller, D.H. (2001). Preliminary evidence for neuronal damage in cortical grey matter and normal appearing white matter in short duration relapsing-remitting multiple sclerosis: a quantitative MR spectroscopic imaging study. *Journal of neurology* *248*, 131-138.
- Kebir, H., Kreymborg, K., Ifergan, I., Dodelet-Devillers, A., Cayrol, R., Bernard, M., Giuliani, F., Arbour, N., Becher, B., and Prat, A. (2007). Human TH17 lymphocytes promote blood-brain barrier disruption and central nervous system inflammation. *Nature medicine* *13*, 1173-1175.
- Keegan, M., Konig, F., McClelland, R., Bruck, W., Morales, Y., Bitsch, A., Panitch, H., Lassmann, H., Weinshenker, B., Rodriguez, M., *et al.* (2005). Relation between humoral pathological changes in multiple sclerosis and response to therapeutic plasma exchange. *Lancet* *366*, 579-582.
- Kerschensteiner, M., Bareyre, F.M., Buddeberg, B.S., Merkler, D., Stadelmann, C., Bruck, W., Misgeld, T., and Schwab, M.E. (2004a). Remodeling of axonal connections contributes to recovery in an animal model of multiple sclerosis. *The Journal of experimental medicine* *200*, 1027-1038.
- Kerschensteiner, M., Stadelmann, C., Buddeberg, B.S., Merkler, D., Bareyre, F.M., Anthony, D.C., Linington, C., Bruck, W., and Schwab, M.E. (2004b). Targeting experimental autoimmune encephalomyelitis lesions to a predetermined axonal tract system allows for

REFERENCES

- refined behavioral testing in an animal model of multiple sclerosis. *The American journal of pathology* *164*, 1455-1469.
- Kidd, D., Barkhof, F., McConnell, R., Algra, P.R., Allen, I.V., and Revesz, T. (1999). Cortical lesions in multiple sclerosis. *Brain : a journal of neurology* *122 (Pt 1)*, 17-26.
- Kivisakk, P., Imitola, J., Rasmussen, S., Elyaman, W., Zhu, B., Ransohoff, R.M., and Khoury, S.J. (2009). Localizing central nervous system immune surveillance: meningeal antigen-presenting cells activate T cells during experimental autoimmune encephalomyelitis. *Annals of neurology* *65*, 457-469.
- Kroenke, M.A., Carlson, T.J., Andjelkovic, A.V., and Segal, B.M. (2008). IL-12- and IL-23-modulated T cells induce distinct types of EAE based on histology, CNS chemokine profile, and response to cytokine inhibition. *The Journal of experimental medicine* *205*, 1535-1541.
- Kuhlmann, T., Lingfeld, G., Bitsch, A., Schuchardt, J., and Bruck, W. (2002). Acute axonal damage in multiple sclerosis is most extensive in early disease stages and decreases over time. *Brain : a journal of neurology* *125*, 2202-2212.
- Kuhlmann, T., Miron, V., Cui, Q., Wegner, C., Antel, J., and Bruck, W. (2008). Differentiation block of oligodendroglial progenitor cells as a cause for remyelination failure in chronic multiple sclerosis. *Brain : a journal of neurology* *131*, 1749-1758.
- Kurtzke, J.F. (1983). Rating neurologic impairment in multiple sclerosis: an expanded disability status scale (EDSS). *Neurology* *33*, 1444-1452.
- Kutzelnigg, A., Lucchinetti, C.F., Stadelmann, C., Bruck, W., Rauschka, H., Bergmann, M., Schmidbauer, M., Parisi, J.E., and Lassmann, H. (2005). Cortical demyelination and diffuse white matter injury in multiple sclerosis. *Brain : a journal of neurology* *128*, 2705-2712.
- Lang, H.L., Jacobsen, H., Ikemizu, S., Andersson, C., Harlos, K., Madsen, L., Hjorth, P., Sondergaard, L., Svejgaard, A., Wucherpfennig, K., *et al.* (2002). A functional and structural basis for TCR cross-reactivity in multiple sclerosis. *Nature immunology* *3*, 940-943.
- Langrish, C.L., Chen, Y., Blumenschein, W.M., Mattson, J., Basham, B., Sedgwick, J.D., McClanahan, T., Kastelein, R.A., and Cua, D.J. (2005). IL-23 drives a pathogenic T cell population that induces autoimmune inflammation. *The Journal of experimental medicine* *201*, 233-240.
- Lassmann, H., Bruck, W., and Lucchinetti, C.F. (2007). The immunopathology of multiple sclerosis: an overview. *Brain pathology* *17*, 210-218.
- Lassmann, H., Brunner, C., Bradl, M., and Linington, C. (1988). Experimental allergic encephalomyelitis: the balance between encephalitogenic T lymphocytes and demyelinating antibodies determines size and structure of demyelinated lesions. *Acta neuropathologica* *75*, 566-576.
- Lassmann, H., van Horssen, J., and Mahad, D. (2012). Progressive multiple sclerosis: pathology and pathogenesis. *Nature reviews. Neurology* *8*, 647-656.

REFERENCES

- Liebetanz, D., and Merkler, D. (2006). Effects of commissural de- and remyelination on motor skill behaviour in the cuprizone mouse model of multiple sclerosis. *Experimental neurology* 202, 217-224.
- Linington, C., Bradl, M., Lassmann, H., Brunner, C., and Vass, K. (1988). Augmentation of demyelination in rat acute allergic encephalomyelitis by circulating mouse monoclonal antibodies directed against a myelin/oligodendrocyte glycoprotein. *The American journal of pathology* 130, 443-454.
- Lovas, G., Szilagyi, N., Majtenyi, K., Palkovits, M., and Komoly, S. (2000). Axonal changes in chronic demyelinated cervical spinal cord plaques. *Brain : a journal of neurology* 123 (Pt 2), 308-317.
- Lucchinetti, C., Bruck, W., Parisi, J., Scheithauer, B., Rodriguez, M., and Lassmann, H. (1999). A quantitative analysis of oligodendrocytes in multiple sclerosis lesions. A study of 113 cases. *Brain : a journal of neurology* 122 (Pt 12), 2279-2295.
- Lucchinetti, C., Bruck, W., Parisi, J., Scheithauer, B., Rodriguez, M., and Lassmann, H. (2000). Heterogeneity of multiple sclerosis lesions: implications for the pathogenesis of demyelination. *Annals of neurology* 47, 707-717.
- Lucchinetti, C.F., Popescu, B.F., Bunyan, R.F., Moll, N.M., Roemer, S.F., Lassmann, H., Bruck, W., Parisi, J.E., Scheithauer, B.W., Giannini, C., *et al.* (2011). Inflammatory cortical demyelination in early multiple sclerosis. *The New England journal of medicine* 365, 2188-2197.
- Lumsden, C.E. (1970). The neuropathology of multiple sclerosis. In *Handbook of clinical neurology*, P.J. Vinken, and G.W. Bruyn, eds. (Amsterdam: Elsevier), pp. 217-309.
- Magliozzi, R., Howell, O., Vora, A., Serafini, B., Nicholas, R., Puopolo, M., Reynolds, R., and Aloisi, F. (2007). Meningeal B-cell follicles in secondary progressive multiple sclerosis associate with early onset of disease and severe cortical pathology. *Brain : a journal of neurology* 130, 1089-1104.
- Magliozzi, R., Howell, O.W., Reeves, C., Roncaroli, F., Nicholas, R., Serafini, B., Aloisi, F., and Reynolds, R. (2010). A Gradient of neuronal loss and meningeal inflammation in multiple sclerosis. *Annals of neurology* 68, 477-493.
- Mancuso, J.J., Chen, Y., Li, X., Xue, Z., and Wong, S.T. (2012). Methods of dendritic spine detection: From Golgi to high-resolution optical imaging. *Neuroscience*.
- Mangiardi, M., Crawford, D.K., Xia, X., Du, S., Simon-Freeman, R., Voskuhl, R.R., and Tiwari-Woodruff, S.K. (2011). An animal model of cortical and callosal pathology in multiple sclerosis. *Brain pathology* 21, 263-278.
- Manrique-Hoyos, N., Jurgens, T., Gronborg, M., Kreutzfeldt, M., Schedensack, M., Kuhlmann, T., Schrick, C., Bruck, W., Urlaub, H., Simons, M., and Merkler, D. (2012). Late motor decline after accomplished remyelination: impact for progressive multiple sclerosis. *Annals of neurology* 71, 227-244.

REFERENCES

- Matsushita, T., Yanaba, K., Bouaziz, J.D., Fujimoto, M., and Tedder, T.F. (2008). Regulatory B cells inhibit EAE initiation in mice while other B cells promote disease progression. *The Journal of clinical investigation* *118*, 3420-3430.
- Mavroudis, I.A., Fotiou, D.F., Manani, M.G., Njaou, S.N., Frangou, D., Costa, V.G., and Baloyannis, S.J. (2011). Dendritic pathology and spinal loss in the visual cortex in Alzheimer's disease: a Golgi study in pathology. *The International journal of neuroscience* *121*, 347-354.
- McCoy, L., Tsunoda, I., and Fujinami, R.S. (2006). Multiple sclerosis and virus induced immune responses: autoimmunity can be primed by molecular mimicry and augmented by bystander activation. *Autoimmunity* *39*, 9-19.
- McDonald, W.I., Compston, A., Edan, G., Goodkin, D., Hartung, H.P., Lublin, F.D., McFarland, H.F., Paty, D.W., Polman, C.H., Reingold, S.C., *et al.* (2001). Recommended diagnostic criteria for multiple sclerosis: guidelines from the International Panel on the diagnosis of multiple sclerosis. *Annals of neurology* *50*, 121-127.
- Medana, I., Martinic, M.A., Wekerle, H., and Neumann, H. (2001). Transection of major histocompatibility complex class I-induced neurites by cytotoxic T lymphocytes. *The American journal of pathology* *159*, 809-815.
- Merkler, D., Boscke, R., Schmelting, B., Czeh, B., Fuchs, E., Bruck, W., and Stadelmann, C. (2006a). Differential macrophage/microglia activation in neocortical EAE lesions in the marmoset monkey. *Brain pathology* *16*, 117-123.
- Merkler, D., Ernsting, T., Kerschensteiner, M., Bruck, W., and Stadelmann, C. (2006b). A new focal EAE model of cortical demyelination: multiple sclerosis-like lesions with rapid resolution of inflammation and extensive remyelination. *Brain : a journal of neurology* *129*, 1972-1983.
- Merkler, D., Klinker, F., Jurgens, T., Glaser, R., Paulus, W., Brinkmann, B.G., Sereda, M.W., Stadelmann-Nessler, C., Guedes, R.C., Bruck, W., and Liebetanz, D. (2009). Propagation of spreading depression inversely correlates with cortical myelin content. *Annals of neurology* *66*, 355-365.
- Mikaeloff, Y., Caridade, G., Tardieu, M., Suissa, S., and group, K.s. (2007). Parental smoking at home and the risk of childhood-onset multiple sclerosis in children. *Brain : a journal of neurology* *130*, 2589-2595.
- Miller, D.H., Rudge, P., Johnson, G., Kendall, B.E., Macmanus, D.G., Moseley, I.F., Barnes, D., and McDonald, W.I. (1988). Serial gadolinium enhanced magnetic resonance imaging in multiple sclerosis. *Brain : a journal of neurology* *111 (Pt 4)*, 927-939.
- Miller, D.J., Sanborn, K.S., Katzmann, J.A., and Rodriguez, M. (1994). Monoclonal autoantibodies promote central nervous system repair in an animal model of multiple sclerosis. *The Journal of neuroscience : the official journal of the Society for Neuroscience* *14*, 6230-6238.
- Minagar, A., and Alexander, J.S. (2003). Blood-brain barrier disruption in multiple sclerosis. *Multiple sclerosis* *9*, 540-549.

REFERENCES

Morris-Downes, M.M., Smith, P.A., Rundle, J.L., Piddlesden, S.J., Baker, D., Pham-Dinh, D., Heijmans, N., and Amor, S. (2002). Pathological and regulatory effects of anti-myelin antibodies in experimental allergic encephalomyelitis in mice. *Journal of neuroimmunology* 125, 114-124.

MSIF Atlas of MS Database (<http://www.atlasofms.org/>).

Nikic, I., Merkler, D., Sorbara, C., Brinkoetter, M., Kreutzfeldt, M., Bareyre, F.M., Bruck, W., Bishop, D., Misgeld, T., and Kerschensteiner, M. (2011). A reversible form of axon damage in experimental autoimmune encephalomyelitis and multiple sclerosis. *Nature medicine* 17, 495-499.

Noseworthy, J.H., Lucchinetti, C., Rodriguez, M., and Weinshenker, B.G. (2000). Multiple sclerosis. *The New England journal of medicine* 343, 938-952.

Olsson, T., Zhi, W.W., Hojeborg, B., Kostulas, V., Jiang, Y.P., Anderson, G., Ekre, H.P., and Link, H. (1990). Autoreactive T lymphocytes in multiple sclerosis determined by antigen-induced secretion of interferon-gamma. *The Journal of clinical investigation* 86, 981-985.

Oppmann, B., Lesley, R., Blom, B., Timans, J.C., Xu, Y., Hunte, B., Vega, F., Yu, N., Wang, J., Singh, K., *et al.* (2000). Novel p19 protein engages IL-12p40 to form a cytokine, IL-23, with biological activities similar as well as distinct from IL-12. *Immunity* 13, 715-725.

Pagany, M., Jagodic, M., Schubart, A., Pham-Dinh, D., Bachelin, C., Baron van Evercooren, A., Lachapelle, F., Olsson, T., and Linington, C. (2003). Myelin oligodendrocyte glycoprotein is expressed in the peripheral nervous system of rodents and primates. *Neuroscience letters* 350, 165-168.

Panitch, H.S., Hirsch, R.L., Haley, A.S., and Johnson, K.P. (1987). Exacerbations of multiple sclerosis in patients treated with gamma interferon. *Lancet* 1, 893-895.

Papadopoulos, D., Dukes, S., Patel, R., Nicholas, R., Vora, A., and Reynolds, R. (2009). Substantial archaeocortical atrophy and neuronal loss in multiple sclerosis. *Brain pathology* 19, 238-253.

Parnavelas, J.G., Lynch, G., Brecha, N., Cotman, C.W., and Globus, A. (1974). Spine loss and regrowth in hippocampus following deafferentation. *Nature* 248, 71-73.

Patani, R., Balaratnam, M., Vora, A., and Reynolds, R. (2007). Remyelination can be extensive in multiple sclerosis despite a long disease course. *Neuropathology and applied neurobiology* 33, 277-287.

Patrikios, P., Stadelmann, C., Kutzelnigg, A., Rauschka, H., Schmidbauer, M., Laursen, H., Sorensen, P.S., Bruck, W., Lucchinetti, C., and Lassmann, H. (2006). Remyelination is extensive in a subset of multiple sclerosis patients. *Brain : a journal of neurology* 129, 3165-3172.

Pearce, J.M. (2005). Historical descriptions of multiple sclerosis. *European neurology* 54, 49-53.

Petermann, F., and Korn, T. (2011). Cytokines and effector T cell subsets causing autoimmune CNS disease. *FEBS letters* 585, 3747-3757.

REFERENCES

- Peterson, J.W., Bo, L., Mork, S., Chang, A., and Trapp, B.D. (2001). Transected neurites, apoptotic neurons, and reduced inflammation in cortical multiple sclerosis lesions. *Annals of neurology* 50, 389-400.
- Pette, M., Fujita, K., Kitze, B., Whitaker, J.N., Albert, E., Kappos, L., and Wekerle, H. (1990). Myelin basic protein-specific T lymphocyte lines from MS patients and healthy individuals. *Neurology* 40, 1770-1776.
- Pollinger, B., Krishnamoorthy, G., Berer, K., Lassmann, H., Bosl, M.R., Dunn, R., Domingues, H.S., Holz, A., Kurschus, F.C., and Wekerle, H. (2009). Spontaneous relapsing-remitting EAE in the SJL/J mouse: MOG-reactive transgenic T cells recruit endogenous MOG-specific B cells. *The Journal of experimental medicine* 206, 1303-1316.
- Polman, C.H., Reingold, S.C., Banwell, B., Clanet, M., Cohen, J.A., Filippi, M., Fujihara, K., Havrdova, E., Hutchinson, M., Kappos, L., *et al.* (2011). Diagnostic criteria for multiple sclerosis: 2010 revisions to the McDonald criteria. *Annals of neurology* 69, 292-302.
- Polman, C.H., Reingold, S.C., Edan, G., Filippi, M., Hartung, H.P., Kappos, L., Lublin, F.D., Metz, L.M., McFarland, H.F., O'Connor, P.W., *et al.* (2005). Diagnostic criteria for multiple sclerosis: 2005 revisions to the "McDonald Criteria". *Annals of neurology* 58, 840-846.
- Pomeroy, I.M., Jordan, E.K., Frank, J.A., Matthews, P.M., and Esiri, M.M. (2008). Diffuse cortical atrophy in a marmoset model of multiple sclerosis. *Neuroscience letters* 437, 121-124.
- Pomeroy, I.M., Matthews, P.M., Frank, J.A., Jordan, E.K., and Esiri, M.M. (2005). Demyelinated neocortical lesions in marmoset autoimmune encephalomyelitis mimic those in multiple sclerosis. *Brain : a journal of neurology* 128, 2713-2721.
- Popescu, B.F., Bunyan, R.F., Parisi, J.E., Ransohoff, R.M., and Lucchinetti, C.F. (2011). A case of multiple sclerosis presenting with inflammatory cortical demyelination. *Neurology* 76, 1705-1710.
- Popescu, B.F., and Lucchinetti, C.F. (2012). Meningeal and cortical grey matter pathology in multiple sclerosis. *BMC neurology* 12, 11.
- Raine, C.S., Cannella, B., Hauser, S.L., and Genain, C.P. (1999). Demyelination in primate autoimmune encephalomyelitis and acute multiple sclerosis lesions: a case for antigen-specific antibody mediation. *Annals of neurology* 46, 144-160.
- Ransohoff, R.M. (2009). Immunology: In the beginning. *Nature* 462, 41-42.
- Ransohoff, R.M. (2012). Animal models of multiple sclerosis: the good, the bad and the bottom line. *Nature neuroscience* 15, 1074-1077.
- Rasmussen, S., Wang, Y., Kivisakk, P., Bronson, R.T., Meyer, M., Imitola, J., and Khoury, S.J. (2007). Persistent activation of microglia is associated with neuronal dysfunction of callosal projecting pathways and multiple sclerosis-like lesions in relapsing--remitting experimental autoimmune encephalomyelitis. *Brain : a journal of neurology* 130, 2816-2829.
- Reboldi, A., Coisne, C., Baumjohann, D., Benvenuto, F., Bottinelli, D., Lira, S., Uccelli, A., Lanzavecchia, A., Engelhardt, B., and Sallusto, F. (2009). C-C chemokine receptor 6-

REFERENCES

regulated entry of TH-17 cells into the CNS through the choroid plexus is required for the initiation of EAE. *Nature immunology* *10*, 514-523.

Richert, J.R., McFarlin, D.E., Rose, J.W., McFarland, H.F., and Greenstein, J.I. (1983). Expansion of antigen-specific T cells from cerebrospinal fluid of patients with multiple sclerosis. *Journal of neuroimmunology* *5*, 317-324.

Rinaldi, F., Calabrese, M., Grossi, P., Puthenparampil, M., Perini, P., and Gallo, P. (2010). Cortical lesions and cognitive impairment in multiple sclerosis. *Neurological sciences : official journal of the Italian Neurological Society and of the Italian Society of Clinical Neurophysiology* *31*, S235-237.

Rinaldi, F., Calabrese, M., Seppi, D., Puthenparampil, M., Perini, P., and Gallo, P. (2012). Natalizumab strongly suppresses cortical pathology in relapsing-remitting multiple sclerosis. *Multiple sclerosis* *18*, 1760-1767.

Rivers, T.M., Sprunt, D.H., and Berry, G.P. (1933). Observations on Attempts to Produce Acute Disseminated Encephalomyelitis in Monkeys. *The Journal of experimental medicine* *58*, 39-53.

Rodriguez, A., Ehlenberger, D.B., Dickstein, D.L., Hof, P.R., and Wearne, S.L. (2008). Automated three-dimensional detection and shape classification of dendritic spines from fluorescence microscopy images. *PloS one* *3*, e1997.

Rodriguez, A., Ehlenberger, D.B., Hof, P.R., and Wearne, S.L. (2006). Rayburst sampling, an algorithm for automated three-dimensional shape analysis from laser scanning microscopy images. *Nature protocols* *1*, 2152-2161.

Roosendaal, S.D., Moraal, B., Pouwels, P.J., Vrenken, H., Castelijns, J.A., Barkhof, F., and Geurts, J.J. (2009). Accumulation of cortical lesions in MS: relation with cognitive impairment. *Multiple sclerosis* *15*, 708-714.

Rossi, S., Lo Giudice, T., De Chiara, V., Musella, A., Studer, V., Motta, C., Bernardi, G., Martino, G., Furlan, R., Martorana, A., and Centonze, D. (2012). Oral fingolimod rescues the functional deficits of synapses in experimental autoimmune encephalomyelitis. *British journal of pharmacology* *165*, 861-869.

Rudick, R.A., Fisher, E., Lee, J.C., Simon, J., and Jacobs, L. (1999). Use of the brain parenchymal fraction to measure whole brain atrophy in relapsing-remitting MS. Multiple Sclerosis Collaborative Research Group. *Neurology* *53*, 1698-1704.

Rudick, R.A., Lee, J.C., Nakamura, K., and Fisher, E. (2009). Gray matter atrophy correlates with MS disability progression measured with MSFC but not EDSS. *Journal of the neurological sciences* *282*, 106-111.

Sailer, M., Fischl, B., Salat, D., Tempelmann, C., Schonfeld, M.A., Busa, E., Bodammer, N., Heinze, H.J., and Dale, A. (2003). Focal thinning of the cerebral cortex in multiple sclerosis. *Brain : a journal of neurology* *126*, 1734-1744.

Sander, M. (1898). Hirnrindenbefunde bei multipler Sklerose. *Monatsschr Psychiatr Neurol*, 427-436.

REFERENCES

- Schluesener, H.J., Sobel, R.A., Linington, C., and Weiner, H.L. (1987). A monoclonal antibody against a myelin oligodendrocyte glycoprotein induces relapses and demyelination in central nervous system autoimmune disease. *Journal of immunology* *139*, 4016-4021.
- Schluesener, H.J., and Wekerle, H. (1985). Autoaggressive T lymphocyte lines recognizing the encephalitogenic region of myelin basic protein: in vitro selection from unprimed rat T lymphocyte populations. *Journal of immunology* *135*, 3128-3133.
- Schwab, C., and McGeer, P.L. (2002). Complement activated C4d immunoreactive oligodendrocytes delineate small cortical plaques in multiple sclerosis. *Experimental neurology* *174*, 81-88.
- Seamons, A., Perchellet, A., and Goverman, J. (2003). Immune tolerance to myelin proteins. *Immunologic research* *28*, 201-221.
- Selmaj, K., Raine, C.S., Cannella, B., and Brosnan, C.F. (1991). Identification of lymphotoxin and tumor necrosis factor in multiple sclerosis lesions. *The Journal of clinical investigation* *87*, 949-954.
- Serafini, B., Rosicarelli, B., Franciotta, D., Magliozzi, R., Reynolds, R., Cinque, P., Andreoni, L., Trivedi, P., Salvetti, M., Faggioni, A., and Aloisi, F. (2007). Dysregulated Epstein-Barr virus infection in the multiple sclerosis brain. *The Journal of experimental medicine* *204*, 2899-2912.
- Serafini, B., Rosicarelli, B., Magliozzi, R., Stigliano, E., and Aloisi, F. (2004). Detection of ectopic B-cell follicles with germinal centers in the meninges of patients with secondary progressive multiple sclerosis. *Brain pathology* *14*, 164-174.
- Sibley, W.A., Bamford, C.R., and Clark, K. (1985). Clinical viral infections and multiple sclerosis. *Lancet* *1*, 1313-1315.
- Siffrin, V., Vogt, J., Radbruch, H., Nitsch, R., and Zipp, F. (2010). Multiple sclerosis - candidate mechanisms underlying CNS atrophy. *Trends in neurosciences* *33*, 202-210.
- Skripuletz, T., Gudi, V., Hackstette, D., and Stangel, M. (2011). De- and remyelination in the CNS white and grey matter induced by cuprizone: the old, the new, and the unexpected. *Histology and histopathology* *26*, 1585-1597.
- Skripuletz, T., Lindner, M., Kotsiari, A., Garde, N., Fokuhl, J., Linsmeier, F., Trebst, C., and Stangel, M. (2008). Cortical demyelination is prominent in the murine cuprizone model and is strain-dependent. *The American journal of pathology* *172*, 1053-1061.
- Smith, P.A., Heijmans, N., Ouwering, B., Breij, E.C., Evans, N., van Noort, J.M., Plomp, A.C., Delarasse, C., t Hart, B., Pham-Dinh, D., and Amor, S. (2005). Native myelin oligodendrocyte glycoprotein promotes severe chronic neurological disease and demyelination in Biozzi ABH mice. *European journal of immunology* *35*, 1311-1319.
- Spatt, J., Chaix, R., and Mamoli, B. (2001). Epileptic and non-epileptic seizures in multiple sclerosis. *Journal of neurology* *248*, 2-9.

REFERENCES

- Spiga, S., Acquas, E., Puddu, M.C., Mulas, G., Lintas, A., and Diana, M. (2011). Simultaneous Golgi-Cox and immunofluorescence using confocal microscopy. *Brain structure & function* 216, 171-182.
- Srivastava, R., Aslam, M., Kalluri, S.R., Schirmer, L., Buck, D., Tackenberg, B., Rothhammer, V., Chan, A., Gold, R., Berthele, A., *et al.* (2012). Potassium channel KIR4.1 as an immune target in multiple sclerosis. *The New England journal of medicine* 367, 115-123.
- Steinman, L. (2001). Multiple sclerosis: a two-stage disease. *Nature immunology* 2, 762-764.
- Storch, M.K., Bauer, J., Linington, C., Olsson, T., Weissert, R., and Lassmann, H. (2006). Cortical demyelination can be modeled in specific rat models of autoimmune encephalomyelitis and is major histocompatibility complex (MHC) haplotype-related. *Journal of neuropathology and experimental neurology* 65, 1137-1142.
- Taylor, E.W. (1892). Zur pathologischen Anatomie der multiplen Sklerose. *Dtsch Z Nervenheilkd* 5, 1-26.
- Terry, R.D., Masliah, E., Salmon, D.P., Butters, N., DeTeresa, R., Hill, R., Hansen, L.A., and Katzman, R. (1991). Physical basis of cognitive alterations in Alzheimer's disease: synapse loss is the major correlate of cognitive impairment. *Annals of neurology* 30, 572-580.
- Thacker, E.L., Mirzaei, F., and Ascherio, A. (2006). Infectious mononucleosis and risk for multiple sclerosis: a meta-analysis. *Annals of neurology* 59, 499-503.
- Torkildsen, O., Brunborg, L.A., Myhr, K.M., and Bo, L. (2008). The cuprizone model for demyelination. *Acta neurologica Scandinavica. Supplementum* 188, 72-76.
- Trapp, B.D., and Nave, K.A. (2008). Multiple sclerosis: an immune or neurodegenerative disorder? *Annual review of neuroscience* 31, 247-269.
- Trapp, B.D., Peterson, J., Ransohoff, R.M., Rudick, R., Mork, S., and Bo, L. (1998). Axonal transection in the lesions of multiple sclerosis. *The New England journal of medicine* 338, 278-285.
- Traugott, U., and Lebon, P. (1988). Interferon-gamma and Ia antigen are present on astrocytes in active chronic multiple sclerosis lesions. *Journal of the neurological sciences* 84, 257-264.
- Tredici, G., Di Francesco, A., Miani, A., Jr., and Pizzini, G. (1993). Real complete three-dimensional reconstruction of Golgi-impregnated neurons by means of a confocal laser scanning microscope. *NeuroImage* 1, 87-93.
- Tzartos, J.S., Friese, M.A., Craner, M.J., Palace, J., Newcombe, J., Esiri, M.M., and Fugger, L. (2008). Interleukin-17 production in central nervous system-infiltrating T cells and glial cells is associated with active disease in multiple sclerosis. *The American journal of pathology* 172, 146-155.
- van Horssen, J., Brink, B.P., de Vries, H.E., van der Valk, P., and Bo, L. (2007). The blood-brain barrier in cortical multiple sclerosis lesions. *Journal of neuropathology and experimental neurology* 66, 321-328.

REFERENCES

- Vercellino, M., Plano, F., Votta, B., Mutani, R., Giordana, M.T., and Cavalla, P. (2005). Grey matter pathology in multiple sclerosis. *Journal of neuropathology and experimental neurology* 64, 1101-1107.
- Waldner, H., Whitters, M.J., Sobel, R.A., Collins, M., and Kuchroo, V.K. (2000). Fulminant spontaneous autoimmunity of the central nervous system in mice transgenic for the myelin proteolipid protein-specific T cell receptor. *Proceedings of the National Academy of Sciences of the United States of America* 97, 3412-3417.
- Warrington, A.E., Bieber, A.J., Ciric, B., Pease, L.R., Van Keulen, V., and Rodriguez, M. (2007). A recombinant human IgM promotes myelin repair after a single, very low dose. *Journal of neuroscience research* 85, 967-976.
- Wearne, S.L., Rodriguez, A., Ehlenberger, D.B., Rocher, A.B., Henderson, S.C., and Hof, P.R. (2005). New techniques for imaging, digitization and analysis of three-dimensional neural morphology on multiple scales. *Neuroscience* 136, 661-680.
- Wegner, C., Esiri, M.M., Chance, S.A., Palace, J., and Matthews, P.M. (2006). Neocortical neuronal, synaptic, and glial loss in multiple sclerosis. *Neurology* 67, 960-967.
- WHO, and MSIF (2008). Atlas multiple sclerosis resources in the world 2008.
- Willenborg, D.O., Fordham, S., Bernard, C.C., Cowden, W.B., and Ramshaw, I.A. (1996). IFN-gamma plays a critical down-regulatory role in the induction and effector phase of myelin oligodendrocyte glycoprotein-induced autoimmune encephalomyelitis. *Journal of immunology* 157, 3223-3227.
- Willing, A., and Friese, M.A. (2012). CD8-mediated inflammatory central nervous system disorders. *Current opinion in neurology* 25, 316-321.
- Wolswijk, G. (1998). Chronic stage multiple sclerosis lesions contain a relatively quiescent population of oligodendrocyte precursor cells. *The Journal of neuroscience : the official journal of the Society for Neuroscience* 18, 601-609.
- Wylezinska, M., Cifelli, A., Jezard, P., Palace, J., Alecci, M., and Matthews, P.M. (2003). Thalamic neurodegeneration in relapsing-remitting multiple sclerosis. *Neurology* 60, 1949-1954.
- York, N.R., Mendoza, J.P., Ortega, S.B., Benagh, A., Tyler, A.F., Firan, M., and Karandikar, N.J. (2010). Immune regulatory CNS-reactive CD8+T cells in experimental autoimmune encephalomyelitis. *Journal of autoimmunity* 35, 33-44.
- Zamvil, S., Nelson, P., Trotter, J., Mitchell, D., Knobler, R., Fritz, R., and Steinman, L. (1985). T-cell clones specific for myelin basic protein induce chronic relapsing paralysis and demyelination. *Nature* 317, 355-358.
- Zhou, D., Srivastava, R., Nessler, S., Grummel, V., Sommer, N., Bruck, W., Hartung, H.P., Stadelmann, C., and Hemmer, B. (2006). Identification of a pathogenic antibody response to native myelin oligodendrocyte glycoprotein in multiple sclerosis. *Proceedings of the National Academy of Sciences of the United States of America* 103, 19057-19062.

REFERENCES

Zhu, B., Luo, L., Moore, G.R., Paty, D.W., and Cynader, M.S. (2003). Dendritic and synaptic pathology in experimental autoimmune encephalomyelitis. *The American journal of pathology* *162*, 1639-1650.

Zhu, J., Yamane, H., and Paul, W.E. (2010). Differentiation of effector CD4 T cell populations (*). *Annual review of immunology* *28*, 445-489.

8 CURRICULUM VITAE

Tanja Jürgens

Rue des Pervenches 9
1227 Carouge / Geneva
Switzerland

E-Mail: Tanja.Juergens@unige.ch
Date of birth: January 22, 1984
Nationality: German

Education

2009 – current

PhD Program Molecular Medicine, University of Göttingen
*Institute of Neuropathology, University of Göttingen and
Department of Pathology and Immunology, University of Geneva*
Theme: Neuronal pathology in targeted cortical experimental
autoimmune encephalomyelitis and multiple sclerosis.
Supervisor: Prof. Dr. D. Merkler

2006 – 2008

Master of Science (M.Sc.) in Biochemistry
Institute of Molecular and Medical Virology, University of Bochum
Theme: Optimization of DNA vaccines against the Respiratory
Syncytial Virus.
Supervisor: Dr. T. Grunwald

2003-2006

Bachelor of Science (B.Sc.) in Biochemistry
Institute of Physical Chemistry II, University of Bochum
Theme: Purification and spectroscopy of ubiquitin mutants.
Supervisor: Prof. Dr. M. Havenith-Newen

Secondary School Education

2003

Abitur
Gymnasium Nordenham

Publications

Late motor decline after accomplished remyelination: impact for progressive multiple sclerosis.

Natalia Manrique-Hoyos, **Tanja Jürgens**, Mads Grønborg, Mario Kreutzfeldt, Mariann Schedensack, Tanja Kuhlmann, Christina Schrick, Wolfgang Brück, Henning Urlaub, Mikael Simons and Doron Merkler. *Annals of Neurology*, 2012.

Toll-like receptor activation reveals developmental reorganization and unmasks responder subsets of microglia.

Jörg Scheffel, Tommy Regen, Denise van Rossum, Stefanie Seifert, Sandra Ribes, Roland Nau, Roham Parsa, Robert A. Harris, Hendrikus W. G. M. Boddeke, Han-Ning Chuang, Tobias Pukrop, Johannes T. Wessels, **Tanja Jürgens**, Doron Merkler, Wolfgang Brück, Mareike Schnaars, Mikael Simons, Helmut Kettenmann and Uwe-Karsten Hanisch. *Glia*, 2012.

Propagation of spreading depression inversely correlates with cortical myelin content.

Doron Merkler*, Florian Klinker*, **Tanja Jürgens**, Raoul Glaser, Walter Paulus, Bastian G. Brinkmann, Michael W. Sereda, Christine Stadelmann-Nessler, Rubem C.A. Guedes, Wolfgang Brück, David Liebetanz. *Annals of Neurology*, 2009. (*equal contribution)
